NTNU – Trondheim
Norwegian University of
Science and Technology

Field Theory at finite Temperature and Density

Applications to Quark Stars

Inga Strumke

Physics

Supervisor: Jens Oluf Andersen, IFY

Norwegian University of Science and Technology
Department of Physics

Abstract

In this thesis, different different thermal field theories are considered, and an equation of state for deconfined matter is derived. This equation of state is used in the Tolman-Oppenheimer-Volkoff (TOV)-equations to calculate the mass and radius of quark stars.

Firstly, a scalar field with a four-point interaction is studied at finite temperature, and the validity of the perturbative expansion is discussed. The pressure is calculated to fifth order.

Secondly, QED and QCD are studied at finite chemical potential and zero temperature, and an equation of state for degenerate quark matter is derived.

Next, general relativity is discussed, and Einstein's field equations as well as the TOV-equations are derived. These last equations are used to model dense stars with different equations of state, and finally the equation describing deconfined matter is used to determine the mass-radius relationship for quark stars with different central pressures.

The results obtained in this thesis indicate in which range of masses and radii quark stars could be observed, and it is discussed how the models used here could be improved and made more realistic.

Acknowledgments

First, I would like to thank professor Jens Oluf Andersen for encouragement and patient supervision, both as a lecturer and especially as my supervisor during this last years work.

My sincere gratitude also goes to professor Jan Myrheim for patiently explaining and answering all my questions in anything from quantum mechanics to theoretical astrophysics.

I am also very grateful to professors Ramon Lapiedra and Pilar Hernandez at the Universidad de Valencia for being so helpful and patient with me while overcoming the language barrier.

My time spent at the NTNU would not have been the same without my friends, and special thanks goes to Haakon Bakka and Peder Galteland for many interesting discussions, leading to both good and some not so good ideas.

Last but not least I want to thank my mother for teaching me the simple, yet valuable lesson that hard work pays off.

Sammendrag

Målet med den følgende oppgaven var å bli kjent med termisk feltteori og mulige astrofysiske anvendelser. Hovedmålet var å finne en tilstandslikning for en degenerert Fermi-gass bestående av masseløse kvarker, ved endelig temperatur og tetthet, og bruke den til forutsi fysiske egenskaper til hypotetiske kvarkstjerner. Tilstandslikningen for sterkt vekselvirkende materie brukes dermed som en forbindelse mellom mangepartikkel- og astrofysikk.

Arbeidet begynner med statistisk mekanikk, og vi har arbeidet oss frem til kvantefeltteori ved endelig temperatur ved å studere likheter mellom partisjonsfunksjonen og veiintegralet.

Den første feltteorien studert ved endelig temperatur i denne oppgaven, er den som beskriver et skalart felt med en firepukts-vekselvirkning. Vi har studert nye effekter som følger av termiske omgivelser, for eksempel termisk masse, tilstandslikningen har blitt utledet til orden g^5 ved endelig temperatur, og gyldigheten til den perturbative rekka diskutert. Det viste seg at konvensjonell perturbasjonsteori bryter sammen med mindre koplingskonstanten er veldig liten, i overensstemmelse med lærebøker og artikler publisert på området.

Etter å ha diskutert trykket i skalar feltteori, fortsatte vi med kvanteelektrodynamikk. Hovedfokuset lå på å utlede partisjonsfunksjonen ved hjelp av metodene utledet i denne oppgavens første kapitler, og å diskutere vekselvirkninger mellom de ulike partiklene. Vekselvirkninger mellom fotoner og deres omgivelser har blitt studert i detalj, og også her førte det til at en termisk masse ble introdusert. Når en beregner trykket i kvanteelektrodynamikk møter en på ringdiagrammer, som også studeres i denne oppgaven, før tilstandslikningen opp til orden $\alpha^2 \ln \alpha$ presenteres. Siden denne tilstandslikningen også er en perturbativ rekke i koplingen, brukte vi litt tid på å diskutere størrelsen og oppførselen til koplingskonstanten i kvanteelektrodynamikk, ved ulike energiskalaer. Dette var første gangen ideen om en løpende koplingskonstant dukket opp.

Diskusjonen rundt termisk feltteori kulminerer i kapittel 6, som inneholder en innføring i kvantekromodynamikk. Vi gir en kort introduksjon til de nye ladningene og partiklene, men hovedfokuset ligger igjen på å utlede tilstandslikningen og å diskutere den perturbative rekkas gyldighet. Som tidligere var det klart at den perturbative ekspansjonen er sterkt avhengig av koplingens oppførsel, og det viser seg her at kvantekromodynamikk er meget ulik de andre teoriene vi har sett på nettopp på grunn av koplingskonstantens egenskaper. Vi bruker derfor en god del tid på å diskutere den løpende koplingens spesielle oppførsel og implikasjoner.

Med tilstandslikningen for kald, kompakt kvarkmaterie på plass, var neste mål å bruke denne likningen til å gjøre astrofysiske forutsigelser, ved å modellere stjerner bestående av en degenerert Fermi-gass. Først var det dog nødvendig å få en forståelse av generelle relativistiske effekter, i og med at materie under ekstreme forhold er i aller høyeste grad relativistisk. Generell relativitetsteori diskuteres i kapittel 7, hvilket inneholder en kort innføring i tensorer og krumning, samt en kort utledning av Einsteins feltlikninger, før strukturlikningene til de enkleste stjernene utledes. Disse strukturlikningene avhenger kun av tilstandslikningen, og vi har gjort numeriske beregninger for stjerner bestående av kompakt materie med forskjellige tilstandslikninger.

Beregningene ble først gjort for en kompakt stjerne bestående av en ikke-relativistisk Fermi-gass, hvilket resulterte i hvite dvergstjerner. Ved å bruke den samme gassen, men forbedre tilstandslikningen til å gjelde i det relativistiske regimet også, ga beregningene resultater som forventet for nøytronstjerner. Til slutt ble tilstandslikningene for kvarkmaterie brukt. Det viste seg at tilstandslikningen med en konstant kopling beskriver en kvarkgass med ufysiske løsninger. Av nysgjerrighet ble MIT bag-modellen kjapt diskutert på dette punktet, da den forutsier en tilstandslikning som likner veldig på den med en konstant kopling, hvilket akkurat hadde feilet. Interessant nok gav MIT bag-modellen forholdsvis realistiske resultater for kvarkstjerner, så vi gjorde numeriske beregninger for ulike verdier av bag-konstanten, for senere å kunne sammenlikne dem med endelige resultater.

Til slutt ble tilstandslikningen for kompakt kvarkmaterie med en løpende koplingskonstant brukt i strukturlikningene, og de oppnådde numeriske resultatene er som forventet for kvarkstjerner.

Angående de numeriske beregningene, brukte jeg først et `Python`-program med en Runge Kutta-rutine jeg hadde implementert selv, for beregningene på hvite dverger, nøytronstjerner og de enkleste kvarkstjernene. Resultatene fra disse beregningene ble sammenliknet med resultater fra innebygde løsningsrutiner i `Mathematica`, og for de enkleste stjernene var resultatene fra min egen kode veldig gode. Likevel er de numeriske pakkene i `Mathematica` veldig mye mer nøyaktige og gjennomførte enn noe jeg kunne håpe på å programmere selv i løpet av et år, og for tilstandslikningen med løpende kopling, har jeg valgt å inkludere kun resultatene fra `Mathematica`. All koden er å finne i appendikset.

Siden vi ikke kan være sikre på at kvarkstjerner faktisk eksisterer, er det så klart umulig å si hvorvidt beskrivelsen av

kvarkmaterie eller de numeriske resultatene presentert i denne oppgaven stemmer overens med virkeligheten. Likevel er disse resultatene i overensstemmelse med det som finnes i litteraturen i dag, og som diskutert i detalj i kapittel 9, er det slettes ikke umulig at vi er bare et lite stykke unna de observasjonene som trengs for å bekrefte kvarkstjerners eksistens. Skulle disse stjernene faktisk observeres, ville dette bekrefte at kvarkmaterie kan finnes, og det ville gi oss ny informasjon om hvordan vi tilstandslikningen for kvarkmaterie må modifiseres.

Contents

Nomenclature

QED	Quantum electrodynamics
QCD	Quantum chromodynamics
TOV	Tolman Oppenheimer Volkoff
EoS	Equation of state
IR	Infrared

List of Figures

Notation and conventions

Throughout this thesis the following notation and conventions are used.

- In Minkowski space the metric is $\eta_{\mu\nu} = \mathrm{diag}(1,-1,-1,-1)$.
- In Euclidean space the metric is $\delta_{\mu\nu}$.
- Unless otherwise stated, natural units $\hbar = c = k_b = 1$ are used.
  This means that mass and temperature are measured in (eV), and time and distance are measured in $(\mathrm{eV})^{-1}$.
- The $n \times n$ unit matrix is denoted by I_n.
- The Einstein summation convention is used, meaning that repeated indices are summed over unless stated otherwise. Greek indices are used for four-vectors in space-time and roman indices otherwise.
- Differentiation with respect to the μ coordinate is denoted by ∂_μ.
- Feynman slash-notation is defined as
$$\not{\partial} \equiv \gamma^\mu \partial_\mu . \tag{1}$$
- The field $\bar{\psi}$ is defined as
$$\bar{\psi} \equiv \psi^\dagger \gamma^0 . \tag{2}$$
- The spatial integral evaluated in d dimensions is
$$\int_p \equiv \left(\frac{e^{\gamma_E} \Lambda_{\overline{\mathrm{MS}}}^2}{4\pi} \right)^\varepsilon \int \frac{d^d p}{(2\pi)^d} . \tag{3}$$
- The shorthand notations for the sum-integrals for bosons and fermions are, respectively
$$\begin{aligned} \sum\!\!\!\!\!\!\int_P &\equiv \left(\frac{e^{\gamma_E} \Lambda_{\overline{\mathrm{MS}}}^2}{4\pi} \right)^\varepsilon T \sum_{p_0 = 2\pi n T} \int \frac{d^{3-2\varepsilon} p}{(2\pi)^{3-2\varepsilon}} \\ \sum\!\!\!\!\!\!\int_{\{P\}} &\equiv \left(\frac{e^{\gamma_E} \Lambda_{\overline{\mathrm{MS}}}^2}{4\pi} \right)^\varepsilon T \sum_{p_0 = (2n+1)\pi T} \int \frac{d^{3-2\varepsilon} p}{(2\pi)^{3-2\varepsilon}} . \end{aligned} \tag{4}$$
- As renormalization is accomplished by the minimal subtraction of poles in ε, the $\Lambda_{\overline{\mathrm{MS}}}$ used in this thesis is the renormalization scale in the $\overline{\mathrm{MS}}$ scheme.

Chapter 1

Introduction

Traditionally, quantum field theory is formalized at zero temperature, and though its theoretical predictions match experimental data extremely well, our real world is certainly not of zero temperature. It is natural to wonder when and to what extent effects arising due to nonzero temperature are relevant, and what new phenomena could arise due to a thermal background.

Non-relativistic field theory at finite temperature and density was invented in the late 1950s for the theoretical description of condensed matter and nuclear matter under laboratory conditions. Relativistic field theory at finite temperature was first studied some time later, the main motivation at the time being describing the phase transition in the electroweak theory, which takes place at a temperature of order 200 MeV. This is also highly relevant for understanding the physics of the early universe, around the inflationatory phase.

Since those early periods, the universe has expanded and cooled to the state in which we find it today. Though this is lucky for our existence, it also means that it is not possible to probe and study the states of matter present at those times.

Moving from the very hot and dense to the cold and dense parts of the universe, there are objects we may very well observe. These are interstellar objects containing matter under extreme pressure, and we can learn very much from them; the stellar remnants.

1.1 A star's life and death

Stars are born in huge interstellar clouds of gas and dust, known as nebulae. The nebulae, extended over several light-years, are not entirely homogeneous, so at some point the denser regions begin to contract and become bound by their own gravitational pull. This slow process first forms a protostar, with a diameter spanning hundred millions of kilometers. As the young star contracts further, the central temperature increases, and nuclear fusion commences. The nuclear processes in the star's center give rise to a radiational pressure outwards, which at some point equalizes the gravitational pressure, so that the star finds an equilibrium state and stabilizes.

A stable star spends almost its entire lifetime fusing light nuclei into heavier ones. What happens when the period of nuclear fusion reaches its end is believed to be predetermined and dependent only on the star's initial mass. Stars with masses lower than the Chandrasekhar limit, of $1.44 M_\odot$ [3], eventually stop the nuclear processes in their interior, and are kept from collapsing by the electron degeneracy pressure, in accordance with Pauli's exclusion principle.

When a more massive star reaches this stage, not even the degeneracy pressure suffices to keep the core from collapsing, and the protons and electrons constituting the star are pressed together to form neutrons. All this happens in a spectacular cosmic event, called a supernova explosion. Supernovae are extremely luminous, and can briefly outshine entire galaxies. A recording of a supernova explosion can be seen in Fig. 1.1. The explosions often expel most of the dying star's material, driving a shock wave through interstellar space. After the explosion, the stellar remnant is likely to be more massive than the Chandrasekhar limit, and so it forms either a very compact star or a black hole.

Figure 1.1: A supernova explosion in the constellation Leo, recorded March 29, 2003. Courtesy of nasa.gov.

A compact star created in such an event is characterized by a mass $M \sim M_\odot$ and a radius $R \sim$ 15km, and was first proposed by Baade and Zwicky in 1933, just after the discovery of the neutron. As it was first assumed that these stars consist mostly out of neutrons, they are called neutron stars. The density inside this kind of star is so high that if the earth were compressed to this density, it would have a diameter of just under 300 meters.

Most of the neutron stars we observe rotate very fast, which follows from conservation of angular momentum. Such stars are called pulsars, and can have rotation periods as short as a few milliseconds [5]. However, there is a lower limit for the rotation period of a neutron star, since the gravitational force is the only thing keeping the star from being ripped apart. This gravitational force stems only from the matter constituting the star, and if the star were to become too massive, it would collapse into a black hole.

The lower limit of the period is about 0.3 milliseconds for a star just above the Chandrasekhar mass [5]. It follows that a star with rotation period below this limit must be made of material that is self-bound at a high equilibrium density. The most probable candidate is strongly interacting matter. Thus, the discovery of a pulsar with period less than about 1 millisecond would constitute strong evidence that the star is not a neutron star or any star bound only by gravity.

1.2 The QCD phase diagram and creation of quark matter

Neutrons are, as the name indicates, electrically neutral. They consist of mainly empty space, as well as one up and two down quarks. The sum of the quark masses is not nearly enough to account for the measured neutron mass, so the quark's binding energies make the neutron much heavier than the sum of its parts.

Quarks have never been observed alone, and are found only in pairs, or, as in the neutron, in groups of three. This phenomenon is called quark confinement, and is believed to be a property of the theory which describes quarks and gluons - the theory of strong interactions, or quantum chromodynamics [1]. Though, does the fact that a quark has never been observed on its own mean that it is impossible for quarks to be deconfined?

We can imagine taking a lump of neutrons and squeezing it so hard that the wave functions begin to overlap. This could cause the individual neutrons to lose their identity, allowing the quarks to move over distances greater than the average size of a neutron. In other words the quarks would become deconfined, as the matter undergoes a phase transition, from hadronic matter to *dense quark matter*. This process has been depicted in Fig. 1.2.

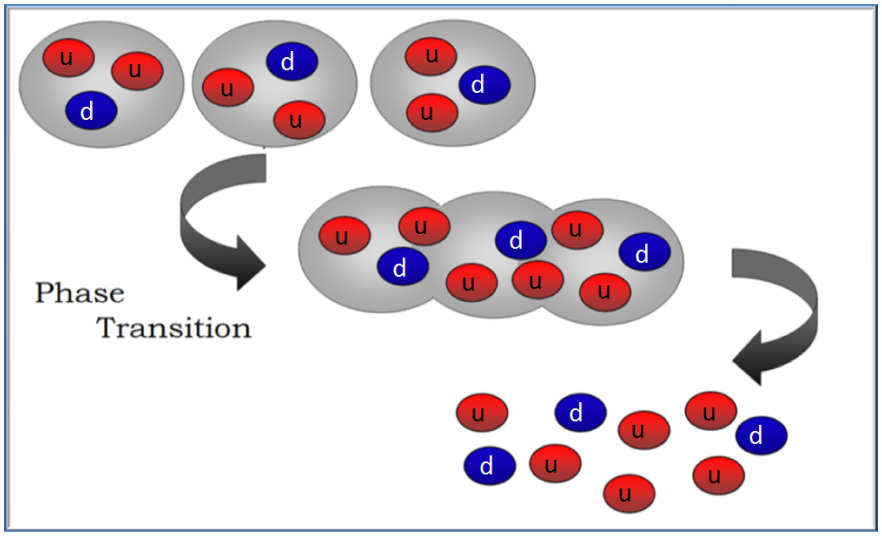

Figure 1.2: Neutrons being pressed together until they overlap, becoming deconfined quark matter.

Under which conditions matter undergoes different phase transitions can be illustrated in a phase diagram, and Fig 1.3 shows qualitatively our current understanding of phase transitions in QCD. The phase transitions are marked in the $\mu_B - T$ plane, where T is the temperature, and μ_B the *baryon chemical potential*. Chemical potentials will be discussed thoroughly later in this thesis, and for understanding the diagram it suffices to say that μ_B is related to the baryon density. The higher the chemical potential, the greater the difference in number density of quarks compared to antiquarks, and $\mu_B = 0$ corresponds to equally many quarks as antiquarks.

The diagram has three distinguished regions: The hadronic phase, the quark-gluon plasma phase and the quark matter phase. The first region is located in the lower left corner of the diagram, i.e. at low temperature and density. This phase represents the conditions of our world and most of the universe, where quarks are confined into hadrons and nuclear matter is stable. A good discussion of the QCD phase diagram can be found in [2].

As mentioned before, quarks are believed to be deconfined at high temperatures and high pressures. At very high temperatures, deconfined matter is expected to be in the quark-gluon plasma phase, represented in the entire upper region of the diagram. Lattice calculations predict the transition temperature at $\mu_b = 0$ to be somewhere in the range $150 \lesssim T_c \lesssim 200$ MeV, corresponding to the conditions of the early universe, as mentioned before.

The last phase is the one which occurs at high chemical potential, but below the critical temperature. In this phase, quarks are deconfined, possibly due to being exposed to great pressure.

It is quite possible that the densities in very compact stars are sufficiently high for exotic forms of matter to be created. In that case, these stars are the perfect laboratories for studying matter which can not yet be created in any laboratory on earth.

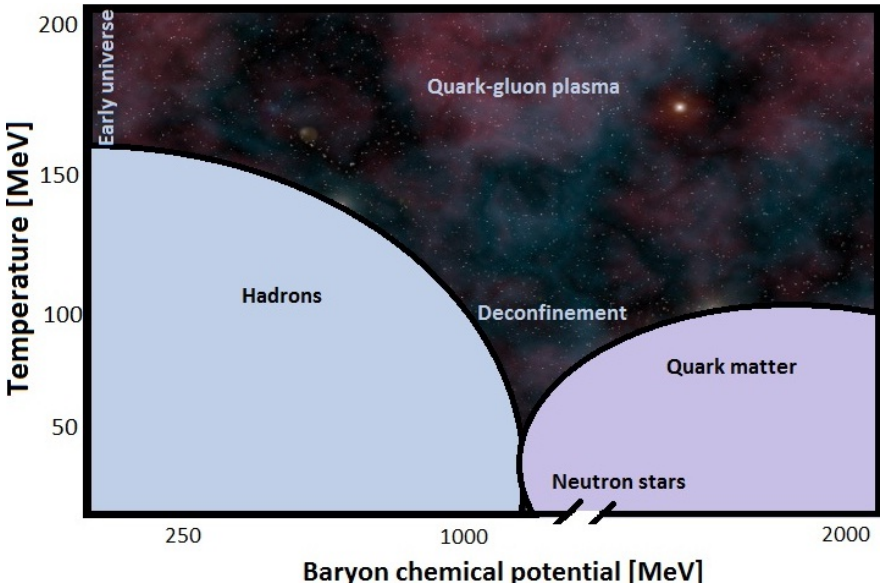

Figure 1.3: The QCD phase diagram for massless quarks.

Chapter 2

Mathematical preliminaries

2.1 Noether's theorem

Noether's theorem states that a continuous symmetry in the Lagrangian gives rise to a conserved current [4]. In infinitesimal form a continuous transformation on the field ϕ can be written as

$$\phi(x) \to \phi'(x) = \phi(x) + \alpha\Delta\phi(x), \tag{2.1}$$

which leads to a change $\Delta\mathcal{L}$ in the Lagrangian density;

$$\begin{aligned}\Delta\mathcal{L} &= \frac{\partial\mathcal{L}}{\partial\phi}\Delta\phi + \left(\frac{\partial\mathcal{L}}{\partial(\partial_\mu\phi)}\right)\Delta(\partial_\mu\phi) \\ &= \frac{\partial\mathcal{L}}{\partial\phi}\Delta\phi + \left(\frac{\partial\mathcal{L}}{\partial(\partial_\mu\phi)}\right)\partial_\mu(\Delta\phi) \\ &= \partial_\mu\left(\frac{\partial\mathcal{L}}{\partial(\partial_\mu\phi)}\Delta\phi\right) + \left[\frac{\partial\mathcal{L}}{\partial\phi} - \partial_\mu\left(\frac{\partial\mathcal{L}}{\partial(\partial_\mu\phi)}\right)\right]\Delta\phi. \end{aligned} \tag{2.2}$$

This is valid under the assumption that the infinitesimal change in the field and the partial derivatives commute. In order for the Lagrangian to be invariant under the transformation, so that $\mathcal{L} \to \mathcal{L}(\phi + \alpha\Delta\phi) = \mathcal{L}(\phi)$, Eq. (2.2) must be zero. The last term in the above equation is the Euler-Lagrange equations of motion

$$\partial_\mu\left(\frac{\partial\mathcal{L}}{\partial(\partial_\mu\phi)}\right) = \frac{\partial\mathcal{L}}{\partial\phi}, \tag{2.3}$$

and defining the Noether current

$$j^\mu(x) \equiv \frac{\partial\mathcal{L}}{\partial(\partial_\mu\phi)}\Delta\phi, \tag{2.4}$$

yields the current conservation equation

$$\partial_\mu j^\mu(x) = 0. \tag{2.5}$$

Integrating the above equation over $\vec{x}$ and writing out the indices yields

$$\int d^3x\left\{\frac{\partial}{\partial t}j^0(\vec{x},t) - \nabla\vec{j}(\vec{x},t)\right\} = 0, \tag{2.6}$$

and applying Gauss' theorem gives

$$\frac{d}{dt}\int d^3x j^0(\vec{x}) = \int_{\partial S}\vec{j}\cdot\vec{n}dS, \tag{2.7}$$

where the term on the right-hand-side is just a surface term, which will vanish in the limit $\vec{x} \to \infty$. Defining the total charge

$$Q \equiv \int d^3x j^0(\vec{x},t), \tag{2.8}$$

Eq. (2.6) becomes a conservation law

$$\frac{d}{dt}Q = 0. \tag{2.9}$$

If the action S of a system is left unchanged by a transformation then the solutions to the equations of motion (2.3) will also be unchanged, hence the system has a symmetry. The action is defined as a functional of the field represented as an integral over time along the path of the system, $S \equiv \int Ldt$. Expressed in terms of the Lagrangian density the action is

$$S[\phi] \equiv \int d^4x \mathcal{L}[\phi, \partial_\mu \phi]. \tag{2.10}$$

From the above definition it is clear that even upon adding a total divergence $\partial_\mu \mathcal{J}^\mu$, i.e. a surface term to the Lagrangian $\mathcal{L} \to \mathcal{L} + \partial_\mu \mathcal{J}^\mu$, the action is left invariant. However, this would alter the above derivation slightly, adding a term to the Noether current

$$j^\mu \equiv \frac{\partial \mathcal{L}}{\partial\left(\partial_\mu \phi\right)}\Delta\phi - \mathcal{J}^\mu. \tag{2.11}$$

2.2 U(1) symmetries

A familiar example in quantum field theory where a symmetry gives rise to a conserved current, is a global phase transformation on a complex scalar field Φ. The Lagrangian describing the field is

$$\mathcal{L} = \left(\partial_\mu \Phi\right)^\dagger \left(\partial^\mu \Phi\right) - m^2 \Phi^\dagger \Phi - \lambda \left(\Phi^\dagger \Phi\right)^2, \tag{2.12}$$

and applying the transformation $\Phi \to e^{i\alpha}\Phi$ clearly leaves the Lagrangian invariant, as the $e^{i\alpha}$ will move right past the partial derivatives. Now, in order to derive the conserved Noether current, the transformation can be made infinitesimal, allowing an expansion of the exponential, so that the transformation can be expressed as $\Phi \to (1 + i\alpha)\Phi$ with $\Delta\Phi = i\Phi$, and its complex conjugate $\Delta\Phi^\dagger = -i\Phi^\dagger$. Inserted into Noether's theorem this yields the conserved current

$$j^\mu = i\left[\left(\partial^\mu \Phi^\dagger\right)\Phi - \Phi^\dagger\left(\partial^\mu \Phi\right)\right]. \tag{2.13}$$

The $U(1)$ symmetry can be extended to describe electromagnetism by making it local. This is done in generalizing the transformation by allowing the phase α to depend on space-time, so that

$$\begin{aligned} \Phi &\to e^{i\alpha(x)}\Phi, \\ \Phi^\dagger &\to e^{-i\alpha(x)}\Phi^\dagger. \end{aligned} \tag{2.14}$$

When applying this transformation, the Lagrangian will clearly not be invariant any more, since $\alpha(x)$ does not commute with the partial derivatives. However, if the Lagrangian can be modified by introducing a field which for every point in space transforms in a way which absorbs the extra terms produced when commuting ∂_μ and $\alpha(x)$, it can be made invariant. Such a field A_μ is called a gauge field, and will be essential when discussing quantum electrodynamics.

The gauge field can be included by introducing the covariant derivative D_μ defined as

$$D_\mu \equiv \partial_\mu - igA_\mu \tag{2.15}$$

and letting $\partial_\mu \to D_\mu$ in the Lagrangian. The constant g is just a coupling constant which may be chosen freely. Under the global transformation the covariant derivatives transform as follows

$$D_\mu \Phi = \left(\partial_\mu - igA_\mu\right)\Phi \to \left(\partial_\mu - igA'_\mu\right)e^{i\alpha(x)}\Phi \tag{2.16}$$

where the transformed gauge field has been denoted by A'_μ. Since what is needed is a transformation on the form $D_\mu\Phi \to e^{i\alpha(x)}D_\mu\Phi$, it is instructive to separate out a factor $e^{i\alpha(x)}$ from the above expression, yielding

$$D_\mu\Phi \to e^{i\alpha(x)}\left(\partial_\mu\Phi + i(\partial_\mu\alpha(x))\Phi - igA'_\mu\right). \tag{2.17}$$

Demanding that A_μ transform as

$$A_\mu \to A'_\mu = A_\mu + \frac{1}{g}\partial_\mu\alpha(x) \tag{2.18}$$

makes sure that the extra partial derivative of $\alpha(x)$ is absorbed in the transformation, thus resulting in a gauge invariant Lagrangian

$$\mathcal{L} = \left(D_\mu\Phi\right)^\dagger\left(D^\mu\Phi\right) - m^2\Phi^\dagger\Phi - \lambda\left(\Phi^\dagger\Phi\right)^2. \tag{2.19}$$

So far, the Lagrangian contains only static terms in A_μ. A kinetic term for the gauge field which preserves gauge invariance can be introduced using the electromagnetic field strength tensor

$$F_{\mu\nu} \equiv \partial_\mu A_\nu - \partial_\nu A_\mu. \tag{2.20}$$

Since the Lagrangian must be a Lorentz scalar the indices of $F_{\mu\nu}$ must be contracted before including it, and the simplest nonzero contraction is $F_{\mu\nu}F^{\mu\nu}$.

2.3 Grassmann variables

The basic feature of Grassmann variables is that they anticommute, so integrals over Grassmann variables are very convenient for dealing with fermionic fields, being described by anticommutation relations. In this section, the Grassmann algebra is defined and some integrals which will be needed later on are calculated.

A Grassmann variable ξ is defined by the anticommutation relation

$$\{\xi, \xi\} = 0, \tag{2.21}$$

which can be generalized to a set of N variables ξ_i, $i = 1, 2, ...N$,

$$\{\xi_i, \xi_j\} = \{\xi_i, \xi_j^\dagger\} = \{\xi_i^\dagger, \xi_j^\dagger\} = 0. \tag{2.22}$$

In particular, the square of any Grassmann number is zero

$$\xi^2 = 0, \tag{2.23}$$

so that the most general function of a single Grassmann variable is

$$f(\xi) = a + b\,\xi. \tag{2.24}$$

Using the anticommutation rules yields the ordering result

$$\xi_1\chi_1...\xi_N\chi_N = \xi_1...\xi_N\chi_1...\chi_N(-1)^{\frac{1}{2}N(N-1)}, \tag{2.25}$$

which holds in general for any Grassmann variables ξ_i and χ_i. Integration is defined by

$$\begin{aligned}\int d\xi &= 0,\\ \int d\xi\,\xi &= 1,\end{aligned} \tag{2.26}$$

and when performing an integral over multiple Grassmann variables, the following sign convention will be used

$$\int d\xi_1 \int d\xi_2\,\xi_2\,\xi_1 = +1 \tag{2.27}$$

that is, doing the inner integral first.

The Gaussian integral over a complex Grassmann variable is

$$\int d\xi^\dagger d\xi e^{-\xi^\dagger b\xi} = \int d\xi^\dagger d\xi (1 - \xi^\dagger b\xi) \tag{2.28}$$

by Taylor expansion, as all higher orders vanish. Anticommuting ξ and $\xi^\dagger$ yields

$$\int d\xi^\dagger d\xi e^{-\xi^\dagger b\xi} = \int d\xi^\dagger d\xi (1 + \xi\xi^\dagger b) = b. \tag{2.29}$$

Generalizing this to N Grassmann variables yields a Gaussian integral involving an $N \times N$ matrix d

$$\int d\xi_1^\dagger d\xi_1 \cdots d\xi_N^\dagger d\xi_N e^{-\xi^\dagger d\xi}. \tag{2.30}$$

This can be calculated by considering N Grassmann variables and components D_{ij} of the matrix which make the exponent hermitean; $(\xi_i^* D_{ij}\xi_j)^* = \xi_j^* D_{ji}\xi_i$, and expanding the integral, keeping in mind that due to (2.23) only one term will be nonzero

$$\int \prod d\xi_i^* d\xi_i e^{-\xi_i^* D_{ij}\xi_j} = \int d\xi_1^* d\xi_1 \ldots d\xi_N^* d\xi_N \frac{1}{N!} \left(-\xi_{i_1}^* D_{i_1 j_1}\xi_{j_1}\right) \ldots \left(-\xi_{i_N}^* D_{i_N j_N}\xi_{j_N}\right). \tag{2.31}$$

Ordering ξ and $d\xi$ according to Eq. (2.25) now yields

$$\begin{aligned} \int \prod d\xi_i^* d\xi_i e^{-\xi_i^* D_{ij}\xi_j} &= \frac{1}{N!} \int d\xi_1^* \ldots d\xi_N^* \xi_{i_1}^* \ldots \xi_{i_N}^* \int d\xi_1 \ldots d\xi_N \xi_{j_1} \ldots \xi_{j_N} D_{i_1 j_1} \ldots D_{i_N j_n} \\ &= \frac{1}{N!} \varepsilon_{i_1 \ldots i_N} \varepsilon_{j_1 \ldots j_N} D_{i_1 j_1} \ldots D_{i_N j_N} \\ &= \det D, \end{aligned} \tag{2.32}$$

where the ε's come from permuting first $\xi_{i_1}^* \ldots \xi_{i_N}^*$ to $\xi_1^* \ldots \xi_N^*$, then $\xi_{j_1} \ldots \xi_{j_N}$, and the ordering result in Eq. (2.25) has been used twice for the integrals. The result is thus

$$\int d\xi_1^\dagger d\xi_1 \cdots d\xi_N^\dagger d\xi_N e^{-\xi^\dagger d\xi} = \det D \tag{2.33}$$

which will be needed later on.

Chapter 3

Thermal field theory

3.1 Statistical mechanics

The most fundamental quantity in statistical physics is the *partition function*, which is used to describe the statistical properties of a system in thermodynamic equilibrium. It is a function of the temperature T and the microstate energies E_i, and is enough to calculate all the other thermodynamic properties of the system. The partition function is denoted by $\mathcal{Z}$, the letter coming from the German word *Zustandssumme*, meaning "sum over states".

Another very important concept in statistical mechanics is the one of *thermal ensembles*. The canonical ensemble describes a system in contact with a heat reservoir, but where the particle number N and the volume V are fixed. For the canonical ensemble the partition function can be written as a trace over the operator $e^{-\beta H}$, and in the basis of discrete energy eigenstates $|n\rangle$, each with energy E_n, it is

$$\mathcal{Z} = \mathrm{Tr}\, e^{-\beta \hat{H}} = \sum_n \langle n|e^{-\beta \hat{H}}|n\rangle = \sum_n e^{-\beta E_n}, \tag{3.1}$$

where the Hamiltonian $\hat{H}$ is the energy operator, $\beta = \frac{1}{T}$ is the inverse temperature, and the sum over n includes all the possible energy eigenstates of the system. In the continuous case the sum becomes an integral, and the eigenstates $|\phi\rangle$ form a complete set, each with energy E_ϕ. The partition function is thus

$$\mathcal{Z} = \int \mathrm{d}\phi\, \langle \phi|e^{-\beta \hat{H}}|\phi\rangle = \int \mathrm{d}\phi e^{-\beta E_\phi}. \tag{3.2}$$

All of the thermodynamic properties of a system can be generated from $\mathcal{Z}$, for example the pressure is given by

$$\mathcal{P} = \frac{\partial (T \ln \mathcal{Z})}{\partial V}. \tag{3.3}$$

Typically, the width L of a system is much larger than the inverse temperature, i.e. $L \gg \frac{2\pi}{T}$, such that one can use the infinite volume limit to describe the thermodynamics of a finite volume to good approximation. In all calculations performed in this thesis, the infinite volume limit is taken. This simplifies the expression for the pressure to

$$\mathcal{P} = \frac{T \ln \mathcal{Z}}{V}. \tag{3.4}$$

The probability of finding the system in microstate ϕ is just

$$P_\phi = \frac{e^{-\beta E_\phi}}{\mathcal{Z}}, \tag{3.5}$$

so since the probabilities must be sum up to 1, the partition function plays the role of a normalizing constant, encoding how the probabilities are partitioned among the different microstates.

When treating a system of fields in a medium, one must turn to the *grand canonical ensemble*, where the system exchanges both energy and particles with the reservoir at temperature T. Its partition function is thus is characterized by both the temperature of the system and the chemical potentials μ_i. The latter makes it possible to treat the number of particles in a system as an intrinsic property of each quantum eigenstate, and is related to the probability of there being N_i particles of type i in the system. The partition function for the grand canonical ensemble is

$$\mathcal{Z} = \mathrm{Tr}\, e^{-\beta(\hat{H}-\mu_i\hat{N}_i)}. \tag{3.6}$$

In general a chemical potential μ can be associated with any conserved charge in the system. These conserved charges can be particle numbers, as described above, but they can also be electrical charge, isospin and so on. Given a system with a set of independently conserved charges Q_i, the grand canonical partition function is

$$\mathcal{Z} = \mathrm{Tr}\, e^{-\beta(\hat{H}-\mu_i\hat{Q}_i)} \tag{3.7}$$

where the $\hat{Q}_i$ are the charge operators. For several charges to be conserved simultaneously, the operators must be diagonalizable in the same basis, i.e. they must commute. The simplest way to include the conserved quantities in field theory is to add them to the Hamiltonian density, so that

$$\mathcal{H} = \mathcal{H}_0 - \mu_i\rho_i \tag{3.8}$$

where $\mathcal{H}_0$ is the zero-density Hamiltonian.

3.1.1 Chemical potential

The chemical potential can also be included by changing the zeroth component of the gauge field, through the substitution $\partial_0 \to \partial_0 - i\mu$ in the Lagrangian. Since this substitution changes only the temporal component while leaving the spatial components of the gauge field unchanged, it decouples space and time and the theory is no longer Lorentz invariant.

This can also be understood by picturing a free particle: When a particle moves in the vacuum, all frames of intertia are equivalent, with no preferred velocities or directions. Meanwhile, a particle moving through a medium will have its speed measured relative to the medium, different velocities no longer being equivalent. Its position in the medium also matters, as the medium might have different properties in different places.

In addition to explicitly breaking Lorentz invariance, the presence of a chemical potential may additionally break other internal symmetries.

3.2 Functional integration

Like the partition function of statistical mechanics completely describes a system in equilibrium, a system in quantum field theory is fully described by its path integral, an integral over all space-time paths allowed. The path-integral formalism was derived by Feynman in a 1948 paper [17]. In this section the basis of path-integrals is derived using a more modern approach, as used in current textbooks on field theory [7].

If a particle is observed in the state $|\phi_a\rangle$ at a time $t_0 = 0$, then the wave function will after some time t have evolved to $|\phi_b\rangle = \exp\left(-i\int_0^t \hat{H}dt\right)|\phi_a\rangle$. Assuming that the Hamiltonian is time-independent this simplifies the transition amplitude for going from a state $|\phi_a\rangle$ to another state $|\phi_b\rangle$ after a time t to

$$\langle\phi_b|e^{-i\hat{H}t}|\phi_a\rangle. \tag{3.9}$$

When working with problems from statistical mechanics the most interesting cases are the ones where the system returns to its initial state, corresponding to the transition amplitude $\langle\phi_a|e^{-iHt}|\phi_a\rangle$. The completeness and orthogonality relations for the field ϕ and the momentum density π are

$$\begin{aligned} \int d\phi(x)|\phi\rangle\langle\phi| &= 1 \\ \langle\phi_a|\phi_b\rangle &= \prod_x \delta(\phi_a(\vec{x}) - \phi_b(\vec{x})) \end{aligned} \tag{3.10}$$

$$\int \frac{1}{2\pi} d\pi(x) |\pi\rangle\langle\pi| = 1$$
$$\langle \pi_a | \pi_b \rangle = \prod_x \delta(\pi_a(\vec{x}) - \pi_b(\vec{x})) \tag{3.11}$$

and the overlap is

$$\langle \phi | \pi \rangle = \exp\left(i \int d^3x \, \pi(\vec{x}) \phi(\vec{x}) \right). \tag{3.12}$$

The probability amplitude is governed by the time evolution from the initial state via all intermediate states at the time intervals Δt, and splitting time interval $(0,t)$ into N equal steps of size $\Delta t = \frac{t}{N}$ yields

$$\langle \phi_a | e^{-i\hat{H}t} | \phi_a \rangle = \langle \phi_a | \underbrace{e^{-i\hat{H}\Delta t} \times \cdots \times e^{-i\hat{H}\Delta t}}_{N \text{ times}} | \phi_a \rangle. \tag{3.13}$$

Next, a complete set of states is inserted after each time interval, alternating between the one in (3.10) and (3.11);

$$\begin{aligned} \langle \phi_a | e^{-i\beta\hat{H}} | \phi_a \rangle = \lim_{N\to\infty} \int \left(\prod_{i=1}^{N} \frac{1}{2\pi} d\pi_i d\phi_i \right) & \langle \phi_a | \pi_N \rangle \langle \pi_N | e^{-i\hat{H}\Delta t} | \phi_N \rangle \\ & \times \langle \phi_N | \pi_{N-1} \rangle \langle \pi_{N-i} | e^{-i\hat{H}\Delta t} | \phi_{N-i} \rangle \cdots \\ & \times \langle \phi_2 | \pi_1 \rangle \langle \pi_1 | e^{-i\hat{H}\Delta t} | \phi_1 \rangle \langle \phi_1 | \phi_a \rangle, \end{aligned} \tag{3.14}$$

where every second term can be rewritten using the overlap, always appearing on the form

$$\langle \phi_{i+1} | \pi_i \rangle = \exp\left(i \int d^3x \, \pi_i(\vec{x}) \phi_{i+1}(\vec{x}) \right), \tag{3.15}$$

and the last term is just

$$\langle \phi_i | \phi_a \rangle = \delta(\phi_1 - \phi_a). \tag{3.16}$$

The terms containing the exponential can be expanded, since the time intervals Δt can be arbitrary small, and keeping terms up to first order yields

$$\langle \pi_i | e^{-i\hat{H}_i \Delta t} | \phi_i \rangle \approx \langle \pi_i | (1 - i\hat{H}_i \Delta t) | \phi_i \rangle. \tag{3.17}$$

In Eq. (3.14), H_i always appears between two states with the same index i, so the Hamiltonian is always evaluated at the same point in time. Proceeding by writing

$$\begin{aligned} \langle \pi_i | (1 - i\hat{H}_i \Delta t) | \phi_i \rangle &= \langle \pi_i | \phi_i \rangle (1 - iH_i \Delta t) \\ &= (1 - iH_i \Delta t) \exp\left(-i \int d^3x \, \pi_i(\vec{x}) \phi_i(\vec{x}) \right), \end{aligned} \tag{3.18}$$

before changing the expansion to first order back into an exponential thus changes it into the following

$$\langle \pi_i | e^{-i\hat{H}_i \Delta t} | \phi_i \rangle \approx \exp(-iH_i \Delta t) \exp\left(-i \int d^3x \, \pi_i(\vec{x}) \phi_i(\vec{x}) \right). \tag{3.19}$$

Finally, using that the Hamiltonian H is just the integral of the Hamiltonian density $\mathcal{H}$

$$H_i = \int d^3x \, \mathcal{H}(\pi_i(\vec{x}), \phi_i(\vec{x})), \tag{3.20}$$

the transition amplitude can be written as

$$\begin{aligned} \langle \phi_a | e^{-i\hat{H}t} | \phi_a \rangle = \frac{1}{2\pi} \lim_{N\to\infty} \prod_{i=1}^{N} \int & d\pi_i d\phi_i \delta(\phi_1 - \phi_a) \\ & \times \exp\left(-i\Delta t \sum_{j=1}^{N} \int d^3x \left[\mathcal{H}(\pi_j, \phi_j) - \pi_j (\phi_{j+1} - \phi_j)/\Delta t \right] \right). \end{aligned} \tag{3.21}$$

Taking the continuum limit in time, so that

$$\lim_{N\to\infty} i\Delta t \sum_{j=1}^{N}\left(\pi_j \frac{\phi_{j+1}-\phi_j}{\Delta t} - \mathcal{H}(\pi_j,\phi_j)\right) \to i\int_0^{t_f} dt\left(\pi(x)\frac{\partial\phi(x)}{\partial t} - \mathcal{H}(\pi(x),\phi(x))\right), \tag{3.22}$$

and using a more compact notation where functional integration is denoted by $\mathcal{D}$, the transition amplitude can be expressed as

$$\langle\phi_a|e^{-iHt}|\phi_a\rangle = \int \mathcal{D}\pi \int \mathcal{D}\phi \exp\left\{i\int_0^{t_f} dt \int d^3x\left(\pi(x)\frac{\partial\phi(x)}{\partial t} - \mathcal{H}(\pi(x),\phi(x))\right)\right\}. \tag{3.23}$$

The the integration runs over all possible momenta $\pi(x)$, while the field $\phi(x)$ is restricted by boundary conditions, starting at $t = 0$ and ending at a final time $t = t_f$.
As the Hamiltonian density of a system is given by

$$\mathcal{H} = \pi(x)\frac{\partial\phi(x)}{\partial t} - \mathcal{L}, \tag{3.24}$$

the exponential can be expressed in terms of the action, Eq. (2.10) as follows

$$\int \mathcal{D}\phi e^{i\int \mathcal{L}d^4x} \equiv \int \mathcal{D}\phi e^{iS[\phi]}. \tag{3.25}$$

This is the so-called path integral, and here a striking simplicity reveals itself; the transition amplitude for a system is simply the sum over all possible paths it may take in going from its initial to its final state.

3.2.1 The partition function revisited

There is a remarkable similarity between the partition function in statistical mechanics and the path integral in quantum mechanics. Comparing Eq. (3.2) to Eq. (3.25) indicates that the time interval $[0,t]$ in the transition amplitude (3.23) takes the role of β in the partition function. In fact, by making the substitution $t \to -i\tau$ and integrating τ from 0 to β, the latter can be interpreted as a path-integral representation of $\mathcal{Z}$. This substitution is called a *Wick rotation*, and rotates the integration in the complex plane by 90°, see Fig. 3.1. The Wick rotation is a transformation from Minkowski to Euclidean space, so the transformed action is called the Euclidean action S_E, defined as

$$S_E \equiv \int_0^\beta d\tau \int d^3x \mathcal{L}_E, \tag{3.26}$$

with the Euclidean Lagrangian

$$\mathcal{L}_E \equiv -\mathcal{L}(t = -i\tau). \tag{3.27}$$

Thus for a scalar field the partition function is

$$\mathcal{Z} = \int_{\phi(\vec{x},0)=\phi(\vec{x},\beta)} \mathcal{D}\phi\, e^{-S_E[\phi]}, \tag{3.28}$$

the integration running over all fields $\phi(\vec{x},\tau)$ that are periodic in imaginary time with period β

$$\phi(\vec{x},0) = \phi(\vec{x},\beta). \tag{3.29}$$

Apparently, it is very useful to think of the temperature as imaginary time, and the origin of the correspondence between the two in principle very distinct arguments is an interesting question. It might be a mere coincidence that the Boltzmann distribution factor $e^{\beta H}$ from statistical mechanics and the quantum mechanical evolution operator e^{-iHt} are related among each other by analytical continuation, but there might also be some deeper reasons yet to be understood.

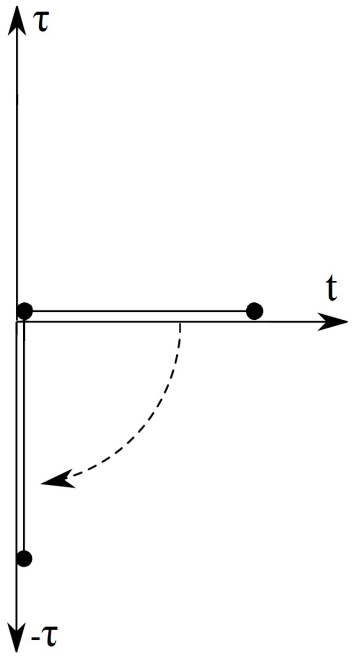

Figure 3.1: The Wick rotation in the complex time plane.

3.3 Periodicity of fields

In this section the Green's function for the Dirac field is used to demonstrate that Dirac fields must be antiperiodic in imaginary time.

The thermal Green's function for the Dirac field is

$$G_\beta(\vec{x}_1,\vec{x}_2;\tau_1,\tau_2) \equiv \frac{1}{Z}\mathrm{Tr}\Big(e^{-\beta\hat{H}}\,T\left[\psi(\vec{x}_1,\tau_1)\psi(\vec{x}_2,\tau_2)\right]\Big), \tag{3.30}$$

where T is the imaginary time ordering operator, which acts as

$$T\left[\psi(\vec{x}_1,\tau_1)\psi(\vec{x}_2,\tau_2)\right] = \begin{cases} \psi(\vec{x}_1,\tau_1)\psi(\vec{x}_2,\tau_2) & \tau_1 > \tau_2 \\ -\psi(\vec{x}_1,\tau_1)\psi(\vec{x}_2,\tau_2) & \tau_1 < \tau_2 \end{cases} \tag{3.31}$$

and the minus sign arises for fermions due to the anticommutativity of the fields. Evaluating the Green's function for

two fields at different times and positions, with $0 < \tau < \beta$, yields

$$\begin{aligned} G_\beta(\vec{x},\vec{y};\tau,0) &= \frac{1}{Z}\mathrm{Tr}\Big(e^{-\beta\hat{H}}\,T\left[\psi(\vec{x},\tau)\psi(\vec{y},0)\right]\Big) \\ &= \frac{1}{Z}\mathrm{Tr}\Big(e^{-\beta\hat{H}}\,\psi(\vec{x},\tau)\psi(\vec{y},0)\Big) \\ &= \frac{1}{Z}\mathrm{Tr}\Big(\psi(\vec{y},0)e^{-\beta\hat{H}}\,\psi(\vec{x},\tau)\Big) \\ &= \frac{1}{Z}\mathrm{Tr}\Big(e^{-\beta\hat{H}}e^{\beta\hat{H}}\psi(\vec{y},0)e^{-\beta\hat{H}}\,\psi(\vec{x},\tau)\Big) \\ &= \frac{1}{Z}\mathrm{Tr}\Big(e^{-\beta\hat{H}}\,\psi(\vec{y},\beta)\psi(\vec{x},\tau)\Big) \\ &= -\frac{1}{Z}\mathrm{Tr}\Big(e^{-\beta\hat{H}}\,T\left[\psi(\vec{x},\tau)\psi(\vec{y},\beta)\right]\Big) = -G_\beta(\vec{x},\vec{y};\tau,\beta). \end{aligned} \tag{3.32}$$

Having used the cyclic properties of the trace operator, inserted the unit operator $1 = e^{-\beta\hat{H}}e^{\beta\hat{H}}$, and used the time evolution of the state ψ:

$$e^{\beta\hat{H}}\psi(\vec{y},0)e^{-\beta\hat{H}} = \psi(\vec{y},\beta). \tag{3.33}$$

Since the Green's function changes sign after one period of β, this means that the Dirac fields must be antiperiodic in imaginary time,

$$\psi(\vec{x},0) = -\psi(\vec{x},\beta). \tag{3.34}$$

The same argument can be used to show that the thermal Green's function is periodic for bosonic fields, yielding the rule

$$G_\beta(\tau,0) = \pm G_\beta(\tau,\beta) \tag{3.35}$$

for bosonic and fermionic fields, respectively. The spatial coordinates have not been written out, since they are not relevant for the further discussion. The thermal Green's functions have the following Fourier transforms

$$\begin{aligned} G_\beta(\tau) &= \frac{1}{\beta}\sum_n e^{-i\omega_n'\tau}G_\beta(\omega_n'), \\ G_\beta(\omega_n') &= \frac{1}{2}\int_{-\beta}^{\beta} d\tau e^{i\omega_n'\tau}G_\beta(\tau), \end{aligned} \tag{3.36}$$

where $\omega_n' = \frac{\pi n'}{\beta}$ for $n' = 0, \pm1, \pm2, \ldots$. Eq. (3.36) can be rewritten by splitting up the integration interval and using Eq. (3.35) as follows

$$\begin{aligned} G_\beta(\omega_n') &= \frac{1}{2}\int_{-\beta}^{0} d\tau e^{i\omega_n'\tau}G_\beta(\tau) + \frac{1}{2}\int_0^{\beta} d\tau e^{i\omega_n'\tau}G_\beta(\tau) \\ &= \pm\frac{1}{2}\int_{-\beta}^{0} d\tau e^{i\omega_n'\tau}G_\beta(\tau+\beta) + \frac{1}{2}\int_0^{\beta} d\tau e^{i\omega_n'\tau}G_\beta(\tau) \\ &= \frac{1}{2}\left(1 \pm e^{-i\omega_n'\beta}\right)\int_0^{\beta} e^{i\omega_n'\tau}G_\beta(\tau) \\ &= \frac{1}{2}\left(1 \pm e^{-i\omega_n' n'}\right)\int_0^{\beta} e^{i\omega_n'\tau}G_\beta(\tau), \end{aligned} \tag{3.37}$$

where the upper sign is for bosonic and the lower sign for fermionic fields. When n' is odd, $G_\beta(\omega_n')$ vanishes for bosonic fields, and when n' is even, $G_\beta(\omega_n')$ vanishes for fermionic fields. Thus for nonzero values of $G_\beta(\omega_n')$, even

numbers of n' are needed for bosonic fields, and odd ones for fermionic fields, yielding the following periodicity rules

$$\omega_n = \begin{cases} \frac{2n\pi}{\beta} & \text{bosonic fields} \\ \frac{(2n+1)\pi}{\beta} & \text{fermionic fields} \end{cases} \tag{3.38}$$

with $n \in Z$. The frequencies ω_n are called Matsubara frequencies, and are essential in the imaginary time formalism.

3.4 Fermion gas

In this section, the partition function for free Dirac fermions is derived. It will be used to find the pressure for the fermion gas, constituting the equation of state. The Lagrangian density for the free fermion gas is

$$\mathcal{L} = \bar{\psi}(i\partial\!\!\!/ - m)\psi, \tag{3.39}$$

and using the Euler-Lagrange equations (2.3) for the field ψ yields its equation of motion, which is just the Dirac equation

$$(i\gamma^\mu \partial_\mu - m)\psi(x) = 0. \tag{3.40}$$

The corresponding Hamiltonian density $\mathcal{H}$ is

$$\mathcal{H} = \pi\partial_0\psi + \partial_0\bar{\psi}\bar{\pi} - \mathcal{L} = \bar{\psi}\left(i\gamma^j\partial_i + m\right)\psi, \tag{3.41}$$

having inserted the conjugate momenta

$$\pi = \frac{\partial\mathcal{L}}{\partial(\partial_0\psi)} = i\psi^\dagger, \qquad \bar{\pi} = \frac{\partial\mathcal{L}}{\partial(\partial_0\bar{\psi})} = 0. \tag{3.42}$$

It is worth noting that ψ and $\psi^\dagger$ must be treated independently in the Hamiltonian formalism. In order to study the thermodynamics of the fermion gas, the Hamiltonian must now be redefined according to Eq. (3.8), so the zeroth component of the current density is needed. It can be derived using the fact that the Lagrangian has a global $U(1)$ symmetry, corresponding to the operations $\psi \to \psi e^{-i\alpha}$ and $\psi^\dagger \to \psi^\dagger e^{i\alpha}$. Performing this transformation and allowing α to depend on x, the new Lagrangian density becomes

$$\begin{aligned} \mathcal{L} \to \mathcal{L}' &= \bar{\psi}e^{i\alpha(x)}\left(i\partial\!\!\!/ - m\right)\psi e^{-i\alpha(x)} \\ &= \bar{\psi}(i\partial\!\!\!/ - m)\psi + \bar{\psi}\partial\!\!\!/\alpha(x)\psi \\ &= \mathcal{L} + \bar{\psi}\partial\!\!\!/\alpha(x)\psi. \end{aligned} \tag{3.43}$$

The Lagrangian density is left unchanged and the original theory recovered if α is constant, that is if the symmetry is global. According to Noether's theorem this symmetry of the Lagrangian will give rise to a conserved current, here found by solving the equation of motion for α

$$\partial_\mu \frac{\partial\mathcal{L}'}{\partial(\partial^\mu\alpha)} = \frac{\partial\mathcal{L}'}{\partial\alpha}. \tag{3.44}$$

The solution is

$$\partial_\mu\left(\bar{\psi}\gamma^\mu\psi\right) = 0, \tag{3.45}$$

so the conserved current is $j^\mu = \bar{\psi}\gamma^\mu\psi$. Inserting the zeroth component, $j^0 = \bar{\psi}\gamma^0\psi$, yields the new Hamiltonian density

$$\begin{aligned} \mathcal{H} \to &\bar{\psi}(i\gamma^j\partial_i + m)\psi - \mu\rho \\ &= \bar{\psi}(i\gamma^j\partial_i + m - \mu\gamma^0)\psi, \end{aligned} \tag{3.46}$$

corresponding to the new Lagrangian

$$\mathcal{L} = \bar{\psi}(i\gamma^\mu \partial_\mu - m + \mu\gamma^0)\psi. \tag{3.47}$$

The Euclidean Lagrangian is now

$$\mathcal{L}_E = -\mathcal{L}(t = -i\tau) = \bar{\psi}\left(\gamma^0\partial_\tau + i\gamma^j\partial_i + m - \mu\gamma^0\right)\psi. \tag{3.48}$$

Using the definition of the Euclidean action in Eq. (3.26) and inserting the above expression into Eq. (3.28) yields the partition function for a free Fermi gas

$$\mathcal{Z} = \int \mathcal{D}\psi^\dagger \mathcal{D}\psi \exp\left\{\int_0^\beta d\tau \int d^3x\, \bar{\psi}\left(\gamma^0\partial_\tau + i\gamma^j\partial_i + m - \mu\gamma^0\right)\psi\right\}. \tag{3.49}$$

Since ψ and $\bar{\psi}$ are independent fields, they must be integrated independently. Due to the antiperiodicity of the fields in Eq. (3.49), it is more convenient to work in momentum space than in position space, and the fields are Fourier transformed as follows

$$\psi(\vec{x},\tau) = \sqrt{\frac{\beta}{V}} \sum_n \sum_{\vec{p}} e^{i(\vec{x}\cdot\vec{p} + \omega_n\tau)} \tilde{\psi}(\vec{p}), \tag{3.50}$$

where the frequencies ω_n are the Matsubara frequencies in Eq. (3.38). Furthermore, the Pauli exclusion principle and spin statistics state that the fields must anticommute. They are therefore treated as Grassmann variables, so the partition function on the form (3.49) resembles a Gaussian Grassmann integral, Eq. (2.30). The action in the exponent of $\mathcal{Z}$ can be written more compactly as

$$\begin{aligned} S &= \sum_n \sum_{\vec{p}} \int_0^\beta \mathrm{d}\tau\, \bar{\psi}\left(\gamma^0\partial_\tau + i\gamma^j\partial_i + m - \mu\gamma^0\right)\psi \\ &= \sum_n \sum_{\vec{p}} \bar{\psi} \underbrace{\left(\gamma^0(i\omega_n) - \vec{\gamma}\cdot\vec{p} + m - \mu\gamma^0\right)}_{D} \psi, \end{aligned} \tag{3.51}$$

having inserted the Fourier expansion (3.50) of the field, integrated over τ and performed the differentiation with respect to τ so that $\partial_\tau\psi = i\omega_n\psi$, and with respect to position so that $\nabla\psi = ip\psi$. Keeping in mind that ψ is a four-component spinor and D is a 4×4 matrix, the partition function is rewritten as

$$\mathcal{Z} = \int \mathcal{D}\bar{\psi}\mathcal{D}\psi\, e^{-\bar{\psi}D\psi}, \tag{3.52}$$

and since it is a Gaussian integral in Grassmann variables, Eq. (2.33) yields

$$\mathcal{Z} = \det D. \tag{3.53}$$

The pressure of the fermion gas depends on the logarithm of $\mathcal{Z}$. The logarithm is related to the determinant of a matrix through the trace operation, Eq. (A.7):

$$\ln\mathcal{Z} = \mathrm{Tr}\ln D. \tag{3.54}$$

Written out explicitly, the matrix D is

$$D = \begin{pmatrix} i\omega_n - \mu & 0 \\ 0 & -i\omega_n + \mu \end{pmatrix} + \begin{pmatrix} 0 & -\vec{p}\cdot\vec{\sigma} \\ \vec{p}\cdot\vec{\sigma} & 0 \end{pmatrix} + m\begin{pmatrix} 1 & 0 \\ 0 & 1 \end{pmatrix} \tag{3.55}$$

$$= \begin{pmatrix} i\omega_n - \mu + m & -\vec{p}\cdot\vec{\sigma} \\ \vec{p}\cdot\vec{\sigma} & -i\omega_n + \mu + m \end{pmatrix}, \tag{3.56}$$

where each of the entries are 2×2 matrices. Calculating the determinant, using the operator identity $(\vec{\sigma}\cdot\vec{p})^2 = \vec{p}^2$ derived in App. A, yields

$$\begin{aligned}
\mathrm{Tr}\ln D &= \sum_n\sum_{\vec{p}} \ln\det\left[\gamma^0(i\omega_n) - \vec{\gamma}\cdot\vec{p} + m - \mu\gamma^0\right] \\
&= \sum_n\sum_{\vec{p}} \ln\left[-\omega_n^2 + \mu^2 - \vec{p}^2 - m^2 - 2i\omega_n\mu\right]^2 \\
&= \sum_n\sum_{\vec{p}} \ln\left[\left(i\omega_n + E_p - \mu\right)\left(i\omega_n - E_p - \mu\right)\right]^2 \\
&= 2\sum_n\sum_{\vec{p}} \Big(\ln\left[i\omega_n + E_p - \mu\right] + \ln\left[i\omega_n - E_p - \mu\right]\Big),
\end{aligned} \tag{3.57}$$

where $E_p = \sqrt{\vec{p}^2 + m^2}$. Considering first the sum over n, it is rewritten as

$$\begin{aligned}
2\sum_{n=-\infty}^{n=\infty} \ln\left[i\omega_n + E_p - \mu\right] &= \sum_{n=-\infty}^{n=\infty} \ln\left[i\omega_n + E_p - \mu\right] + \sum_{n=-\infty}^{n=\infty} \ln\left[-i\omega_n + E_p - \mu\right] \\
&= \sum_{n=-\infty}^{n=\infty} \ln\left[\omega_n^2 + (E_p + \mu)^2\right].
\end{aligned} \tag{3.58}$$

The second term can be rewritten in the same manner; $2\sum_n \ln\left[i\omega_n - E_p - \mu\right] = \sum_n \ln\left[\omega_n^2 + (E_p - \mu)^2\right]$. Inserting this and taking the continuum limit, yields the following for the grand canonical ensemble

$$\ln\mathcal{Z} = V\sum_n \int \frac{\mathrm{d}^3p}{(2\pi)^3}\Big\{\ln\left[\omega_n^2 + (E_p - \mu)^2\right] + \ln\left[\omega_n^2 + (E_p + \mu)^2\right]\Big\}. \tag{3.59}$$

The summation and integration are usually abbreviated using the sum-integral sign $\not\int$, with the shorthand notation $\omega_n = -i\omega = -ip_0$. The sum-integral sign is defined in Eq. (4), and includes some prefactors necessary for dimensional regularization.

3.4.1 Matsubara sums

In order to perform the sum over n in Eq. (3.59), the following quantity is defined

$$\sigma_\pm \equiv \sum_{n=-\infty}^{n=\infty} \ln\left(\omega_n^2 + \varepsilon_\pm^2\right), \tag{3.60}$$

essentially when $\varepsilon_\pm \equiv E_p \pm \mu$. Since the calculation is the same for the positive and negative cases, only the one for σ_+ is performed here, and from now in the sign is omitted. The expression for σ is first rewritten as

$$\sigma = \sum_n \ln\left(-(i\omega_n)^2 + \varepsilon^2\right), \tag{3.61}$$

and next differentiated with respect to ε

$$\frac{d\sigma}{d\varepsilon} = -2\varepsilon\sum_n \frac{1}{(i\omega_n^2) - \varepsilon^2}. \tag{3.62}$$

Inserting the hyperbolic tangent and summing over its residues, this can be rewritten as

$$\frac{d\sigma}{d\varepsilon} = -2\varepsilon\sum_n \frac{\beta}{2}\mathrm{Res}\left\{\frac{1}{\omega^2 - \varepsilon^2}\tanh\tfrac{\beta\omega}{2};\ \ \omega = i\omega_n = (2n+1)\pi iT\right\}, \tag{3.63}$$

since the hyperbolic tangent has poles at $\tanh\left(\frac{\pi i}{2} + n\pi i\right)$ with residue 1, which corresponds to poles at

$$\tanh\tfrac{\beta\omega}{2} = \tanh\left(\frac{\pi i}{2} + n\pi i\right) \ \ \Rightarrow\ \ \omega = \frac{(2n+1)\pi i}{\beta}, \tag{3.64}$$

i.e. at $\omega = i\omega_n$, where the residues are $\frac{2}{\beta}$. Using the residue theorem in reverse the sum over residues can now be expressed as an integral over a contour C enclosing the poles of the hyperbolic tangent

$$\frac{d\sigma}{d\varepsilon} = -\frac{\varepsilon\beta}{2\pi i}\oint_C \frac{1}{\omega^2-\varepsilon^2}\tanh\tfrac{\beta\omega}{2}. \tag{3.65}$$

The poles of the hyperbolic tangent lie on the imaginary axis, and the function is bounded everywhere else. The contour can therefore be split into two half circles not enclosing the imaginary axis, see Fig. 3.2. This can be done since the factor $\frac{1}{\omega^2-\varepsilon^2}$ decreases fast, and the two new contours $C^{\pm}$ enclose the two poles of the denominator; $\pm\varepsilon$ respectively. The integral is now

$$\frac{d\sigma}{d\varepsilon} = -\frac{\varepsilon\beta}{2\pi i}\oint_{(C_+\cup C_-)} \frac{1}{\omega^2-\varepsilon^2}\tanh\tfrac{\beta\omega}{2} \tag{3.66}$$

$$= \varepsilon\beta\sum_{\omega=\pm\varepsilon}\mathrm{Res}\left\{\frac{1}{\omega^2-\varepsilon^2}\tanh\tfrac{\beta\omega}{2}\right\}, \tag{3.67}$$

having again used the theorem of residues, but now as mentioned only summing the residues of $\frac{1}{\omega^2-\varepsilon^2}$, as these are the only poles the contours enclose. The sign has switched due to the orientation of the contours. The residues are found by using the following formula valid for all simple poles c

$$\mathrm{Res}(f(z),c) = \lim_{z\to c}(z-c)f(z). \tag{3.68}$$

This yields

$$\begin{aligned}\frac{d\sigma}{d\varepsilon} &= -\varepsilon\beta\left(\frac{1}{2\varepsilon}\tanh\tfrac{\beta\varepsilon}{2} - \frac{1}{2\varepsilon}\tanh\tfrac{\beta(-\varepsilon)}{2}\right)\\ &= \beta\left(\frac{e^{\beta\varepsilon}-1}{e^{\beta\varepsilon}+1}\right)\\ &= \beta\left(1-\frac{2}{1+e^{\beta\varepsilon}}\right),\end{aligned} \tag{3.69}$$

and upon integration this expression is

$$\sigma = \int d\sigma = \beta\int\left(1-\frac{2}{1+e^{\beta\varepsilon}}\right)d\varepsilon \tag{3.70}$$

$$= \beta\varepsilon + 2\ln\left(1+e^{-\beta\varepsilon}\right). \tag{3.71}$$

To sum up, the final result for the Matsubara sum is

$$\sum_n \ln\left(\omega_n^2+\varepsilon_\pm^2\right) = \beta\varepsilon_\pm + 2\ln\left(1+e^{-\beta\varepsilon_\pm}\right). \tag{3.72}$$

The expression for the sum over n can now be inserted into Eq. (3.59), yielding

$$\begin{aligned}\ln\mathcal{Z} &= 2V\int\frac{\mathrm{d}^3p}{(2\pi)^3}\left\{\frac{\beta\varepsilon_+}{2}+\ln\left(1+e^{-\beta\varepsilon_+}\right)+\frac{\beta\varepsilon_-}{2}+\ln\left(1+e^{-\beta\varepsilon_-}\right)\right\}\\ &= 2V\int\frac{\mathrm{d}^3p}{(2\pi)^3}\left\{\beta E_p+\ln\left(1+e^{-\beta(E_p-\mu)}\right)+\ln\left(1+e^{-\beta(E_p+\mu)}\right)\right\}.\end{aligned} \tag{3.73}$$

The pressure of an ideal gas of massless fermions can now be found by using Eq. (3.4), as well as the fact that massless particles have $E_p = \sqrt{p^2+m^2} = p$. Furthermore, the first term in Eq. (3.73) will be omitted, since it is only a shift in

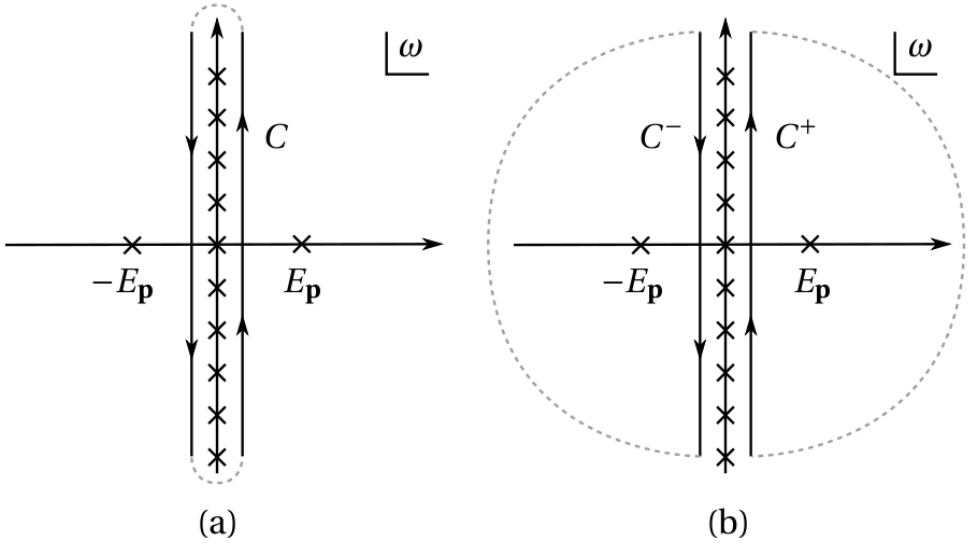

Figure 3.2: (a) The original contour C, enclosing the poles of the hyperbolic tangent. (b) The contours C^+ and C^-, enclosing the poles of $\pm\varepsilon$.

the vacuum energy, which can not be measured experimentally. The pressure is thus

$$\begin{aligned}\mathcal{P} &= 2T\int\frac{\mathrm{d}^3p}{(2\pi)^3}\left\{\ln\left(1+e^{-\beta(p-\mu)}\right)+\ln\left(1+e^{-\beta(p+\mu)}\right)\right\}\\ &= -\frac{2T^4}{\pi^2}\left\{Li_4(-e^{\beta\mu})+Li_4(e^{\beta\mu})\right\}\\ &= \frac{7\pi^2T^4}{180}+\frac{\mu^2T^2}{6}+\frac{\mu^4}{12\pi^2},\end{aligned} \tag{3.74}$$

where the polylogarithmic function Li_n has been Taylor expanded around $\mu = 0$. When doing sums over Matsubara frequencies one often encounters the distribution

$$n_f = \frac{1}{e^{-\beta(E_p\pm\mu)}+1}, \tag{3.75}$$

which is the Fermi-Dirac distribution function for fermions and antifermions respectively.

Chapter 4

Scalar field theory at finite temperature

A well-known [16] problem in high-temperature field theory is the breakdown of the conventional perturbative expansion at some order in the coupling constant. The aim of this chapter is to study this phenomenon by performing a series expansion with weak-coupling approximations for a scalar field, and demonstrate that these series are poorly convergent.

4.1 Free field partition function and pressure

The simplest non-interacting field theory is that of a single massless scalar field, with the following Lagrangian

$$\mathcal{L} = \frac{1}{2}\partial_\mu \phi \partial^\mu \phi, \tag{4.1}$$

where the abbreviation $\phi \equiv \phi(x)$ is used. Going to imaginary time where $x = (\tau, \vec{x})$ with $\tau = it$, and inserting this Lagrangian into Eq. (3.28) yields the following partition function

$$\mathcal{Z} = \int \mathcal{D}\phi \exp\left\{ -\int_0^\beta d\tau \int d^3x \left(\frac{1}{2}(\partial_\tau \phi)^2 + \frac{1}{2}(\nabla \phi)^2 \right) \right\}, \tag{4.2}$$

with the same periodicity constraint as earlier. Just as before it is convenient to insert the field in terms of a Fourier series;

$$\phi(x) = \sqrt{\frac{\beta}{V}} \sum_n \sum_{\vec{p}} e^{i(\vec{x}\cdot\vec{p} + \omega_n \tau)} \phi(\omega_n, \vec{p}), \tag{4.3}$$

where the allowed Matsubara frequencies for a scalar field are the bosonic ones, i.e. $\omega_n = 2\pi n T$. Substituting the Fourier expansion of the field ψ in Eq. (4.3) into the partition function yields

$$\mathcal{Z} = \int \mathcal{D}\phi \exp\left\{ \frac{\beta}{V} \int_0^\beta d\tau \int d^3\vec{x} \sum_{m,\vec{q}} \phi_{m,\vec{q}} e^{i(\vec{x}\cdot\vec{q} + \omega_m \tau)} \sum_{n,\vec{p}} \frac{-\omega_n^2 - \vec{p}^2}{2} \phi_{n,\vec{p}} e^{i(\vec{x}\cdot\vec{p} + \omega_n \tau)} \right\}. \tag{4.4}$$

With the following representations for the δ-functions

$$\begin{aligned} \int_0^\beta d\tau e^{i(\omega_m + \omega_n)\tau} &= \beta \delta(m+n), \\ \int d^3\vec{x} e^{i(\vec{q}+\vec{p})\vec{x}} &= V \delta^{(3)}(\vec{q}+\vec{p}), \end{aligned} \tag{4.5}$$

carrying out the integration over τ and $\vec{x}$, as well as performing the summation over m and $\vec{q}$ yields

$$\begin{aligned}
\mathcal{Z} &= \int \mathcal{D}\phi \exp\left\{-\frac{\beta^2}{2}\sum_{n,\vec{p}}(\omega_n^2+\vec{p}^2)\phi_{-n,-\vec{p}}\phi_{n,\vec{p}}\right\} \\
&= \int \mathcal{D}\phi \exp\left\{-\frac{\beta^2}{2}\sum_{n,\vec{p}}(\omega_n^2+\vec{p}^2)\phi *_{n,\vec{p}}\phi_{n,\vec{p}}\right\} \\
&= \prod_{n,\vec{p}}\int d\phi_n \exp\left\{-\frac{\beta^2}{2}\sum_{n,\vec{p}}(\omega_n^2+\vec{p}^2)\phi_{-n,-\vec{p}}\phi_{n,\vec{p}}\right\} \\
&= N\prod_{n,\vec{p}}\left(\beta^2(\omega_n^2+\vec{p}^2)\right)^{-\frac{1}{2}},
\end{aligned} \tag{4.6}$$

where the integration constant N can be dropped, since it is independent of temperature. The quantity of interest is the logarithm of the partition function, which is

$$\begin{aligned}
\ln\mathcal{Z} &= -\frac{1}{2}\sum_{n,\vec{p}}\ln\left\{\beta^2(\omega_n^2+\vec{p}^2)\right\} \\
&= -\frac{1}{2}\sum_{n,\vec{p}}\ln\left\{((2\pi n)^2+\beta^2\vec{p}^2)\right\} \\
&= -\frac{1}{2}\sum_{n,\vec{p}}\left\{\int_1^{\beta^2\vec{p}^2}\frac{dx^2}{(2\pi n)^2+x^2}+\ln\left\{(2\pi n)^2+1\right\}\right\}.
\end{aligned} \tag{4.7}$$

The last step, which can be verified by evaluating the integral and might thereby seem like going backwards, has been performed in order to rewrite the frequency sum as a contour integral again. The procedure is the same as described in Section 3.4.1, only for bosonic Matsubara frequencies the poles are produced by a hyperbolic cotangent. The frequency sum is thus

$$\begin{aligned}
\sum_n \frac{1}{(2\pi n)^2+x^2} &= \frac{1}{2x}\coth\frac{x}{2} \\
&= \frac{1}{2x}\left(1+\frac{2}{e^x-1}\right),
\end{aligned} \tag{4.8}$$

which after dropping temperature independent terms yields

$$\begin{aligned}
\ln\mathcal{Z} &= -\frac{1}{2}\sum_{\vec{p}}\int_1^{\beta^2\vec{p}^2} dx^2\,\frac{1}{2x}\left(1+\frac{2}{e^x-1}\right) \\
&= \sum_{\vec{p}}\int_1^{\beta\vec{p}} dx\left(-\frac{1}{2}-\frac{2}{e^x-1}\right) \\
&= \sum_{\vec{p}}\left\{-\frac{1}{2}\beta\vec{p}-\ln(1-e^{-\beta\vec{p}})\right\} \\
&= V\int\frac{d^3p}{(2\pi)^3}\left\{-\frac{1}{2}\beta\vec{p}-\ln(1-e^{-\beta\vec{p}})\right\},
\end{aligned} \tag{4.9}$$

having taken the continuum limit in the last line. As before, the first term can be dropped, since it is just the zero-point energy. In the high energy limit the pressure can be obtained from Eq. (3.4) by expanding the logarithm as follows

$$\begin{aligned}\mathcal{P} &= T\int \frac{d^3p}{(2\pi)^3}\left(e^{-\beta\vec{p}}+e^{-2\beta\vec{p}}+e^{-3\beta\vec{p}}+...\right)\\ &= T\int \frac{dp}{2\pi^2}p^2\sum_{n=1}^{\infty}\frac{e^{-n\beta p}}{n}\\ &= \frac{T^4}{\pi^2}\sum_{n=1}^{\infty}\frac{1}{n}\\ &= \frac{\pi^2T^4}{90}.\end{aligned} \tag{4.10}$$

The T^4 behaviour can be expected by dimensional analysis, since T is the only characteristic scale in the free scalar field theory. This result for the pressure is exactly half the pressure from black body radiation, which can be understood from statistical mechanics. The mean energy of a system is proportional to the independent degrees of freedom. Black body radiation consists of photons, which have two transverse propagating modes, while the scalar particles discussed here are spin zero particles, and thus have only one degree of freedom.

4.2 Interactions and Feynman diagrams

The Lagrangian for a scalar field can be modified to include interactions as follows

$$\begin{aligned}\mathcal{L} &= \frac{1}{2}\partial_\mu\phi\partial^\mu\phi-\frac{g^2}{4!}\phi^4\\ &\equiv \mathcal{L}_0+\mathcal{L}_{int},\end{aligned} \tag{4.11}$$

i.e. it consists of a free part and an interaction part. The coupling constant g is dimensionless and assumed to be small, so the contributions from the interacting term will be studied perturbatively in g. This involves series expanding in terms of the coupling, so introducing $\lambda \equiv \frac{g^2}{4!}$ simplifies the process of keeping track of the order. Inserting the above Lagrangian into the partition function, and splitting also the action into a free and an interaction piece yields

$$\mathcal{Z} = \int \mathcal{D}\phi e^{S} = \int \mathcal{D}e^{S_0+S_I} = \int \mathcal{D}\phi e^{S_0}\left(1+S_I+\frac{1}{2}S_I^2+...\right) \tag{4.12}$$

$$\equiv \mathcal{Z}_0+\mathcal{Z}_I. \tag{4.13}$$

Doing the same with the partition function, i.e. breaking it into two separate pieces, its logarithm is

$$\begin{aligned}\ln\mathcal{Z} &= \ln\left(\mathcal{Z}_0+\mathcal{Z}_I\right)\\ &= \ln\int\mathcal{D}\phi\left(e^{S_0}+e^{S_0}\sum_{n=1}^{\infty}\frac{S_I^n}{n!}\right)\\ &= \ln\mathcal{Z}_0+\frac{\mathcal{Z}_I}{\mathcal{Z}_0}-\frac{\mathcal{Z}_I^2}{2\mathcal{Z}_0^2}+...,\end{aligned} \tag{4.14}$$

after expanding the logarithm around the free partition function. The first order perturbation expansion in λ stems only from the term $\frac{\mathcal{Z}_I}{\mathcal{Z}_0}$, and extracting this piece yields

$$\left(\ln\mathcal{Z}\right)_1 = \frac{\int\mathcal{D}\phi S_I e^{S_0}}{\int\mathcal{D}\phi e^{S_0}}, \tag{4.15}$$

where the subscript 1 denotes that this is first order in λ. Substituting the field expansion in Eq. (4.3) into the above expression yields

$$(\ln \mathcal{Z})_1 = \frac{1}{\mathcal{Z}_0} \int \mathcal{D}\phi_{n,\vec{q}} (-\lambda) \int_0^\beta d\tau \int d^3x \frac{\beta^2}{V^2} \sum_{n_1,\ldots,n_4} \sum_{\vec{p}_1,\ldots,\vec{p}_4} \phi_{n_1,\vec{p}_1} \ldots \phi_{n_4,\vec{p}_4}$$
$$\times e^{i(\omega_{n_1}+\ldots+\omega_{n_4})\tau} e^{i(\vec{p}_1+\ldots+\vec{p}_4)\vec{x}} \exp\left\{ -\frac{\beta^2}{2} \sum_{n,\vec{q}} |\phi_{n,\vec{q}}|^2 (\omega_n + \vec{q}^2) \right\}, \tag{4.16}$$

where the denominator $\mathcal{Z}_0$ is

$$\mathcal{Z}_0 = \int \mathcal{D}\phi_{n,\vec{p}} \exp\left\{ -\frac{\beta^2}{2} \sum_{n,\vec{q}} |\phi_{n,\vec{q}}|^2 (\omega_n + \vec{q}^2) \right\}. \tag{4.17}$$

The integrations over τ and $\vec{x}$ give rise to two delta-functions which only allow for three nonzero permutations of the ω_{n_i} and $\vec{p}_{n_i}$. Thus

$$\begin{aligned}(\ln \mathcal{Z})_1 &= 3 \frac{1}{\mathcal{Z}_0} (-\lambda) \beta V \prod_{n,\vec{q}} \int \mathcal{D}\phi_{n,\vec{q}} \frac{\beta^2}{V^2} \sum_{l,m} \sum_{\vec{p},\vec{r}} |\phi_{l,\vec{p}}|^2 |\phi_{m,\vec{r}}|^2 \exp\left\{ -\frac{\beta^2}{2} \phi^2_{n,\vec{q}} (\omega_n + \vec{q}^2) \right\} \\ &= -3\lambda\beta V \left(\frac{V}{\beta} \sum_{n,\vec{p}} \frac{1}{\omega_n^2 + \vec{p}^2} \right)^2 \\ &= -3\lambda\beta V \left(\frac{1}{\beta} \sum_n \int \frac{d^3p}{(2\pi)^3} \frac{1}{\omega_n^2 + \vec{p}^2} \right)^2, \end{aligned} \tag{4.18}$$

after taking the continuum limit in the last line. The term in the bracket is recognized as the free scalar propagator in imaginary time [10]. Thus this last expression contains one vertex factor λ as well as the square of the propagator, and it can be represented in terms of a diagram as follows

$$(\ln \mathcal{Z})_1 = -3\beta V \times$$  . (4.19)

The diagram consists of two lines, closed and connected in a single point, which fits the expression above. This is an example of a *Feynman diagram*, which is a very useful tool and will be explored further in the following. The $\frac{\mathcal{Z}_I}{\mathcal{Z}_0}$ term also gives rise to terms of second order in λ, namely

$$\frac{1}{\mathcal{Z}_0} \int \mathcal{D}e^{S_0} \frac{S_I^2}{2} = \frac{1}{\mathcal{Z}_0} \int \mathcal{D}\phi e^{S_0} \frac{1}{2} \left(-\lambda \int d^4x \phi^4 \right)^2, \tag{4.20}$$

which corresponds to three topologically distinct diagrams:

$$\frac{9}{2}(\beta V)^2$$ $$\times$$ 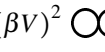 $$+ 36(\beta V)^2$$ 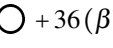 $$+ 12(\beta V)^2$$ 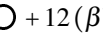 . (4.21)

The prefactors in front of the diagrams are symmetry factors, which embody in how many ways the diagrams can be constructed. All the diagrams are made of two vertices and four lines, and the first one is simply constructed by twice connecting the lines coming out of each vertex, which can be done in 3×3 ways. To obtain the second diagram, two legs from one vertex are connected with two legs from the other, which there are $4 \times \frac{3}{2}$ ways of doing each time. In total there are thus $6 \times 6 \times 2 = 72$ ways to connect the two. The last diagram connects all the lines coming out from one vertex to the other vertex, so the combinatorial factor here is simply $4! = 24$. Including the factor one half from the Taylor expansion thus yields the prefactors in agreement with the above expression. Continuing to find contributions to second order, the term $\frac{\mathcal{Z}_I^2}{2\mathcal{Z}_0^2}$ gives rise to only one part of order λ^2, it is

$$-\frac{1}{2} \left(\frac{\mathcal{D}\phi S_I e^{S_0}}{\mathcal{D}\phi e^{S_0}} \right)^2 = -\frac{1}{2} \left(3\beta V$$ 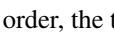 $$\right)^2,$$ (4.22)

so it exactly cancels the first term in Eq. (4.21), and the full second-order part is

$$(\ln \mathcal{Z})_2 = 36(\beta V)^2 \quad + 12(\beta V)^2 \quad . \tag{4.23}$$

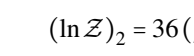

The fact that the disconnected diagrams have cancelled is not a coincidence. It happens at all orders of the perturbation expansion, though it is only demonstrated to second order here.

The Feynman diagrams are very useful for bypassing much of the path-integral formalism and proceeding directly to calculate probability amplitudes. The preceding discussion can be summed up by writing down the following *Feynman rules* for $g^2\phi^4$-theory

- To each vertex assign a factor $-\lambda = -\frac{g^2}{4!}$.
- Assign a factor of $\frac{1}{\beta}\sum_n \int \frac{d^3p}{(2\pi)^3}\Delta(\omega_n, \vec{p})$ to each line.
- Include a factor of $\frac{(2\pi)^3}{\beta}\delta(\omega_{in} - \omega_{out})\delta^{(3)}(\vec{p}_{in} - \vec{p}_{out})$ at each vertex for energy-momentum conservation.
- Determine the overall symmetry factor.
- An overall factor of $\beta(2\pi)^3\delta(0) = \beta V$ is left over.

4.3 Thermal effects

The thermal background produces an effective mass for scalar particles. This can be seen by using the Feynman rules derived in the last section to derive an expression for the self energy of the scalar field. At lowest order it reads the following, including the symmetry factor 4×3 for ways of connecting two of the four legs;

$$\begin{aligned}
\Pi &= -12 \quad \\
&= -12(-\frac{g^2}{4!})\frac{1}{\beta}\sum_n \int \frac{d^3p}{(2\pi)^3}\frac{1}{\omega_n^2 + \vec{p}^2} \\
&= \frac{g^2}{2}\int \frac{d^3p}{(2\pi)^3}\frac{1}{2\vec{p}}\left(1 + \frac{2}{e^{\beta\vec{p}} - 1}\right),
\end{aligned} \tag{4.24}$$

and it consists of one part independent and one dependent on temperature. Dropping the first part as earlier, the second part is interpreted as the *thermal mass generated at one-loop*, and evaluates to the following

$$\begin{aligned}
m_T^2 &= \frac{g^2}{2}\int \frac{d^3p}{(2\pi)^3}\frac{1}{\vec{p}}\frac{2}{e^{\beta\vec{p}} - 1} \\
&= 2g\pi \int \frac{dp}{(2\pi)^3}\frac{p}{e^{\beta p} - 1} \\
&= \frac{g^2T^2}{24}.
\end{aligned} \tag{4.25}$$

Thus the interactions generate an effective thermal mass that increases with temperature, meaning that it is not a perturbation.

When evaluating higher order vacuum diagrams, one encounters divergences in the infrared (IR) regime. These divergences may be counted by using the Euclidean propagators with discrete energies, meaning that only the propagators with zero Matsubara frequencies do not have an IR cutoff of order T. This problem can be solved by using the thermal mass as a cutoff, which is incorporated into the theory by changing the Lagrangian (4.11) to

$$\begin{aligned}
\mathcal{L}_0 &= \frac{1}{2}\partial_\mu\phi\,\partial^\mu\phi - \frac{1}{2}m_T^2\phi^2\delta_{p_0,0}, \\
\mathcal{L}_{int} &= -\frac{g^2}{4!}\phi^4 + \frac{1}{2}m_T^2\phi^2\delta_{p_0,0}.
\end{aligned} \tag{4.26}$$

The physics of the problem at hand do not change when this is done, since the same term is added and subtracted in the Lagrangian. Though, formally, the term with the thermal mass is once treated as an actual mass, and once as a perturbation. Just as the g^2-term in the Lagrangian represents an interaction which couples four fields in one vertex, the m_T^2-term can also be interpreted as an interaction, now coupling two fields. Due to this it is expected that in addition to diagrams consisting of loops and four-point vertices, new diagrams will be encountered. Thus an extra element must be added to the Feynman rules, and this will be discussed when the diagrams arise. The propagator from the modified Lagrangian is [19]

$$\Delta(P) \equiv \frac{1-\delta_{p_0,0}}{P^2} + \frac{\delta_{p_0,0}}{\vec{p}^2 + m_T^2}, \tag{4.27}$$

where the last term is referred to as the dressed propagator.

In the following sections the pressure up to order g^5 is calculated for a system described by the Lagrangian and propagator above, at finite temperature T, and the results from [19] are recovered. We use the compact notation $\Lambda^2 = \frac{e^{\gamma_E}\Lambda_{\overline{\text{MS}}}^2}{4\pi}$.

4.4 Calculation of sum-integrals

In thermal field theory the vacuum diagrams are most easily evaluated using the imaginary-time formalism, and the sum-integral notation will be used in the following calculations. In particular, there are two sum-integrals frequently encountered, namely

$$\sum\!\!\!\!\!\!\int_P \Delta(P)^2 \quad \text{and} \quad \Big(\sum\!\!\!\!\!\!\int_P \Delta(P)\Big)^2. \tag{4.28}$$

The first one, with the propagator inserted reads

$$\begin{aligned}\Big(\sum\!\!\!\!\!\!\int_P \Delta(P)\Big)^2 &= \left(\sum\!\!\!\!\!\!\int_P \frac{1-\delta_{p_0,0}}{P^2} + \sum\!\!\!\!\!\!\int_P \frac{\delta_{p_0,0}}{\vec{p}^2+m_T^2}\right)^2 \\ &= \left(\sum\!\!\!\!\!\!\int_P{}' \frac{1}{P^2} + T\int_p \frac{1}{\vec{p}^2+m_T^2}\right)^2,\end{aligned} \tag{4.29}$$

where the prime on the sum-integral indicates that the zero mode has been excluded, and that the sum should be taken from $n = 1$. In the second term the sum-integral has collapsed to a 3-dimensional integral due to the delta function. When working in dimensional regularization, an integral which does not contain a mass scale, the integral in Eq. (B.10) with $m = 0$, is zero and so

$$\sum\!\!\!\!\!\!\int_P{}' \frac{1}{(P^2)^n} \to \sum\!\!\!\!\!\!\int_P \frac{1}{(P^2)^n} \tag{4.30}$$

by adding the $n = 0$ mode. From now on the primes will be omitted on the sum-integrals where this can be done. A general expression for sum-integrals on the form $\sum\!\!\!\!\!\!\int \frac{1}{(P^2)^n}$ can be found in App. (B.3), and the spatial integral is calculated in App. (B.2). The final result for the integral is

$$\Big(\sum\!\!\!\!\!\!\int_P \Delta(P)\Big)^2 = \frac{T^4}{12^2} + \frac{m_T^2 T^2}{(4\pi)^2} - \frac{m_T T^3}{24\pi}. \tag{4.31}$$

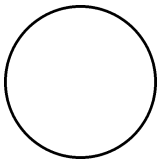

Figure 4.1: Diagram a, the one-loop contribution to the pressure in scalar field theory.

The second sum-integral of interest is

$$\begin{aligned}\sum\!\!\!\!\!\!\int_P \Big(\Delta(P)\Big)^2 &= \sum\!\!\!\!\!\!\int_P \frac{1-\delta_{p_0,0}}{P^4} + \sum\!\!\!\!\!\!\int_P \frac{\delta_{p_0,0}}{(\vec{p}^2+m_T^2)^2} \\ &= \sum\!\!\!\!\!\!\int_P \frac{1}{P^4} + T\int_p \frac{1}{(\vec{p}^2+m_T^2)^2} \\ &= \frac{1}{(4\pi)^2}\left(\frac{1}{\varepsilon}+2\gamma_E+2\ln\frac{\mu}{4\pi T}\right)+\frac{T}{8\pi m_T}. \end{aligned} \tag{4.32}$$

4.5 Pressure to lowest orders

The lowest order correction to the pressure stems from the one-loop vacuum diagram in Fig. 4.5, and reads

$$\begin{aligned}\mathcal{P}_a &= \frac{1}{2}\sum\!\!\!\!\!\!\int_P \ln\Delta(P) \\ &= -\frac{1}{2}\sum\!\!\!\!\!\!\int_P \ln\left\{P^2(1-\delta_{p_0,0})+(\vec{p}^2+m_T^2)\delta_{p_0,0}\right\} \\ &= \frac{1}{2}\sum\!\!\!\!\!\!\int_P \ln P^2 - \frac{1}{2}T\int_p \ln\left(1+\frac{m_T^2}{\vec{p}^2}\right). \end{aligned} \tag{4.33}$$

The sum-integral has been calculated in the Appendix, Eq. (B.20), and the integral can be evaluated by rewriting it as

$$\int_p \ln\left(1+\frac{m_T^2}{\vec{p}^2}\right) \;=\; \int_p \ln\left(\vec{p}^2+m_T^2\right) - \int_p \ln\vec{p}^2, \tag{4.34}$$

where the first term has been calculated in Eq. (B.16), and the second term is zero in dimensional regularization. Collecting terms and inserting the thermal mass $m_T^2 = \frac{g^2T^2}{24}$ yields

$$\mathcal{P}_a = \frac{\pi^2T^4}{90} + \frac{\pi^2T^4}{9\sqrt{6}}\left(\frac{g}{4\pi}\right)^3, \tag{4.35}$$

where the first term is the same as in Eq. (4.10), and the second term is of order $g^3 \sim \lambda^{\frac{3}{2}}$, which is not a behaviour one would expect in a series expansion. It arises due to the inclusion of the thermal mass in the propagator, which obviously gives rise to terms with a novel behaviour.

The second order correction to the pressure stems from the two-loop diagrams in Fig. 4.2. The first one of these diagrams is the same as already encountered in Eq. (4.19), while the other one is new. This new diagram has an *insertion of the thermal mass*, depicted as a small cross. As mentioned earlier, this can be treated as an interaction. According to the Lagrangian (4.26), this is a two-point interaction with vertex factor $-\frac{1}{2}m_T^2\delta_{p_0,0}$. The diagram with

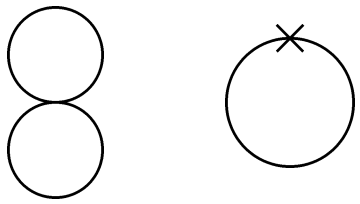

Figure 4.2: Diagrams b and c, the two-loop contributions to the pressure.

one mass insertion thus contributes as a two-loop diagram, since $m_T \sim g$. The contribution from the first diagram is

$$\begin{aligned}
\mathcal{P}_b &= -3\frac{g^2}{24}\left(\sum\!\!\!\!\!\!\int_P \Delta(P)\right)^2 \\
&= -\frac{g^2}{8}\left(\sum\!\!\!\!\!\!\int_P \frac{1}{P^2} + \int_p \frac{1}{\vec{p}^2+m_T^2}\right)^2 \\
&= -\frac{g^2}{8}\left(\frac{T^4}{12^2} - \frac{mT^3}{24\pi} + \frac{m_T^2T^2}{(4\pi)^2}\right) \\
&= -\frac{\pi^2T^4}{2^3\,3^2}\left(\frac{g}{4\pi}\right)^2 + \frac{\pi^2T^4}{6\sqrt{6}}\left(\frac{g}{4\pi}\right)^3 - \frac{\pi^2T^4}{2^2\,3}\left(\frac{g}{4\pi}\right)^4,
\end{aligned} \tag{4.36}$$

while the second diagram yields

$$\begin{aligned}
\mathcal{P}_c &= \frac{1}{2}m_T^2\delta_{p_0,0}\sum\!\!\!\!\!\!\int_P \Delta(P) \\
&= \frac{1}{2}m_T^2T\int_p \frac{1}{\vec{p}^2+m_T^2} \\
&= -\frac{m_T^3T}{8\pi} \\
&= -\frac{\pi^2T^4}{6\sqrt{6}}\left(\frac{g}{4\pi}\right)^3.
\end{aligned} \tag{4.37}$$

Upon summing the two-loop diagrams, the g^3 contributions cancel. The final expression for the second order correction to the pressure is thus

$$\mathcal{P}_b + \mathcal{P}_c = -\frac{\pi^2T^4}{2^3\,3^2}\left(\frac{g}{4\pi}\right)^2 - \frac{\pi^2T^4}{2^2\,3}\left(\frac{g}{4\pi}\right)^4. \tag{4.38}$$

4.6 Higher orders

When going to higher orders, different diagrams are produced and some of these diagrams are divergent. The first kind of diagrams which will be discussed are the so-called ring diagrams or daisy diagrams, see Fig. 4.3. A daisy diagram with n vertices yields the following contribution to the pressure

$$V\frac{(-1)^{n+1}}{n}\left(\frac{g^2}{2}\sum\!\!\!\!\!\!\int_P \frac{1}{P^2}\right)^n \sum\!\!\!\!\!\!\int_Q \frac{1}{(Q^2)^n}, \tag{4.39}$$

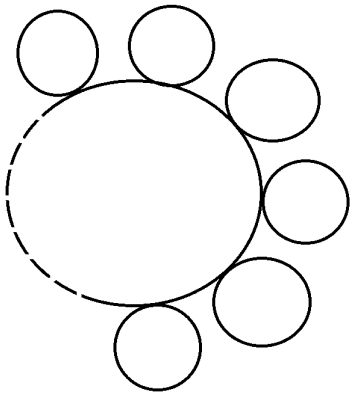

Figure 4.3: A ring diagram, or daisy diagram, which can in principle have an arbitrary number of loops.

where the topological factor V makes sure the expression have the right symmetry factor for the diagram. By analysing many diagrams the factor V has been determined for a diagram with n vertices

$$V = \frac{1}{n!}\,6^n(2n-2)!! \quad n \geq 2. \tag{4.40}$$

The first daisy diagram produced is diagram e in Fig. 4.4, and this is the first in an infinite series of diagrams which are increasingly infrared divergent. Due to the similarity in this series of diagrams it is possible to sum them, and although every term is IR-divergent, the sum turns out to be convergent both in the infrared and in the ultraviolet. The fact that these infrared divergences arise reflects the fact that an improved propagator must be used in the perturbative expansion. This is exactly the propagator in Eq. (4.27), which leads to insertions of the thermal mass.

The thermal mass insertions furthermore produce diagrams with only mass insertions, and there are also diagrams with both mass insertions and loops. The third order correction to the pressure is given by the three diagrams in Fig. 4.4, which yield the following contribution

$$\begin{aligned}
\mathcal{P}_e + \mathcal{P}_f + \mathcal{P}_g &= \frac{g^4}{16}\left(\sum\!\!\!\!\!\!\int_P \Delta\right)^2 \sum\!\!\!\!\!\!\int_P \Delta^2 - \left(\frac{1}{2}m_T^2\delta_{p_0,0}\sum\!\!\!\!\!\!\int_P \Delta^2\right)\left(\frac{g^2}{2}\sum\!\!\!\!\!\!\int_P \Delta\right) + \frac{1}{4}m_T^4\delta_{p_0,0}\sum\!\!\!\!\!\!\int_P \Delta^2 \\
&= \frac{g^4}{16}\left(\sum\!\!\!\!\!\!\int_P \frac{1}{P^2} + T\int_p \frac{1}{\vec{p}^2+m_T^2}\right)^2\left(\sum\!\!\!\!\!\!\int_P \frac{1}{(P^2)^2} + T\int_p \frac{1}{(\vec{p}^2+m_T^2)^2}\right) \\
&- \frac{m_T^2 g^2 T}{4}\int_p \frac{1}{(\vec{p}^2+m_T^2)^2}\sum\!\!\!\!\!\!\int_P \frac{1}{P^2} + \frac{m_T^4}{4}T\int_p \frac{1}{(\vec{p}^2+m_T^2)^2} \\
&= \frac{g^4}{16}\left(\frac{T^4}{12^2} + \frac{m_T^2T^2}{(4\pi)^2} - \frac{m_TT^3}{24\pi}\right)^2\left(\frac{1}{(4\pi)^2}\left[\frac{1}{\varepsilon} + 2\ln\frac{\Lambda}{4\pi T} + 2\gamma_E\right] + \frac{T}{8\pi m_T}\right) + \\
&- \frac{m_T^2g^2T}{4}\frac{1}{8\pi m_T}\frac{T^2}{12} + \frac{m_T^3T}{32\pi} + \mathcal{O}(\varepsilon) \\
&= \frac{g^4T^4}{2^{12}3\pi^2\varepsilon}\left(\frac{1}{3} - \frac{g}{\pi\sqrt{6}} + \frac{g^2}{2^3\pi^2}\right) + \frac{g^4T^4}{2^{12}3^2\pi^2}\left(3\ln\frac{\Lambda^2}{4\pi T^2} + 4 - \gamma_E + 4\frac{\xi'(-1)}{\xi(-1)}\right) + \\
&- \frac{g^5T^4}{2^{12}3\sqrt{6}\pi^3}\left(\ln\frac{3\Lambda^6}{2\pi g^2T^6} + 1 - \gamma_E + 2\frac{\xi'(-1)}{\xi(-1)}\right) + \mathcal{O}(g^6).
\end{aligned} \tag{4.41}$$

As predicted a divergence has arisen, produced by the ring diagram. This divergence will be dealt with shortly, after the last contributing diagram has been included.

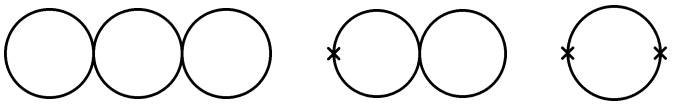

Figure 4.4: The three diagrams e, f and g, contributing to three-loop order.

4.6.1 Basketball diagram

The last diagram which must be included in order to obtain the pressure to order g^5 is the one in Fig. 4.5, the so-called basketball diagram. In terms of the propagator (4.27) it yields the following sum-integral

$$\mathcal{P}_h = \frac{g^4}{48} \sum\!\!\!\!\!\!\int_{PQR} \Delta(P)\Delta(Q)\Delta(R)\Delta(P+Q+R). \tag{4.42}$$

Writing out the expressions for the propagator explicitly and multiplying out yields

$$\begin{aligned}
\mathcal{P}_h = \frac{g^4}{48} \sum\!\!\!\!\!\!\int_{PQR} \Bigg\{ & \frac{1}{P^2}\frac{1}{Q^2}\frac{1}{R^2}\frac{1}{(P+R+Q)^2} \\
& -4\frac{m_T^2\delta_{p_0,0}}{\vec{p}^2(\vec{p}^2+m_T^2)}\frac{1}{Q^2}\frac{1}{R^2}\frac{1}{(P+Q+R)^2} \\
& +6\frac{m_T^2\delta_{p_0,0}}{\vec{p}^2(\vec{p}^2+m_T^2)}\frac{m_T^2\delta_{q_0,0}}{\vec{q}^2(\vec{q}^2+m_T^2)}\frac{1}{R^2}\frac{1}{(P+Q+R)^2} \\
& -4\frac{m_T^2\delta_{p_0,0}}{\vec{p}^2(\vec{p}^2+m_T^2)}\frac{m_T^2\delta_{q_0,0}}{\vec{q}^2(\vec{q}^2+m_T^2)}\frac{m_T^2\delta_{r_0,0}}{\vec{r}^2(\vec{r}^2+m_T^2)}\frac{1}{(P+Q+R)^2} \\
& +\frac{m_T^2\delta_{p_0,0}}{\vec{p}^2(\vec{p}^2+m_T^2)}\frac{m_T^2\delta_{q_0,0}}{\vec{q}^2(\vec{q}^2+m_T^2)}\frac{m_T^2\delta_{r_0,0}}{\vec{r}^2(\vec{r}^2+m_T^2)}\frac{m_T^2\delta_{p_0+q_0+r_0,0}}{(\vec{p}+\vec{q}+\vec{r})^2\left((\vec{p}+\vec{q}+\vec{r})^2+m_T^2\right)} \Bigg\} \\
& \equiv \mathcal{P}_{h1}+\mathcal{P}_{h2}+\mathcal{P}_{h3}+\mathcal{P}_{h4}+\mathcal{P}_{h5}.
\end{aligned} \tag{4.43}$$

The first sum-integral is known as the massless basketball diagram, and was first calculated by Arnold and Zhai in [18]:

$$\mathcal{P}_{h1} = \frac{g^4T^4}{3^3 2^{12}\pi^2}\left(\frac{6}{\varepsilon}+36\ln\frac{\Lambda}{4\pi T}-12\frac{\xi'(-3)}{\xi(-3)}+48\frac{\xi'(-1)}{\xi(-1)}+\frac{182}{5}\right). \tag{4.44}$$

The term $\mathcal{P}_{h2}$ contains only one zero Matsubara mode, which can happen in four different ways, giving rise to the combinatorial factor in front of the integral. Written out explicitly it becomes

$$\begin{aligned}
\mathcal{P}_{h2} &= -\frac{g^4}{12}\frac{m_T^2\delta_{p_0,0}}{\vec{p}^2(\vec{p}^2+m_T^2)}\frac{1}{Q^2}\frac{1}{R^2}\frac{1}{(P+Q+R)^2} \\
&= -\frac{g^4T}{12}m_T^{1-2\varepsilon}\int_p \frac{1}{\vec{p}^2(\vec{p}^2+1)} \sum\!\!\!\!\!\!\int_{QR} \frac{1}{Q^2R^2\left[(q_0+r_0)^2+(\vec{q}+\vec{r}+m_T\vec{p})^2\right]},
\end{aligned} \tag{4.45}$$

after scaling $\vec{p}\to m_T\vec{p}$. The sum-integral can be written as

$$T^2\int_{qr}\frac{1}{\vec{q}^2r^2(\vec{q}+\vec{r}+m_T\vec{p})^2}+\sum\!\!\!\!\!\!\int_{QR}\frac{1-\delta_{q_0,0}\delta_{r_0,0}}{Q^2R^2\left[(q_0+r_0)^2+(\vec{q}+\vec{r}+m_T\vec{p})^2\right]} \tag{4.46}$$

by extracting the two zero modes. The denominator in the second term can be expanded, and it becomes a sum of one massless term, one term which is linear in $m_T\vec{p}$ and terms of higher order in $m_T\vec{p}$. The first of these is zero in dimensional regularization, and the second yields zero upon integration over $\vec{p}$, the integrand being asymmetrical. Since $m_T \sim g$ and this discussion includes only terms up to order g^5, only the following part must be evaluated

$$-\frac{g^4T^2}{12}m_T^{1-2\varepsilon}\int_p \frac{1}{\vec{p}^2(\vec{p}^2+1)}\int_{qr}\frac{1}{\vec{q}^2\vec{r}^2(\vec{q}+\vec{r}+m_T\vec{p})^2}. \tag{4.47}$$

The procedure used by [19] consists in evaluating first the $\vec{q}$ and $\vec{r}$ integrals in $d = 3-2\varepsilon$ dimensions, dropping all terms linear in ε and then performing the $\vec{p}$ integral. The result is

$$\mathcal{P}_{h2} = -\frac{g^5T^4}{2^9\sqrt{6}\pi^3}\left\{\frac{1}{\varepsilon}+3\ln\frac{6\Lambda^2}{4\pi m_T^2}+8+\ln\frac{16}{\pi^3}\right\}. \tag{4.48}$$

The term $\mathcal{P}_{h3}$ contains two zero and one nonzero mode, so the same procedure as earlier can be used. Scaling in m_T

$$\begin{aligned}\mathcal{P}_{h3} &= \frac{g^4}{8}\int_{pq}\frac{m_T^2\delta_{p_0,0}}{\vec{p}^2(\vec{p}^2+m_T^2)}\frac{m_T^2\delta_{q_0,0}}{\vec{q}^2(\vec{q}^2+m_T^2)}\sum\!\!\!\!\!\!\int_R\frac{1}{R^2}\frac{1}{(P+Q+R)^2}\\ &= \frac{g^4T^2}{8}m_T^{2(1-2\varepsilon)}\int_{pq}\frac{1}{\vec{p}^2(\vec{p}^2+1)\vec{q}^2(\vec{q}^2+1)}\sum\!\!\!\!\!\!\int_R\frac{1}{R^2}\frac{1}{r_0^2+(\vec{r}+m_T\vec{p}+m_T\vec{q})^2},\end{aligned} \tag{4.49}$$

and next extracting the zero-mode from the sum-integral over R. The latter is

$$T\int_r\frac{1}{\vec{r}^2(\vec{r}+m_T\vec{p}+m_T\vec{q})^2}+\sum\!\!\!\!\!\!\int_R\frac{1}{R^2}\frac{1-\delta_{r_0,0}}{r_0^2+(\vec{r}+m_T\vec{p}+m_T\vec{q})^2}. \tag{4.50}$$

Scaling again, both $\vec{p}$ and $\vec{q}$, the second term contributes only to order g^6, while the first term results in the integral

$$\frac{g^4T^3}{8}m_T^{1-6\varepsilon}\int_{pqr}\frac{1}{\vec{p}^2(\vec{p}^2+1)\vec{q}^2(\vec{q}^2+1)\vec{r}^2(\vec{r}+\vec{p}+\vec{q})^2}. \tag{4.51}$$

The $\vec{p},\vec{q}$ and $\vec{r}$ integrals can be decoupled using the 3-dimensional integral delta function

$$\begin{aligned}\frac{1}{(\vec{p}+\vec{q}+\vec{r})^2} &= \int\frac{d^3\omega}{\omega^2}\delta^3(\vec{p}+\vec{q}+\vec{r}+\vec{\omega})\\ &= \int\frac{d^3\omega}{\omega^2}\int\frac{d^3R}{(2\pi)^3}e^{iR\cdot(\vec{p}+\vec{q}+\vec{r}+\vec{\omega})},\end{aligned} \tag{4.52}$$

thus the integral in Eq. (4.51) becomes

$$\begin{aligned}&\int d^3R\left(\frac{1-e^{-R}}{4\pi R}\right)^2\left(\frac{1}{4\pi R}\right)^2\\ &= \frac{1}{(4\pi)^3}\int_0^\infty\frac{dR}{R^2}\left(1-e^{-R}\right)^2\\ &= \frac{1}{(4\pi)^3}2\ln 2.\end{aligned} \tag{4.53}$$

Including prefactors and dropping terms linear in ε yields

$$\begin{aligned}\mathcal{P}_{h3} &= \frac{g^4m_TT^3}{8(4\pi)^3}2\ln 2\\ &= \frac{g^5T^4}{2^9\sqrt{6}\pi^3}\ln 2.\end{aligned} \tag{4.54}$$

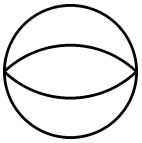

Figure 4.5: The basketball diagram.

In $\mathcal{P}_{h4}$, all Matsubara modes are zero independently. Scaling all three vectors $\vec{p}$, $\vec{q}$ and $\vec{r}$ and proceeding in the same way as above yields

$$\begin{aligned}
\mathcal{P}_{h4} &= -\frac{g^4}{12} \sum\!\!\!\!\!\!\int_{PQR} \frac{m_T^2 \delta_{p_0,0}}{\vec{p}^2(\vec{p}^2+m_T^2)} \frac{m_T^2 \delta_{q_0,0}}{\vec{q}^2(\vec{q}^2+m_T^2)} \frac{m_T^2 \delta_{r_0,0}}{\vec{r}^2(\vec{r}^2+m_T^2)} \frac{1}{(P+Q+R)^2} \\
&= -\frac{g^4 m_T T^3}{12} \int dR \left(\frac{1-e^{-R}}{4\pi R}\right)^3 \left(\frac{1}{4\pi R}\right) \\
&= -\frac{g^4 m_T T^3}{12} \frac{1}{(4\pi)^3} \int_0^\infty \frac{dR}{R^2} \left(e^{-R-1}\right)^3 \\
&= -\frac{g^4 m_T T^3}{12(4\pi)^3} (3\ln 3 - 6\ln 2) \\
&= \frac{g^5 T^4}{2^9\sqrt{6}\pi^3} (\ln 3 - 2\ln 2) .
\end{aligned} \tag{4.55}$$

The last term, $\mathcal{P}_{h5}$, is purely spatial. The integral is rewritten as

$$I = \int_{pqr} \frac{1}{p^2+m_T^2} \frac{1}{q^2+m_T^2} \frac{1}{r^2+m_T^2} \frac{1}{(p+q+r)^2+m_T^2} = \int_R V^4(R), \tag{4.56}$$

having defined the function

$$\begin{aligned}
V(R) &\equiv \int_k e^{i\vec{k}\cdot\vec{R}} \frac{1}{k^2+m_T^2} \\
&= \left(\frac{e^{\gamma_E}\Lambda^2}{4\pi}\right)^\varepsilon \frac{1}{(2\pi)^{3/2-\varepsilon}} \left(\frac{m}{R}\right)^{1/2-\varepsilon} \mathcal{K}_{\frac{1}{2}-\varepsilon}(mR),
\end{aligned} \tag{4.57}$$

which reduces to the coulomb potential at $\varepsilon = 0$;

$$V_0(R) = \frac{e^{-mR}}{4\pi R}. \tag{4.58}$$

The $\mathcal{K}$ are the modified Bessel functions, and for small R the potential can be written as a sum of two Laurent expansions in R^2, one beginning with an $R^{-1+2\varepsilon}$ term and one with an R^0 term,

$$\begin{aligned}
V(R) \simeq &\left(\frac{e^{\gamma_E}\Lambda^2}{4}\right)^\varepsilon \frac{\Gamma(\frac{1}{2}-\varepsilon)}{\Gamma(\frac{1}{2})} \frac{R^{-1+2\varepsilon}}{4\pi} \left(1 + \frac{m_T^r}{2(1+2\varepsilon)} + \mathcal{O}(m_T^4 R^4)\right) - \\
&\left(e^{\gamma_E}\Lambda^2\right)^\varepsilon \frac{\Gamma(-\frac{1}{2}+\varepsilon)}{\Gamma(-\frac{1}{2})} \frac{m_T^{1-2\varepsilon}}{4\pi} \left(1 + \frac{m_T^2 R^2}{2(3-2\varepsilon)} + \mathcal{O}(m_T^4 R^4)\right).
\end{aligned} \tag{4.59}$$

Since all divergences come from the region where $R \to 0$, the integral from 0 to ∞ can be split into one part from 0 to some small r, and one integral from r to ∞. In the lower region the small-R expansion in Eq. (4.59) may be used, and

in the upper region it is safe to set $\varepsilon = 0$ before starting the calculation. Splitting up the integral and inserting yields

$$I = \underbrace{4\pi\left(\frac{e^{\gamma_E}\Lambda^2}{4}\right)^{-\varepsilon}\frac{\Gamma(\frac{3}{2})}{\Gamma(\frac{3}{2}-\varepsilon)}\int_0^r \mathrm{d}R\,R^{2-2\varepsilon}V^4(R)}_{I_1} + \underbrace{4\pi\int_r^\infty \mathrm{d}R\,R^2V_0^4(R)}_{I_2}. \tag{4.60}$$

Evaluating the first term by performing the straightforward integrations over R and next Taylor expanding in ε, yields

$$I_1 = \frac{1}{(4\pi)^3}\left[-\frac{1}{r} - m_T\left(\frac{1}{\varepsilon} + 2\ln\frac{r^2\Lambda^3}{2m} + 4\gamma_E + 4\right)\right] + \mathcal{O}(\varepsilon). \tag{4.61}$$

The second term is evaluated using the incomplete gamma-functions;

$$\begin{aligned} I_2 &= 4\pi\int_r^\infty \mathrm{d}R\,R^2V_0^4(R) \\ &= 4\pi\int_r^\infty \mathrm{d}R\frac{e^{-4mR}}{(4\pi)^4R^2} \\ &= \frac{1}{(4\pi)^3}\left[\frac{e^{-4mR}}{r} - 4m_T\Gamma(0,4mr)\right]_{R=(r,\infty)} \\ &= \frac{1}{(4\pi)^3}\left\{\frac{1}{r} + 4m_T\left(\gamma_E - 1 + \ln 4mr\right)\right\}. \end{aligned} \tag{4.62}$$

When adding the two integrals, the r-dependence cancels, as was expected since there was nothing physical about it, and the result is

$$\begin{aligned} \mathcal{P}_{h5} &= \frac{g^4T^3}{48}I = -\frac{g^4T^3m}{48(4\pi)^3}\left\{\frac{1}{\varepsilon} + 6\ln\frac{\Lambda}{2m} + 8 - 4\ln 2\right\} \\ &= -\frac{g^5T^4}{2^{11}3\sqrt{6}\pi^3}\left\{\frac{1}{\varepsilon} + 6\ln\frac{\Lambda}{2m} + 8 - 4\ln 2\right\}. \end{aligned} \tag{4.63}$$

Collecting terms, the full contribution up to order g^5 for the thermal basketball diagram is

$$\mathcal{P}_h = \frac{g^4T^4}{3^3\,2^{12}\,\pi^2}\left(\frac{6}{\varepsilon} + 36\ln\frac{\Lambda}{4\pi T} - 12\frac{\xi'(-3)}{\xi(-3)} + 48\frac{\xi'(-1)}{\xi(-1)} + \frac{182}{5}\right) - \frac{g^5T^4}{2^{11}3\sqrt{6}\pi^3}\left(\frac{1}{\varepsilon} + 6\ln\frac{\Lambda}{2m} + 8 - 4\ln 2\right). \tag{4.64}$$

4.6.2 Renormalized coupling

The three-loop diagrams have yielded ultraviolet divergences, appearing in the first terms of Eqs. (4.41) and (4.64). As all vacuum diagrams stem from a perturbative expansion in g, it is natural that g be expanded also. It is thus a series in itself, and the coupling appearing in the Lagrangian is only the leading order term, or the *bare coupling*, g_b. Upon series expanding $g_b = g + \delta g$ and thus renormalizing g_b, all diagrams will yield contributions to ever increasing orders in g. From this follows that to order g^5, only diagram b in Fig. 4.6 must be renormalized. Upon renormalization, this diagram is then required to produce a $\frac{g^4}{\varepsilon}$ piece which exactly cancels the encountered divergences. Thus to lowest order,

$$g_b^2 = g^2 + \frac{3g^4}{32\pi^2\varepsilon}, \tag{4.65}$$

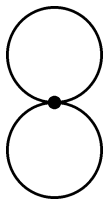

Figure 4.6: Diagram d, the two-loop diagram with a renormalized coupling.

and diagram b changes as follows

$$\begin{aligned}
\mathcal{P}_d &= \mathcal{P}_b + \frac{1}{8}\frac{3g^4}{32\pi^2\varepsilon}\left(\sum\!\!\!\!\!\!\int_P \Delta\right)^2 \\
&= \mathcal{P}_b + \frac{3g^4}{32\pi^2\varepsilon}\left(\sum\!\!\!\!\!\!\int_P \frac{1}{P^2} + T\int_p \frac{1}{\vec{p}^2+m^2}\right)^2 \\
&= \mathcal{P}_b + \frac{3g^4}{32\pi^2\varepsilon}\left(1+\left[2\ln\frac{\Lambda}{4\pi T}+2+2\frac{\xi'(-1)}{\xi(-1)}\right]\varepsilon - \frac{mT}{4\pi}\left\{1+\left[2\ln\frac{\Lambda}{2m}+2\right]\varepsilon\right\}\right)^2 \\
&= \mathcal{P}_b + \frac{T^4}{2^4\pi^2\varepsilon}\left(\frac{g}{4\pi}\right)^4\left(-\frac{1}{3}+\frac{g}{\sqrt{6}\pi}-\frac{g^2}{2^3\pi^2}\right) - \frac{T^4}{2^4 3\pi^2}\left(\frac{g}{4\pi}\right)^4\left(4\ln\frac{\Lambda}{4\pi T}+4+4\frac{\xi'(-1)}{\xi(-1)}\right) + \\
&+ \frac{\pi^2 T^4}{2^2\sqrt{6}}\left(\frac{g}{4\pi}\right)^5\left(2\ln\frac{\Lambda^2}{4\pi T^2}+4+2\frac{\xi'(-1)}{\xi(-1)}+\ln\frac{6}{g^2}\right).
\end{aligned} \tag{4.66}$$

The renormalized coupling is depicted as a dot, and the new diagram is shown in Fig. 4.6.

4.7 Total pressure to order g^5

The sum of diagrams, including the extra term from diagram d, yields the following total pressure

$$\mathcal{P} = \mathcal{P}_{ideal}\left\{1-\frac{5}{4}\alpha+\frac{5\sqrt{6}}{3}\alpha^{3/2}+\frac{15}{4}\alpha^2\left(\frac{1}{2}\ln\frac{\Lambda^2}{4\pi T^2}+C_4\right)-\frac{15\sqrt{6}}{2}\alpha^{5/2}\left(\frac{1}{2}\ln\frac{\Lambda^2}{4\pi T^2}-\frac{2}{3}\ln\alpha+C_5\right)\right\}, \tag{4.67}$$

where $\mathcal{P}_0 = \mathcal{P}_{ideal} = \frac{\pi^2 T^2}{90}$, $\alpha = \left(\frac{g}{4\pi}\right)^2$ and the constants appearing are

$$C_4 = -\frac{2}{3}\frac{\xi'(-3)}{\xi(-3)}+\frac{4}{3}\frac{\xi'(-1)}{\xi(-1)}-\frac{\gamma}{6}-\frac{59}{45}, \tag{4.68}$$

$$C_5 = \frac{5}{6}-\frac{\gamma}{6}-\frac{2}{3}\frac{\xi'(-1)}{\xi(-1)}-\frac{2}{3}\ln\frac{2}{3}. \tag{4.69}$$

There are no divergent terms in Eq. (4.67), so all divergences have cancelled up to the current order. Furthermore, a logarithm of the coupling constant has appeared, and the first time this happens is at fifth order.

Numerical values for the constants are

$$C_4 = 0.809138, \tag{4.70}$$

$$C_5 = -0.315928, \tag{4.71}$$

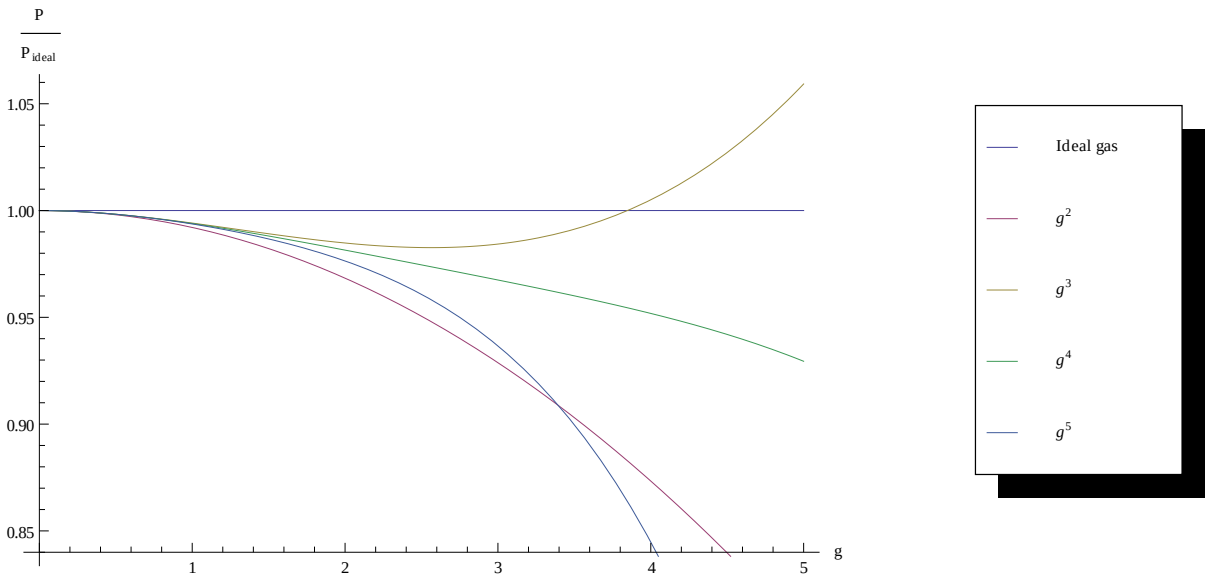

Figure 4.7: The pressure $\mathcal{P}$ normalized to $\mathcal{P}_{ideal}$ to order g^2, g^3, g^4 and g^5.

and a plot of $\mathcal{P}$ normalized to $\mathcal{P}_{ideal}$ has been made, with $\Lambda = 2\pi T$. The plot can be seen in Fig. 4.7 and shows the pressure to order g^0 through all orders up to g^5.

Since Eq. (4.67) is a perturbative expansion, the nth term in the series must be smaller than the $(n-1)$th one. Thus the expansion parameter α must be small, and an upper bound can be found by applying the condition to the second and third terms. This yields $\alpha < \frac{3}{4\sqrt{6}}$, i.e. $g \approx 3.85$, which can be seen in Fig 4.7, as the pressure up to order g^3 equals the ideal gas pressure at this value of g. The same argument can be applied further and including higher order terms. From this, or from simply studying the graph, it is evident that the expansion only holds for very small α. Thus the perturbative expansion is poorly convergent, unless the coupling is tiny.

In the following chapters we will see that the magnitude of the coupling constant is critical for the validity of any perturbational theory.

As long as the coupling constant is small, the perturbative expansion holds, but if the coupling increases in order, or ever exceeds unity, series problems arise.

Chapter 5

QED

The following chapter is devoted to the discussion of quantum electrodynamics (QED), which, mathematically speaking, is an Abelian gauge theory with the $U(1)$ symmetry group. Abelian groups are also called commutative groups and have the property that the group operation can be applied on two group elements regardless of the order. In QED the interaction between charged spin$-\frac{1}{2}$ fields is mediated by the electromagnetic field A_μ; the gauge field. It is therefore natural to start this discussion with the introduction of a gauge and a treatment of gauge fixing, before moving on to find the partition function in QED. The aim is to arrive at an EoS for a completely degenerate Fermi gas at $T = 0$, so the quantum corrections to the pressure of a gas consisting of photons and electrons are calculated by evaluating self-energies. The interactions in QED plasma and propagating photons are also studied, and the self-energy tensor is derived. Finally, the contribution to the pressure from ring diagrams up to order $e^4 \ln e$ is calculated in the zero temperature limit.

5.1 Partition function for a U(1) gauge theory

In electromagnetic quantum theory the observables are the electric field $\vec{E}$ and the magnetic field $\vec{B}$, and within a class of gauges, there are infinitely many A_μ with the same electric and magnetic fields. Thus the fields A_μ are not observables, and they are all connected by gauge transformations. This is usually taken care of by fixing the gauge, which formally corresponds to integrating over a delta-function [11]. The generalized covariant Lorentz gauge is used throughout this thesis, and it is expressed by the gauge fixing condition

$$F(A) = \partial_\mu A^\mu - \omega(x) = 0, \tag{5.1}$$

where $\omega(x)$ can be any scalar function. As demonstrated in Section 2.1, the equations of motion for a field do not change if the action S is changed only up to a surface term. The change in S is given rise to by transformations on the field, and for the QED Lagrangian to be invariant under these transformations, corresponding transformations must be applied to the gauge fields, as discussed in Section 2.2. The Lagrangian is invariant if the Dirac and gauge fields transform as follows

$$\psi \rightarrow e^{i\alpha(x)}\psi, \tag{5.2}$$
$$A^\mu \rightarrow A^\mu + \partial^\mu \alpha(x). \tag{5.3}$$

Under this transformation the gauge fixing condition in Eq. (5.1) changes as well;

$$F(A) \rightarrow \partial_\mu A^\mu + \partial_\mu \partial^\mu \alpha(x) - \omega(x). \tag{5.4}$$

Now, $\alpha(x)$ is some arbitrary scalar function which can itself, as well as its derivative and higher order derivatives, take on any value for all x. The integral over all $\alpha(x)$ and the gauge fixing condition is

$$\int \mathcal{D}\alpha(x)\delta\left(\partial_\mu A^\mu + \partial_\mu \partial^\mu \alpha(x) - \omega(x)\right) = 1, \tag{5.5}$$

meaning that there are no constraints defining the path of integration. This also means that the variables can be changed as follows

$$\alpha(x) \rightarrow \partial_\mu \partial^\mu \alpha(x), \tag{5.6}$$
$$d\alpha(x) \rightarrow \det(\partial_\mu \partial^\mu) d\alpha(x), \tag{5.7}$$

which in turn changes the integral defined above to

$$\int \mathcal{D}\alpha'(x) \frac{1}{\det(\partial_\mu \partial^\mu)} \delta\left(\partial_\mu A^\mu + \partial_\mu \partial^\mu \alpha(x) - \omega(x)\right) = \frac{1}{\det(\partial_\mu \partial^\mu)}. \tag{5.8}$$

The partition function can now be expressed as an integral over all gauge fields and given a gauge constraint by inserting the above integral, yielding the following expression

$$\mathcal{Z} = \int_{periodic} \mathcal{D}A_\mu(x) \mathcal{D}\alpha(x) \delta\left(\partial_\mu A^\mu + \partial_\mu \partial^\mu \alpha(x) - \omega(x)\right) \det(\partial_\mu \partial^\mu) e^{-S_E}. \tag{5.9}$$

This can be rewritten as

$$\mathcal{Z} = \int_{periodic} \mathcal{D}A_\mu(x) \mathcal{D}\alpha(x) \delta\left(\partial_\mu A^\mu - \omega(x)\right) \det(\partial_\mu \partial^\mu) e^{-S_E}, \tag{5.10}$$

since the gauge fields are related to each other by linear shifting. The integral over $\alpha(x)$ now only contributes as an infinite constant, which is interpreted as the gauge volume. It is therefore just a normalization constant, and can be dropped from here on.

According to [8], the most general form of the integral, and thereby the proper expression for the partition function, is

$$\mathcal{Z} = \int_{periodic} \mathcal{D}A_\mu(x) \delta(F) \det\left(\frac{\partial F}{\partial \alpha}\right) e^{-S_E} \tag{5.11}$$

where F is the gauge fixing condition in Eq. (5.1). What makes this integral most difficult to evaluate is the fact that the function $\omega(x)$ in the gauge fixing condition is an arbitrary function of x. As long as one does not know anything about the behaviour of this function, the integral contained in the partition function cannot be solved. One can get rid of this problem by arguing that multiplying by

$$e^{-\frac{1}{2\alpha}\int d^4x \omega^2}, \tag{5.12}$$

and next performing a functional integral over ω, will not change the physics in $\mathcal{Z}$. Integrating over all possible functions $\omega(x)$, assuming that they have a Gaussian distribution around $\omega(x)$=0, reduces the partition function to the following expression in Euclidean space

$$\int \mathcal{D}A^\mu(x) \det(-\partial^2) e^{S_E}, \tag{5.13}$$

with the Euclidean action

$$S_E = \int d^4x \mathcal{L}_E - \frac{1}{2\alpha}(\partial_\mu A^\mu)^2. \tag{5.14}$$

The last term in the action is known as a gauge fixing term, and the constant α is any real number, which has nothing to do with the scalar function from before. The Landau gauge corresponds to the choice $\alpha = 0$ and the Feynman gauge to $\alpha = 1$. The latter one is used in this thesis.

It is perhaps easier to understand the meaning of the determinant in Eq. (5.13) by using Eq. (2.29) to express it as an integral over a complex Grassmann variable as follows

$$\det(-\partial^2) = \int \mathcal{D}C^\dagger \mathcal{D}C e^{\int d^4x (\partial_\mu C)^\dagger (\partial^\mu C)}. \tag{5.15}$$

The C and $C^\dagger$ are thus scalar Grassmann fields, which are allowed to interact with the gauge fields A_μ, and their quanta are spin-zero fermions [10]. They are called *ghost fields*, and we will not dwell with them for long, just note that they

can not represent real physical states, since that would violate spin statistics. This notion is supported by the fact that the ghost fields could have been eliminated by choosing a different gauge, as

$$\det\left(\frac{\partial F}{\partial \alpha(x)}\right) = \det(-\partial^2) \tag{5.16}$$

only with the gauge fixing condition stated in Eq. (5.4) and in Euclidean space. The ghost fields do however contribute to the effective degrees of freedom, and thereby also to the corrections to the pressure, and so they play an important part in the theory.

5.2 The partition function and pressure for free photons, electrons and ghosts

The Lagrangian density for a gas of photons and electrons is

$$\mathcal{L}_0 = \bar{\psi}(i\partial\!\!\!/ - m_e)\psi - \frac{1}{4}F_{\mu\nu}F^{\mu\nu}, \tag{5.17}$$

where m_e is the electron mass, and the electromagnetic field tensor $F_{\mu\nu}$ is defined in Eq. (2.20). This Lagrangian is called the free Lagrangian density, as it does not contain any cross terms in A and ψ. It is also invariant under global $U(1)$ transformations, and therefore has a conserved current.

Using this Lagrangian, as well as including the gauge fixing term and the ghost fields in the partition function (5.13), yields the non-interacting partition function in QED:

$$\mathcal{Z} = \int \mathcal{D}\bar{C}(x)\mathcal{D}C(x)\mathcal{D}\bar{\psi}(x)\mathcal{D}\psi(x)\mathcal{D}A_\mu(x) e^{\int d^4x\left(-\frac{1}{4}F_{\mu\nu}F^{\mu\nu} - \frac{1}{2\alpha}(\partial_\mu A^\mu)^2 - \bar{C}(x)\partial^2 C(x) + \bar{\psi}(i\partial\!\!\!/ - m_e)\psi\right)}. \tag{5.18}$$

The pressure is given by Eq. (3.4), so the logarithm of Eq. (5.18) is needed. The calculation becomes more clearly laid by splitting the exponential into one part containing the gauge field $A_\mu(x)$, one containing the ghost fields $C(x)$ and one containing the electrons $\psi(x)$. The first part is

$$\begin{aligned}
-\frac{1}{4}F^{\mu\nu}F_{\mu\nu} - \frac{1}{2\alpha}\left(\partial_\mu A^\mu\right)^2 &= -\frac{1}{2}\left(A_\mu \partial_\nu \partial^\mu A^\nu - A_\mu \partial_\nu \partial^\nu A^\mu\right) - \frac{1}{2\alpha}\left(\partial_\mu A^\mu\right)\left(\partial_\nu A^\nu\right) \\
&= -\frac{1}{2}A_\mu\left((1-\alpha^{-1})\partial^\mu\partial^\nu - \partial^2\delta^{\mu\nu}\right)A_\nu \\
&= -\frac{1}{2}A_\mu\left((1-\alpha^{-1})P^\mu P^\nu + P^2\delta^{\mu\nu}\right)A_\nu,
\end{aligned} \tag{5.19}$$

after having integrated by parts and dropped two total derivatives which are just surface terms in the Lagrangian, and therefore do not change the action. The transition to the last line comes to when going to momentum space, where P^μ is the four-momentum of the photons. Using the expression for a Gaussian integral of a matrix M_{ij} in d dimensions

$$\int_{-\infty}^{\infty} e^{-\frac{1}{2}\sum M_{ij}x_i x_j} d^d x = \sqrt{\frac{(2\pi)^d}{\det(M)}} \tag{5.20}$$

and choosing the Feynman gauge with $\alpha = 1$ yields

$$\int \mathcal{D}A(x) e^{-\frac{1}{2}\int d^4x A_\mu (P^2\delta^{\mu\nu})A_\nu} = \prod_{n,\vec{p}} \frac{1}{\sqrt{(\omega_n^2 + \vec{p}^2)^d}}. \tag{5.21}$$

The term with the ghost-fields does not need to be rewritten before evaluating it, and since the ghost fields are defined in the same basis as the gauge fields, it yields

$$\begin{aligned}
\int \mathcal{D}\bar{C}(x)\mathcal{D}C(x) e^{-\int d^4x\left(\bar{C}(x)\partial^2 C(x)\right)} &= \det(-\partial^2) \\
&= \prod_{n,\vec{p}} (\omega_n^2 + \vec{p}^2).
\end{aligned} \tag{5.22}$$

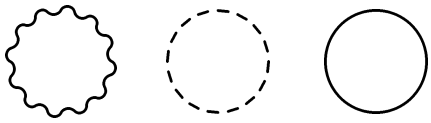

Figure 5.1: One-loop vacuum diagrams. The undulating lines are photons, the dashed lines ghosts and the solid lines electrons.

The electron part can be rewritten by using the Fourier expansion of the wave function $\psi(x)$ given in Eq. (3.50) to go to momentum space, and next the fact that the ψ and $\bar{\psi}$ are independent Grassmann fields, so that Eq. (2.29) yields

$$\begin{aligned}\int \mathcal{D}\bar{\psi}(x)\mathcal{D}\psi(x)e^{\int d^4x\bar{\psi}(i\partial\!\!\!/-m_e)\psi} &= \int \mathcal{D}\bar{\psi}(x)\mathcal{D}\psi(x)e^{\int d^4x\bar{\psi}(p\!\!\!/-m_e)\psi} \\ &= \prod_{n,\vec{p}} \det\left(p\!\!\!/ - m_e\right). \end{aligned} \tag{5.23}$$

Putting everything together, the expression for the pressure becomes

$$\frac{T}{V}\ln\mathcal{Z} = \sum_{n,\vec{p}}\left\{\left(1-\tfrac{d}{2}\right)\ln\left(\omega_n^2+\vec{p}^2\right) + \ln\det\left(p\!\!\!/ - m_e\right)\right\}. \tag{5.24}$$

This is the lowest-order contribution to the pressure of a non-interacting gas in QED, and the corresponding Feynman vacuum diagrams can be seen in Fig. 5.1. From now on the electrons will be treated as massless, i.e. $m_e = 0$. Taking the continuum limit, the sums again become sum-integrals and the above expression yields

$$\begin{aligned}\mathcal{P}_0 &= \left(1-\tfrac{d}{2}\right)\sum\!\!\!\!\!\!\int_P \ln P^2 + \sum\!\!\!\!\!\!\int_{\{P\}} \ln\det p\!\!\!/ \\ &= \left(1-\tfrac{d}{2}\right)\sum\!\!\!\!\!\!\int_P \ln P^2 + \frac{d}{2}\sum\!\!\!\!\!\!\int_{\{P\}} \ln P^2. \end{aligned} \tag{5.25}$$

The calculation of the bosonic sum-integral is done in the Appendix, see Eq. (B.24), and the fermonic sum-integral was evaluated in Eq. (3.74). Finally, the expression for the pressure to lowest order is

$$\mathcal{P}_0 = \frac{\pi^2T^4}{45} + \left(\frac{7\pi^2T^4}{180} + \frac{\mu^2T^2}{6} + \frac{\mu^4}{12\pi^2}\right) \quad \varepsilon \to 0. \tag{5.26}$$

5.3 QED Feynman rules and the two-loop contribution

As mentioned earlier, QED is an Abelian gauge theory. Since physical quantities must be preserved under gauge transformations, so must the derivatives. In order to satisfy this, the ordinary derivatives must be replaced with gauge covariant derivatives, Eq. (2.15). In the present discussion the covariant derivative is defined as

$$D_\mu \equiv \partial_\mu + ieA_\mu, \tag{5.27}$$

thus changing the Lagrangian in Eq. (5.17) to

$$\mathcal{L}_{QED} = \bar{\psi}(i\partial\!\!\!/ - m_f)\psi - e\bar{\psi}A\!\!\!/\psi - \frac{1}{4}F_{\mu\nu}F^{\mu\nu}. \tag{5.28}$$

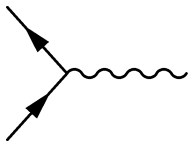

Figure 5.2: The QED vertex, connecting the solid lines representing an incoming and an outgoing electron with a photon, represented by an undulating line.

A new term has arisen in the Lagrangian. The second term in the expression couples the three physical fields, and hence describes an interaction. This interaction is the annihilation of an electron-positron pair into a photon, and is represented graphically in Fig. 5.2. [1] The vertex contains a three-point interaction, and it connects different kinds of lines. The undulating line represents a photon, while the solid lines are electrons. The arrows on the lines indicate in *which direction in time* the electron is moving, or interpreted in another way: Whether it is an electron or a positron. This vertex represents the only kind of interaction present in QED, thus all higher order diagrams can be constructed from it. For instance, the second order contribution to the pressure in QED is given by the two-loop diagram shown in Fig. 5.3.

Just as earlier, diagrams can be evaluated by following a set of rules, now the Feynman rules in QED:

- To each vertex assign a factor $ie\gamma^\mu$.
- Assign a photon propagator $\mathcal{D}_0$ to each photon line.
- Assign a Fermi propagator $\mathcal{S}$ to each fermion line.
- Multiply by a factor -1 for each closed fermion loop.
- Perform a trace operation over each closed fermion loop.
- Integrate over the momentum of each independent loop.
- Multiply by the symmetry factor of the diagram.

The free photon propagator in a covariant gauge is

$$\mathcal{D}^0_{\mu\nu} = \frac{1}{P^2}\left(g_{\mu\nu} - (1-\alpha)\frac{P_\mu P_\nu}{P^2}\right), \tag{5.29}$$

and the Fermi propagator is

$$\mathcal{S} = \frac{i}{\not{P} - m}. \tag{5.30}$$

In the Feynman gauge where $\alpha = 1$, and treating the electrons as massless, the two-loop diagram yields the following expression

[1] The process depicted in Fig 5.2 can not happen isolated in the vacuum, since the photon has zero mass, and it is thus impossible to conserve energy and momentum in this process.

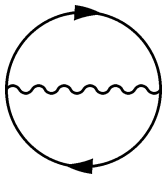

Figure 5.3: The second order contribution to the pressure in QED, often called the Sunset diagram.

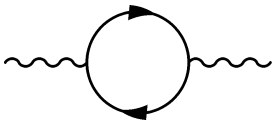

Figure 5.4: One-loop self-energy of the photon.

$$
\begin{aligned}
\mathcal{P}_2 &= \frac{1}{2}\sum\!\!\!\!\!\!\int_{\{PQ\}} \mathrm{Tr}\left\{\frac{1}{\not{P}} ie\gamma^\mu \frac{g_{\mu\nu}}{(P-Q)^2} ie\gamma^\nu \frac{1}{\not{Q}}\right\} \\
&= -(2-d)e^2 \sum\!\!\!\!\!\!\int_{\{PQ\}} \frac{\mathrm{Tr}\left\{\gamma^\alpha\gamma^\beta P_\alpha Q_\beta\right\}}{P^2(P-Q)^2Q^2} \\
&= -(2-d)\frac{d}{2}e^2\left(\sum\!\!\!\!\!\!\int_{\{PQ\}} \frac{1}{Q^2(P-Q)^2} + \sum\!\!\!\!\!\!\int_{\{PQ\}} \frac{1}{P^2(P-Q)^2} - \sum\!\!\!\!\!\!\int_{\{PQ\}} \frac{1}{P^2Q^2}\right) \\
&= -(2-d)\frac{d}{2}e^2\left(2\sum\!\!\!\!\!\!\int_{P} \frac{1}{P^2}\cdot\sum\!\!\!\!\!\!\int_{\{P\}} \frac{1}{P^2} - \Big(\sum\!\!\!\!\!\!\int_{\{P\}} \frac{1}{P^2}\Big)^2\right),
\end{aligned}
\tag{5.31}
$$

after a change of variable in the last line, so that $P' = P - Q = P$. Due to this those frequency sums run over $\omega_n - \omega_m = [(2n+1) - (2m-1)]i\pi T = 2(n-m)i\pi T = 2ki\pi T = \omega_k$, i.e. bosonic Matsubara frequencies. Both the bosonic and fermionic integrals are calculated in the Appendices, see Eqs. (B.18) and (B.26) respectively. Putting it all together and setting $d = 4$ in the end, the pressure to second order is

$$
\begin{aligned}
\mathcal{P}_2 &= (2-d)\frac{d}{2}e^2\left(\frac{T^2}{12\pi^2}\left(\frac{\mu^2}{4} + \frac{\pi^2T^2}{12}\right) + \frac{1}{4\pi^4}\left(\frac{\mu^2}{4} + \frac{\pi^2T^2}{12}\right)^2\right) \\
&= (2-d)\frac{d}{2}e^2\left(\frac{T^2\mu^2}{32\pi^2} + \frac{\mu^4}{64\pi^4} + \frac{5T^4}{576}\right) \\
&= -\frac{e^2}{288}\left(5T^4 + \frac{18\mu^2T^2}{\pi^2} + \frac{9\mu^4}{\pi^4}\right).
\end{aligned}
\tag{5.32}
$$

This is the same result as the one derived in [8], though the procedure is entirely different.

5.4 Photon self-energy tensor

When a photon propagates in a medium of charged particles, interactions cause it to acquire properties it does not have when propagating in the vacuum. This is referred to as the self-energy of the photon. What happens is that a

propagating photon may fluctuate into pairs of electrons and positrons, which propagate for a short period of time before annihilating, see Fig. 5.4. In QED, the photon self-energy is also referred to as *vacuum polarization*, an effect caused by the presence of charged particles. Using the QED Feynman rules, the expression for this process is

$$\begin{aligned}\Pi^{\mu\nu}(Q) &= e^2 \sum\!\!\!\!\!\!\int_{\{P\}} Tr\left\{\gamma^\mu \frac{1}{\not{P}}\gamma^\nu \frac{1}{\not{P}+\not{Q}}\right\} \\ &= 4e^2 \sum\!\!\!\!\!\!\int_{\{P\}} \frac{P^\mu (P+Q)^\nu + P^\nu (P+Q)^\mu - \delta^{\mu\nu} P\cdot(P+Q)}{P^2(P+Q)^2} \\ &= 8e^2 \sum\!\!\!\!\!\!\int_{\{P\}} \frac{P^\mu P^\nu}{P^2(P+Q)^2} + 4e^2 \sum\!\!\!\!\!\!\int_{\{P\}} \frac{P^\mu Q^\nu + Q^\mu p^\nu}{P^2(P^2+Q^2)} - 2e^2\delta^{\mu\nu} \sum\!\!\!\!\!\!\int_{\{P\}} \left(\frac{1}{P^2} + \frac{1}{(P+Q)^2} - \frac{Q^2}{P^2(P^2+Q^2)}\right). \end{aligned} \tag{5.33}$$

Under the assumption that the external photon momentum is zero, $Q \to 0$, the simplifies to

$$\Pi^{\mu\nu}(0) = 8e^2 \sum\!\!\!\!\!\!\int_{\{P\}} \frac{P^\mu P^\nu}{P^4} - 4e^2\delta^{\mu\nu} \sum\!\!\!\!\!\!\int_{\{P\}} \frac{1}{P^2}. \tag{5.34}$$

The temporal and spatial components are, with no summing over repeated indices implied,

$$\Pi^{00}(0) = 4e^2 \sum\!\!\!\!\!\!\int_{\{P\}} \frac{1}{P^2} - 8e^2 \sum\!\!\!\!\!\!\int_{\{P\}} \frac{\vec{p}^2}{P^4}, \tag{5.35}$$

$$\Pi^{ii}(0) = \frac{8}{d}e^2 \sum\!\!\!\!\!\!\int_{\{P\}} \frac{\vec{p}^2}{P^4} - 4e^2 \sum\!\!\!\!\!\!\int_{\{P\}} \frac{1}{P^2}, \tag{5.36}$$

having used that with zero external momentum, $\Pi^{\mu\nu} = 0$ when $\mu \neq \nu$, due to the fact that

$$\sum\!\!\!\!\!\!\int p^\mu = 0 \tag{5.37}$$

since the integrand is antisymmetric. Using Eq. (B.29) yields

$$\begin{aligned}\Pi^{00}(0) &= -4e^2(1+d) \sum\!\!\!\!\!\!\int_{\{P\}} \frac{1}{P^2}, \\ \Pi^{ij}(0) &= 0. \end{aligned} \tag{5.38}$$

And after evaluating the sum-integral,

$$\Pi^{00} = \frac{e^2T^2}{3} + \frac{e^2\mu^2}{\pi^2}, \tag{5.39}$$

where the chemical potential μ has been included through the substitution $p_0 \to p_0 \pm i\mu$. This equation defines the thermal mass of the photon, $m^2 \equiv \frac{e^2T^2}{3} + \frac{e^2\mu^2}{\pi^2}$.

The self-energy with nonzero external momentum can be calculated under the assumption that the four-momentum of the photon is much smaller than that of the fermions, so that $\not{Q}$ can be neglected with respect to $\not{P}$. Taylor expanding and keeping only terms to first order thus yields $\frac{1}{(P+Q)^2} \approx \frac{1}{P^2}$, and within this approximation the self-energy in Eq. (5.33) becomes

$$\Pi^{\mu\nu}(Q) \quad \simeq \quad e^2 \sum\!\!\!\!\!\!\int_{\{P\}} \frac{-4P^2\delta_{\mu\nu} + 8P_\mu P_\nu}{P^2(P-Q)^2}. \tag{5.40}$$

Now, the first term is easily evaluated using the Taylor expansion;

$$-4e^2 \sum\!\!\!\!\!\!\int_{\{P\}} \frac{P^2}{P^2(P-Q)^2} \simeq -4e^2 \sum\!\!\!\!\!\!\int_{\{P\}} \frac{1}{P^2} = \frac{e^2T^2}{6}, \tag{5.41}$$

while the second term is a little more cumbersome. Defining

$$I_{\mu\nu} \equiv \sum\!\!\!\!\!\!\int_{\{P\}} \frac{P_\mu P_\nu}{P^2(P-Q)^2}, \tag{5.42}$$

and evaluating first the spatial part

$$\begin{aligned} I_{ij} &= \sum\!\!\!\!\!\!\int_{\{P\}} \frac{p_i p_j}{P^2(P-Q)^2} \\ &= \sum\!\!\!\!\!\!\int_{\{P\}} \frac{\vec{p}^2\delta_{ij}}{P^2} + \sum\!\!\!\!\!\!\int_{i\neq j} \frac{p_i p_j}{P^2(P-Q)^2} \\ &= -\frac{T^2}{24}\delta_{ij} + \frac{T^2}{24}\int \frac{d\Omega}{4\pi}\frac{q_0}{Q\cdot\hat{P}}\hat{p}_i\hat{p}_j, \end{aligned} \tag{5.43}$$

where the integral has been split into one diagonal and one off-diagonal part. The diagonal part has been calculated assuming small Q again, and making use of Eq. (B.29). In the off-diagonal part, the sum over Matsubara frequencies is done first. Next the integral over momenta p is evaluated, while the angular integral is not. The light-like four-vectors are defined as $\hat{P} = (1, \hat{p})$.

Moving on to the temporal parts, these can be evaluated using the same methods;

$$\begin{aligned} I_{00} &= \sum\!\!\!\!\!\!\int_{\{P\}} \frac{p_0^2}{P^2(P-Q)^2} \\ &= \sum\!\!\!\!\!\!\int_{\{P\}} \frac{1}{(P-Q)^2} - \sum\!\!\!\!\!\!\int_{\{P\}} \frac{\vec{p}^2}{P^2(P-Q)^2} \\ &= -\frac{T^2}{24}\left(1 - \int \frac{\mathrm{d}\Omega}{4\pi}\frac{q_0}{Q\cdot\hat{P}}\right), \end{aligned} \tag{5.44}$$

and

$$I_{0i} = \frac{T^2}{24}\int \frac{\mathrm{d}\Omega}{4\pi}\frac{q_0}{Q\cdot\hat{P}}. \tag{5.45}$$

Collecting the results and identifying thermal photon mass $m^2 = \frac{e^2T^2}{3}$ at zero chemical potential, yields the self-energy

$$\Pi_{\mu\nu} = m^2\left(\int \frac{\mathrm{d}\Omega}{4\pi}\frac{q_0\hat{P}_\mu\hat{P}_\nu}{Q\hat{P}} - \delta_{\mu 0}\delta_{\nu 0}\right). \tag{5.46}$$

The self-energy can also be expressed in terms of the transverse and longitudinal projectors $P^{T/L}_{\mu\nu}$ as follows [6]

$$\Pi_{\mu\nu} = -\Pi_T P^T_{\mu\nu} - \frac{1}{n_p^2}\Pi_L P^L_{\mu\nu}, \tag{5.47}$$

where Π_T and Π_L are the transverse and longitudinal self-energies respectively. They are functions of the photon momentum and will be determined in the following. The projectors obey the relations

$$(P^{T/L})^2 = P^{T/L}, \qquad P^L P^T = P^T P^L = 0, \tag{5.48}$$

as well as the Ward identity $P_\mu \Pi_{\mu\nu} = 0$. In Euclidean space where $P_\mu = (p_0, \vec{p})$, they are given by

$$P^T_{\mu\nu} = \delta_{\mu\nu} - \frac{P_\mu P_\nu}{P^2} - P^L_{\mu\nu}, \tag{5.49}$$

$$P^L_{\mu\nu} = \frac{n_{p\mu} n_{p\nu}}{n_p^2}, \tag{5.50}$$

so they are both transverse in four dimensions, and $P^T_{\mu\nu}$ is transverse also in three dimensions, while $P^L_{\mu\nu}$ is longitudinal in three dimensions. The vector n_p^μ also satisfies $P \cdot n_p$=0, and

$$n_p^\mu \equiv n^\mu - \frac{n\cdot p}{P^2} P^\mu = n^\mu - \frac{p_0}{P^2} P^\mu, \tag{5.51}$$

$$n_p^2 = 1 - \frac{(n\cdot P)^2}{P^2} = 1 - \frac{p_0^2}{P^2}. \tag{5.52}$$

In the thermal rest frame, defined by $n^\mu = (1, \vec{0})$, its components are

$$n_p^0 = 1 - \frac{p_0^2}{P^2} = n_p^2, \tag{5.53}$$

$$n_p^i = -\frac{p_0 p_i}{P^2}.$$

This can be used to determine the components of the projection operators

$$P^L_{00} = n_p^2, \quad P^L_{i0} = -\frac{p_0 p_i}{P^2}, \quad P^L_{ij} = \frac{p_0^2}{n_p^2 P^2} \hat{p}_i \hat{p}_j,$$

$$P^T_{00} = P^T_{i0} = 0, \quad P^T_{ij} = \delta_{ij} - \hat{p}_i \hat{p}_j \left(1 + \frac{p_0^2}{n_p^2 P^2}\right). \tag{5.54}$$

Inserting the projection operators into Eq. (5.47) and writing out the components of the self-energy, yields the following relations for the longitudinal and transverse components

$$\Pi_L = -\Pi^{00}, \tag{5.55}$$

$$\Pi_T = \frac{1}{d-1}\left(\delta^{ij} - \frac{p^i p^j}{p^2}\right)\Pi^{ij}. \tag{5.56}$$

For a more explicit representation of Π_T and Π_L, $\Pi_{\mu\nu}(Q)$ is expressed in the frame where $Q = (q_0, 0, 0, q)$, with $\hat{Q} = (1, 0, 0, 1)$, i.e. $\vec{q}$ parallel to the z-axis. All other vectors $\vec{p}$ will then have components

$$p_x = \sin\theta \cos\phi, \tag{5.57}$$

$$p_y = \sin\theta \sin\phi, \tag{5.58}$$

$$p_z = \cos\theta, \tag{5.59}$$

with both angles θ and ϕ relative to the z-axis. From Eq. (5.55)

$$\begin{aligned}\Pi_L(q_0, q) &= -\Pi_{00} \\ &= -m^2\left(\int \frac{\mathrm{d}\Omega}{4\pi} \frac{q_0}{q_0 + q\cos\theta} - 1\right) \\ &= m^2\left(1 - \frac{q_0}{2q} \ln\frac{q_0+q}{q_0-q}\right),\end{aligned} \tag{5.60}$$

and from Eq. (5.56)

$$\begin{aligned}\Pi_T(\omega,q) &= \frac{1}{2}\left(\delta^{ij}-\frac{p^i p^j}{p^2}\right)\Pi^{ij}\\ &= \frac{1}{2}\left(\Pi_{xx}+\Pi_{yy}\right)\\ &= \frac{m^2}{2}\int\frac{\mathrm{d}\Omega}{4\pi}\left(\frac{q_0\sin^2\theta\cos^2\phi}{q_0+q\cos\theta}+\frac{q_0\sin^2\theta\sin^2\phi}{q_0+q\cos\theta}\right)\\ &= \frac{m^2 q_0}{2(d-1)}\int_0^\pi \mathrm{d}\theta\,\frac{\sin^3\theta}{q_0+q\cos\theta}\\ &= \frac{m^2 q_0^2}{(d-1)\,q^2}\left(1+\frac{q^2+q_0^2}{2q_0 q}\ln\frac{q_0+q}{q_0-q}\right).\end{aligned} \tag{5.61}$$

In order to express the total self-energy more compactly in d dimensions, the following tensor is introduced

$$\mathcal{T}^{\mu\nu}(p,-p) = \left\langle y^\mu y^\nu \frac{p\cdot n}{p\cdot y}\right\rangle_{\hat{y}}, \tag{5.62}$$

where the angular brackets indicate averaging over the spatial directions of the light-like vector $y=(1,\hat{y})$. The angular average can be expressed as an integral over the cosine of an angle, and doing this the expression for the 00 component of the tensor yields

$$\begin{aligned}\mathcal{T}^{00}(p,-p) &= \frac{\Gamma(2-2\varepsilon)}{\Gamma^2(1-\varepsilon)}2^{2\varepsilon-1}\int_{-1}^{1}\mathrm{d}x\,(1-x^2)^{-\varepsilon}\frac{p_0}{p_0-px}\\ &= \frac{p_0}{2p}\ln\frac{p_0+p}{p_0-p}, \qquad \varepsilon\to 0.\end{aligned} \tag{5.63}$$

In terms of this tensor the self-energy is

$$\Pi_{\mu\nu} = m^2\left(\mathcal{T}_{\mu\nu}(p,-p)-n_\mu n_\nu\right), \tag{5.64}$$

and its components are

$$\Pi_L(p) = m^2\Big(1-\mathcal{T}^{00}(p,-p)\Big), \tag{5.65}$$

$$\Pi_T(p) = \frac{m^2}{(d-1)n_p^2}\Big(\mathcal{T}^{00}(p,-p)-1+n_p^2\Big). \tag{5.66}$$

5.5 Pressure of photons to one-loop

As mentioned earlier in this chapter, propagating photons are affected by other particles present, causing the photons to acquire new properties due to interactions. The thermal mass is an example of such a property, and this section is dedicated to studying how the thermal photon mass could contribute to the pressure. The first order contribution to the pressure from the photons is

$$\mathcal{P}_{0a} = \frac{1}{2}\sum\!\!\!\!\!\!\int_P\Big\{(d-1)\ln\Delta_T(P)+\ln\Delta_L(P)\Big\}. \tag{5.67}$$

The propagator has thus split up, into a transverse part with $d-1$ degrees of freedom, and the remaining longitudinal part. This behaviour is described by introducing the transverse and longitudinal propagators

$$\Delta_L(P) = \frac{1}{-n_p^2P^2+\Pi_L(P)}, \tag{5.68}$$

$$\Delta_T(P) = \frac{1}{-P^2+\Pi_T(P)},$$

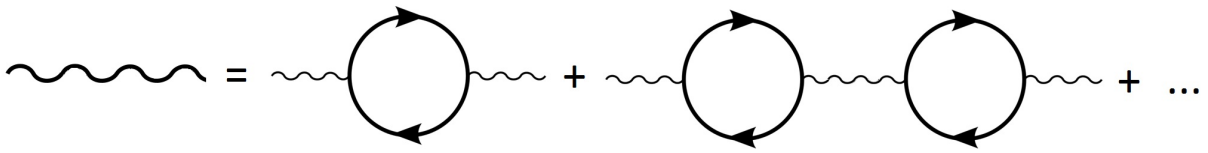

Figure 5.5: Diagrammatic representation of the sum of self-energy insertions in the photon propagator.

with the projectors and self-energy components derived earlier. Inserting for the propagators yields

$$\mathcal{P}_{0a} = -\frac{1}{2}\sum\!\!\!\!\!\!\int_P \left\{(d-1)\left(\ln P^2 + \ln\left(\tfrac{\Pi_T(P)}{P^2} - 1\right)\right) + \ln n_p^2 P^2 + \ln\left(\tfrac{\Pi_L(P)}{n_p^2 P^2} - 1\right)\right\}. \tag{5.69}$$

Using Eq. (5.52) to write $n_p^2 P^2 = P^2 - p_0^2 = \vec{p}^2$ in $\Pi_L(P)$ and $\Pi_T(P)$ from Eq. (5.65), and next Taylor expanding to second order in m results in

$$\begin{aligned}
\ln\left(\frac{\Pi_T}{P^2} - 1\right) &= i\pi - \frac{\Pi_T}{P^2} - \left(\frac{\Pi_T}{P^2}\right)^2 \\
&= i\pi - \frac{m^2}{(d-1)\vec{p}^2}\left(\mathcal{T}^{00} - 1\right) - \frac{m^2}{(d-1)P^2} + \mathcal{O}(m^4) \qquad (5.70)\\
\ln\left(\frac{\Pi_L}{\vec{p}^2} - 1\right) &= i\pi - \frac{\Pi_L}{\vec{p}^2} - \left(\frac{\Pi_L}{\vec{p}^2}\right)^2 \\
&= i\pi - \frac{m^2}{\vec{p}^2}\left(1 - \mathcal{T}^{00}\right) + \mathcal{O}(m^4). \qquad (5.71)
\end{aligned}$$

Inserting this into Eq. (5.67), both the imaginary terms as well as those containing $\mathcal{T}^{00}$ cancel, and the expression becomes

$$\mathcal{P}_{0a} = -\frac{1}{2}\sum\!\!\!\!\!\!\int_P \left\{(d-1)\ln P^2 + \frac{m^2}{P^2} + \frac{1}{2}\ln\vec{p}^2\right\}, \tag{5.72}$$

where the last term vanishes in dimensional regularization. Using the sum-integrals listed in App. (B.3) yields the final expression for the pressure

$$\mathcal{P}_{0a} = \frac{\pi^2 T^4}{45} - \frac{m^2 T^2}{12}. \tag{5.73}$$

First, it should be noted that the first term in the above expression is the same as the first one in Eq. (5.26), as it should be, since this is just the one-loop contribution from the photons, and should not depend on which method is used for calculating it. The other one, namely the mass-term, is a result of the Taylor expansion of the self-energies. Expanding to higher orders in m would have yielded contributions of order m^4, and so forth. Since m is proportional to the coupling constant, which must be small, these contributions are smaller in increasing order.

5.6 Ring diagrams

Just as in scalar field theory, there are ring diagrams in QED as well. Here, the ring diagrams are a consequence of the interactions between photons and their environment. The effective photon propagator $\mathcal{D}_{\mu\nu}$ in an interacting environment can be expressed as a series with the free propagator $\mathcal{D}^0_{\mu\nu}$ and insertions of the self-energy. The series is a recursive relation, expressed as follows

$$\mathcal{D}_{\mu\nu} = \mathcal{D}^0_{\mu\nu} + \mathcal{D}^0_{\mu\alpha}\Pi^{\alpha\beta}\mathcal{D}_{\beta\nu}, \tag{5.74}$$

where the free propagator is the one in Eq. (5.29). Using perturbation theory the expression for the effective photon propagator can be written as an infinite series in terms of the free propagator $\mathcal{D}^0_{\mu\nu}$. This procedure is illustrated pictorially in Fig. 5.5, displaying that each of the rings are just insertions of the self-energy. Writing out the expression yields

$$\frac{1}{2}\mathcal{D}^0_{\mu\alpha}\Pi^{\alpha\beta}\mathcal{D}^0_{\beta\nu}\Pi^{\nu\mu} - \frac{1}{3}\mathcal{D}^0_{\mu\alpha}\Pi^{\alpha\beta}\mathcal{D}^0_{\beta\nu}\Pi^{\nu\rho}\mathcal{D}^0_{\rho\sigma}\Pi^{\sigma\mu} + ..., \tag{5.75}$$

and using a more compact notation where the indices are not written out, this is identified as a logarithmic series;

$$\begin{aligned}
&\frac{1}{2}\Pi\mathcal{D}\Pi\mathcal{D} - \frac{1}{3}\Pi\mathcal{D}\Pi\mathcal{D}\Pi\mathcal{D} + ... \\
&= \sum_{n=2}^{\infty} \frac{(-1)^n}{n} (\Pi\mathcal{D})^n \\
&= \sum_{n=1}^{\infty} \frac{(-1)^n}{n} (\Pi\mathcal{D})^n - \Pi\mathcal{D} \\
&= \ln(1+\Pi\mathcal{D}) - \Pi\mathcal{D}.
\end{aligned} \tag{5.76}$$

So again the sum of an infinite series turns out to be convergent, yielding a finite contribution to the pressure. Inserting the free photon propagator from Eq. (5.29) and the self-energy from Eq. (5.47) yields

$$\begin{aligned}
\ln \mathcal{Z}_{ring} &= -\frac{1}{2} \sum\!\!\!\!\!\!\int_P \mathrm{Tr}\left\{\ln(1+\mathcal{D}_0\Pi) - \mathcal{D}_0\Pi\right\} \\
&= -\frac{1}{2} \sum\!\!\!\!\!\!\int_P \left\{2\ln\left(1-\frac{\Pi_T}{P^2}\right) + \ln\left(1-\frac{\Pi_L}{n_p^2 P^2}\right) + 2\frac{\Pi_T}{P^2} + \frac{\Pi_L}{n_p^2 P^2}\right\}.
\end{aligned} \tag{5.77}$$

The sum over Matsubara frequencies contained in the sum-integral is essentially a sum over n, since $\omega_n = 2\pi nT$ for bosons. As long as $n \neq 0$ it is safe to expand the logarithms, and the only potential infrared divergence, is the one that will arise if Π_T and Π_L do not vanish when $n = 0$ and $p \to 0$. This potential divergence would occur in the following part of the above integral

$$-\frac{1}{2}T\int_p \left\{2\ln\left(1+\frac{\Pi_T(0,0)}{P^2}\right) + \ln\left(1+\frac{\Pi_L(0,0)}{n_p^2 P^2}\right) - \frac{2\Pi_T(0,0)}{P^2} - \frac{\Pi_L(0,0)}{n_p^2 P^2}\right\}, \tag{5.78}$$

while the remaining terms are infrared safe. Rewriting them by Taylor expanding about $\Pi_T = 0$ and $\Pi_L = 0$, using $\ln(1-x) = -x - \frac{x^2}{2} + ...$, and then extracting the zero-mode from the sum over n yields

$$\begin{aligned}
\ln \mathcal{Z}_{ring} &\simeq \frac{1}{4}T\int_p \sum_n \left\{2\left(\frac{\Pi_T(n,p)}{P^2}\right)^2 + \left(\frac{\Pi_L(n,p)}{n_p^2 P}\right)^2\right\} \\
&= \frac{1}{4}T\int_p \left(\sum_{n\neq 0}\left\{2\left(\frac{\Pi_T(n,p)}{P^2}\right)^2 + \left(\frac{\Pi_L(n,p)}{n_p^2 P^2}\right)^2\right\}\right. \\
&\left. + 2\left(\frac{\Pi_T(0,p)}{p^2}\right)^2 + \left(\frac{\Pi_L(0,p)}{p^2}\right)^2 - 2\left(\frac{\Pi_T(0,0)}{p^2}\right)^2 - \left(\frac{\Pi_L(0,0)}{p^2}\right)^2\right),
\end{aligned} \tag{5.79}$$

where the last two terms have been subtracted to avoid double counting.

At $T = 0$ the frequency of the photon becomes continuous, the sum-integral turns into a four-dimensional integral, and the $n = 0$ mode can no longer be extracted. In the zero temperature limit,

$$\lim_{T\to 0} T\sum_n = \frac{1}{2\pi}\int_{-\infty}^{\infty} dp_0 \tag{5.80}$$

and $P^2 = p_0^2 + \vec{p}^2$ in Euclidean space. The new integration measure to be used is $d^4P = d\phi d\phi \sin^2\phi dP^2 P^2$, since $p_0 = P\sin\phi$. Both Π_L and Π_T are now functions of the momentum P and the angle ϕ, and Eq. (5.77) becomes

$$\ln \mathcal{Z}_{ring} = -\frac{1}{2}\frac{1}{(2\pi)^4}\int_0^{2\pi} d\theta \int_0^{\pi} d\phi \sin^2\phi \int_0^{\infty} dP^2 P^2 \times \tag{5.81}$$
$$\left\{2\ln\left(1-\frac{\Pi_T(\phi,P^2)}{P^2}\right)+\ln\left(1-\frac{\Pi_L'(\phi,P^2)}{P^2}\right)+2\frac{\Pi_T(\phi,P^2)}{P^2}+\frac{\Pi_L'(\phi,P^2)}{P^2}\right\},$$

where Π_L' is shorthand for $\frac{P^2}{p^2}\Pi_L$. Now, both Π_L and Π_T are proportional to m^2, and $m \sim e$. As the aim here is to find the pressure up to order $e^4 \ln e$, the terms which yield these contributions may be isolated, and the rest left out. Furthermore, the infrared divergences can be handled by introducing a fictious mass scale σ, which will be set to zero at the end. Introducing the mass scale where it is needed changes the above expression to the following

$$\ln \mathcal{Z}_{ring} = -\frac{1}{(2\pi)^3}\int_0^{\pi/2} d\phi \sin^2\phi \int_0^{\infty} dP^2 P^2 \left\{2\ln\left(1-\frac{\Pi_T(\phi,0)}{P^2}\right)+\right.$$
$$\left.+\ln\left(1-\frac{\Pi_L'(\phi,0)}{P^2}\right)+2\frac{\Pi_T(\phi,0)}{P^2}+\frac{\Pi_L'(\phi,0)}{P^2}+\frac{\Pi_L'(\phi,0)^2+2\Pi_T(\phi,0)^2}{2p^2(p^2+\sigma^2)}\right\},$$

which can be integrated analytically. Integrating over P^2 under the assumption that $\sigma \neq 0$ and σ^2 is real yields

$$\ln \mathcal{Z}_{ring} = -\frac{1}{(2\pi)^3}\int_0^{\pi/2} d\phi \sin^2\phi \times \tag{5.82}$$
$$\left\{\Pi_L'^2(\phi,0)\left(\ln\frac{-\Pi_L'(\phi,0)}{\sigma^2}-\frac{1}{2}\right)+2\Pi_T^2(\phi,0)\left(\ln\frac{-\Pi_T(\phi,0)}{\sigma^2}-\frac{1}{2}\right)\right\},$$

from which the $\mathcal{O}(e^4\ln e^2)$ terms can be isolated in

$$\ln \mathcal{Z}_{ring}^{(1)} = -\frac{\ln e}{(2\pi)^3}\int_0^{\pi/2} d\phi \sin^2\phi \left(2\Pi_T^2(\phi,0)+\Pi_L'^2(\phi,0)\right). \tag{5.83}$$

Evidently, the mass scale σ does not enter up to the current order, so it will not be necessary to subtract it from the final result. Using $\tan\phi = \frac{q}{q_0}$ and $Q^2 = q_0^2 + \vec{q}^2 = 0$ in Eqs. (5.55) and (5.56), yields

$$\Pi_L'(\phi,0) = \frac{1}{\sin^2\phi}\Pi_L(\phi,0) = -\frac{m^2}{\sin^2\phi}\left(1-\frac{\cot\phi}{2}\ln\frac{1+\tan\phi}{1-\tan\phi}\right) \tag{5.84}$$

$$\Pi_T(\phi,0) = \frac{m^2}{(d-1)}\left(\cot^2\phi - \frac{P^2}{2p^2}\cot\phi\ln\frac{1+\tan\phi}{1-\tan\phi}\right). \tag{5.85}$$

In Euclidean space, $\arctan x = \frac{i}{2}\ln\frac{i-x}{i+x}$. It looks much nicer in Minkowski space, and upon Wick rotating from imaginary to real time, the above expressions change to

$$\Pi_L'(\phi,0) = -m^2\left(\frac{1-\phi\cot\phi}{\sin^2\phi}\right) \tag{5.86}$$

$$\Pi_T(\phi,0) = \frac{m^2}{(d-1)}\left(\frac{\cos^2\phi-\phi\cot\phi}{\sin^2\phi}\right). \tag{5.87}$$

Inserting these expressions into Eq. (5.83) and evaluating the integral over ϕ in $d = 3$ spatial dimensions yields

$$\begin{aligned}\ln \mathcal{Z}^{(1)}_{ring} &= -\frac{m^4 \ln e}{(2\pi)^3} \int_0^{\pi/2} d\phi \frac{1}{\sin^2\phi} \left\{ \frac{1}{2} (\cos^2\phi - \phi \cdot \cot\phi)^2 + (1 - \phi \cdot \cot\phi)^2 \right\} \\ &= -\frac{\mu^4 e^4 \ln e^2}{128\pi^6},\end{aligned} \tag{5.88}$$

having inserted the thermal mass $m^2 = \frac{e^2\mu^2}{\pi^2}$ at $T = 0$. The total contribution to the pressure at $T = 0$ through order $e^4 \ln e^2$ is thus

$$\mathcal{P} = \frac{\mu^4}{12\pi^2} \left(1 - \frac{3}{2} \frac{e^2}{4\pi^2} - \frac{3}{2} \left(\frac{e^2}{4\pi^2} \right)^2 \ln e^2 \right). \tag{5.89}$$

The first term in the above expression is the one obtained when setting $T = 0$ in Eq. (5.26), and the second term corresponds in the same way to Eq. (5.32). It is worth noting that all the terms come from loops with fermions, i.e. at $T = 0$ neither photons nor ghosts contribute to the pressure. This is due to the fact that they are massless and have no chemical potential, thus T is the only relevant scale.

5.7 Fine structure constant

Just as in scalar field theory, the above expression for the pressure is a perturbative expansion. Defining $\alpha \equiv \frac{e^2}{4\pi}$, or $\alpha = \frac{e^2}{4\pi\varepsilon_0\hbar c}$ in standard units, this is called the *fine structure constant* in QED. It is dimensionless, i.e. it has the same value of $\alpha \simeq \frac{1}{137}$ in all unit systems. Furthermore, since it is quite small, QED is said to be weakly coupled. This means that each extra correction, or each extra electron-positron pair, contribute less by a factor 0.007299..., i.e. much smaller than one, making the perturbative expansion valid. The value of the fine structure constant is not predicted by the theory, so it must be measured experimentally.

Due to fluctuations in and out of the vacuum, space-time is full of electron-positron pairs being created and annihilated. If one tries to measure the charge of the electron at large distances, the described phenomenon makes this task difficult. The electrons popping into existence are repelled by the electron one tries to measure, and the positrons are attracted to it. A photon propagating in the vicinity of said electron, has a weaker coupling to it the farther it moves away. Conversely, at short distances the photon has a strong coupling to the electron. This phenomenon is called *charge screening*, and since the coupling constant is a measure of the strength of interactions, its value is altered by this effect.

From the above discussion it follows that the quantum vacuum is just as much a dielectric as ordinary matter, which poses an experimental problem: At which energy scale is the fine structure "constant" measured? It is obviously not constant since it depends on the energy scale, and more properly it should be defined as

$$\alpha(\Lambda) = \frac{e^2(\Lambda)}{4\pi}, \tag{5.90}$$

where Λ is the energy scale. This effect was first measured by [21], and has since then been studied extensively, proving vacuum polarization to be a real physical effect, increasing over distance.

As it turns out, the effective charge measured in QED increases with the energy scale, and the true scaling behaviour of $\alpha(\Lambda)$ at large energy scales is not known. However, the behaviour of the coupling at small energy scales, which correspond to large distances, is well understood. The coupling decreases as one moves farther away from the charge, and the electric potential decreases as

$$V(r) = \frac{e^2}{4\pi r} = \frac{\alpha}{r}, \tag{5.91}$$

the well-known Coulomb potential.

Chapter 6

QCD

The following chapter is devoted to the discussion of the strong interaction, and the ultimate goal is to find an equation of state at zero temperature. The previous discussion of QED serves as a good starting point for discussing strong interactions, since these two theories are described using the same formalism. The theory of strong interactions, or quantum chromodynamics (QCD), is a non-Abelian $SU(3)$ gauge theory. Since QED is a $U(1)$ gauge theory, the generalization of previous results to QCD will involve mostly group-theoretical factors, in addition so some other corrections.

QCD is the theory describing quarks and gluons in the same way as QED describes electrons and photons. The main difference between the two is that QCD has three charges, called colours. A quark can thus be written as a vector with the three colour states

$$\Psi = \begin{pmatrix} \Psi_r \\ \Psi_g \\ \Psi_b \end{pmatrix}, \tag{6.1}$$

for the three colours red, green and blue. The colour charge is mediated by the QCD gauge field, the gluon. In addition to being colour mediators, the gluons themselves carry colour charge and are thereby able to interact amongst themselves, another contrast to QED.

The special unitary group $SU(N)$ has $N_g = N^2 - 1$ generators, corresponding to the number of charge mediating particles. Thus with $N = 3$ the group is said to have dimension eight, corresponding to eight gluons in QCD. The group thus has a set of eight linearly independent generators, and one choice of a possible representation are the Gell-Mann matrices λ_i. These matrices obey the commutation relations

$$\left[\lambda_i, \lambda_j\right] = i\varepsilon^{ijk}\lambda_k, \tag{6.2}$$

are traceless, and have the normalization relation Tr $\lambda_i\lambda_j = 2\delta_{ij}$. These properties are most convenient and also quite elegant, since they generalize the Pauli matrices, which form a basis for $SU(2)$; the spin group. The ε^{ijk} are numbers, called the *structure constants* of the group, and they are totally antisymmetric, so that ε^{ijk} vanishes if two of the indices are equal.

As mentioned earlier, this group is non-Abelian, reflected by the fact that its generators do not commute. This has implications on the gauge field carrying the charge of the theory, which will be discussed further on.

The following discussion starts with a presentation of the QCD Lagrangian and a short treatment of interactions in QCD. The interactions result in new kinds of vertices not present in QED, which in turn give rise to diagrams not encountered before. All these extra challenges will be handled step by step, and the discussion ends with the calculation of ring diagrams and derivation of the pressure for quark matter.

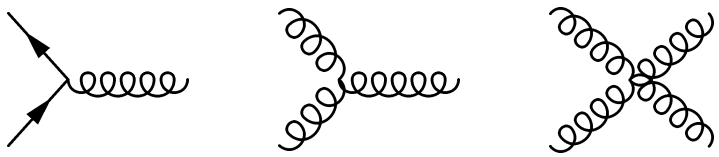

Figure 6.1: The QCD vertices. The first one connects the solid lines representing incoming and outgoing quarks with a spiral line, representing a gluon. The last two are three- and four-point interactions between gluons.

6.1 Lagrangian and interactions

The QCD Lagrangian is

$$\mathcal{L} = \bar{\Psi}_{ab}\left(i\partial\!\!\!/ - m_q\right)\Psi_{ab} - g\left(\bar{\Psi}_{ab}\lambda_i\Psi_{ab}\right)A\!\!\!/^i - \frac{1}{4}G^i_{\mu\nu}G^{\mu\nu}_i, \tag{6.3}$$

where the Ψ_{ab} are quark spinors with colour $a = (r,g,b)$ and b denotes the quark type, or flavour. There are six quark flavours in total. The above Lagrangian is very similar to the full QED Lagrangian (5.17), with the differences that another set of indices has appeared, and the electromagnetic field strength tensor has been replaced by the gluonic field strength tensor $G^i_{\mu\nu}$. Analysing the Lagrangian step by step, the first term describes non-interacting quarks with mass m_q. The second term is the quark-gluon interaction with the QCD coupling g, depicted first in Fig 6.1. One feature not present in QED is the presence of the λ_i matrices mentioned earlier, which change the colour (or "colour charge"?) of the interacting particles. Finally, $G^i_{\mu\nu}$ represents the gluon fields. These fields must be invariant under gauge transformations, which can be accomplished by defining [10]

$$G^{\mu\nu}_i \equiv F^{\mu\nu}_i + g\varepsilon_{ijk}A^\mu_j A^\nu_i, \tag{6.4}$$

and the second term in this expression gives rise to gluon-gluon interactions. This can be seen by multiplying out the last term in the Lagrangian (6.3), which yields the following

$$\mathcal{L}_G = -\frac{1}{4}F_{i\mu\nu}F^{\mu\nu}_i + g\varepsilon ijkA_{i\mu}A_{j\nu}\partial^\mu A^\nu_k - \frac{1}{4}g^2\varepsilon_{ijk}\varepsilon_{ilm}A^\mu_j A^\nu_k A_{l\mu}A_{m\nu}. \tag{6.5}$$

The first term is the Lagrangian for eight non-interacting, massless spin 1 gluon fields. Meanwhile, the second and third terms represent interactions of gluon fields amongst themselves. This generates three- and four-point vertices in perturbation theory, depicted in Fig. 6.1. This last feature has no analogue in QED, as photons do not interact amongst themselves.

A fundamental property of QCD is *flavour independence*; the strength of the quark-gluon interactions do not depend on the quark flavour. This will be most convenient when calculating vacuum diagrams and deriving the EoS, as it will not be necessary to specify which quarks participate in the interactions.

6.2 From QED to QCD

To lowest order, quark matter is an ideal gas of quarks and gluons, so just as in QED the first order correction to the pressure is of zeroth order in the coupling. Recalling the expression for the pressure of a non-interacting gas in QED, Eq. (5.26) can now be modified to suit QCD. In the $T = 0$ limit, neither purely gluonic nor ghost contributions are present, analogous to the case for photons. All interactions involving quarks must now be multiplied by 3 for each of the colour states, and the assumption that all quarks have equal chemical potentials is made. In the zero temperature limit, the pressure to lowest order is thus

$$\mathcal{P}_0 = N_f\frac{\mu^4}{4\pi^2}, \tag{6.6}$$

where N_f denotes the number of quark flavours.

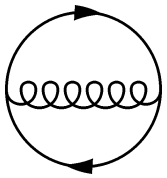

Figure 6.2: The sunset diagram in QCD.

Before moving on to treat corrections due to interactions, a closer look at the λ matrices and the structure constants is due. These objects characterize the group structure by two more relations;

$$\varepsilon^{ikl}\varepsilon^{jkl} = N\delta^{ij}, \tag{6.7}$$

$$\sum_i \lambda^i\lambda^i = \frac{N^2-1}{2N}\mathrm{I}_N, \tag{6.8}$$

and taking the trace of the last equation yields

$$\begin{aligned}\mathrm{Tr}\,\lambda_i\lambda_i &= \frac{N^2-1}{2N}\mathrm{Tr}\,\mathrm{I}_N \\ &= \tfrac{1}{2}N_g.\end{aligned} \tag{6.9}$$

Recalling the Feynman rules in QED, they state that a trace operation must be made for each closed fermion loop. According to the QCD Lagrangian, a matrix λ is present at each vertex, so each fermion loop with interactions gives rise to the trace of two λ matrices. The first QCD vacuum diagram with interactions is the equivalent to the sunset diagram, Fig. 6.2. It is evaluated in the same way as in QED, but the replacement $e^2 \to \frac{1}{2}g^2N_g$ must be made in Eq. (5.32), in correspondence with the above calculation of the trace. In addition, a factor N_g must be included, counting the number of gluons which could be present in the interaction. Making these two changes, the second order contribution to the pressure at zero temperature becomes

$$\begin{aligned}\mathcal{P}_2 &= -N_f N_g \frac{\mu^4 g^2}{64\pi^4} \\ &= -N_f N_g \frac{\mu^4 \alpha_s}{16\pi^2},\end{aligned} \tag{6.10}$$

having introduced the fine structure constant of the strong interaction $\alpha_s = \frac{g^2}{4\pi}$, which will be discussed later.

Other two-loop diagrams which might have contributed to the pressure are the ones shown in Fig. 6.3. The first one of these has ghost-gluon interactions, and another contrast to QED is that the ghosts which arise in QCD can not be eliminated by a change of gauge [25]. However, since all ghost-gluon and gluon-gluon contributions are purely of order T^4, they vanish at zero temperature and need not be taken into account in the present discussion.

6.3 Ring diagrams in QCD

Proceeding in the same way as in Section 5.6 when calculating the ring sum in QED, yields

$$\begin{aligned}\ln \mathcal{Z}_{ring} = &-\frac{1}{(2\pi)^3}\int_0^{\pi/2}\phi\sin^2\phi\times \\ &\left\{\Pi_L'^2(\phi,0)\left(\ln\frac{-\Pi_L'(\phi,0)}{\sigma^2}-\frac{1}{2}\right)+2\Pi_T^2(\phi,0)\left(\ln\frac{-\Pi_T(\phi,0)}{\sigma^2}-\frac{1}{2}\right)\right\}.\end{aligned} \tag{6.11}$$

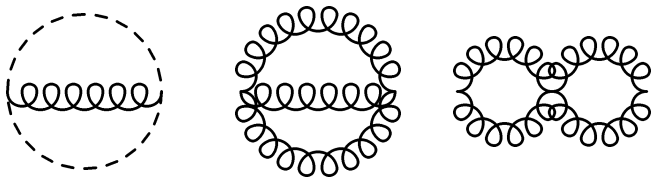

Figure 6.3: Interactions between ghosts and gluons at two-loop order.

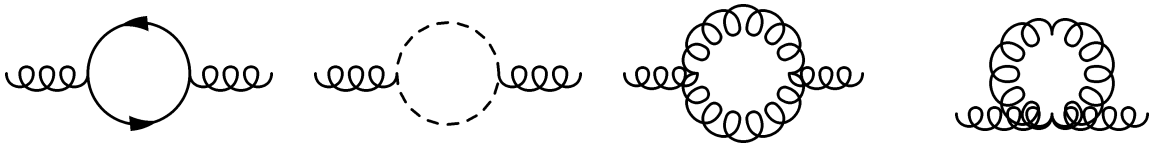

Figure 6.4: The one-loop gluon self-energies.

Since both Π_L and Π_T are proportional to the thermal mass squared, an expression for the thermal mass for gluons is needed. At zero temperature this is just Eq. (5.39) with the modification that the quark chemical potentials μ must be summed up. Under the assumption that all chemical potentials are equal, the summation only gives rise to a factor N_f, and the thermal gluon mass is

$$m_g^2 = N_f \frac{\mu^2 g^2}{\pi^2}. \tag{6.12}$$

Extracting the interesting pieces, that is everything up to order $\alpha_s^2 \ln \alpha_s$, from $\ln \mathcal{Z}_{ring}$ and inserting the thermal gluon mass yields

$$\begin{aligned} \ln \mathcal{Z}_{ring} &= -\frac{m_g^4 \ln m_g}{(2\pi)^3} \frac{\pi}{8} \\ &= -N_f^2 \frac{\mu^4}{4\pi^2} \left(\frac{\alpha_s}{\pi} \right)^2 \ln \frac{\alpha_s}{\pi} + \mathcal{O}(\alpha_s^2). \end{aligned} \tag{6.13}$$

The final expression for the pressure in QCD through order $\alpha_s^2 \ln \alpha_s$ is thus

$$\mathcal{P} = N_f \frac{\mu^4}{4\pi^2} \left\{ 1 - \frac{N_g}{4} \frac{\alpha_s}{\pi} - N_f \left(\frac{\alpha_s}{\pi} \right)^2 \ln \frac{\alpha_s}{\pi} \right\}. \tag{6.14}$$

This is the EoS for quark matter at zero temperature, in accordance with [26].

6.4 Running coupling

In QED the vacuum acquires dielectric properties due to the creation of virtual electron-positron pairs, causing the effective electric charge, and thereby also the coupling constant, to decrease at large distances. The described phenomenon is also present in QCD, as gluons split into virtual quark-antiquark pairs. This process is depicted first in Fig. 6.4. Additionally, since the gauge fields in non-Abelian gauge theories carry charge and couple amongst themselves, they also produce a screening effect. Just as in QED, there are also ghost fields with non-physical degrees of freedom

present, and they also couple to the gluons. The extra corrections are represented by the remaining diagrams in Fig. 6.4, and as it turns out, the net effect of polarization of virtual gluons in the vacuum is not to screen the field, but to augment it. The contribution is thus *opposite in sign*, giving rise to an *antiscreening* effect, which competes with the conventional charge screening. Which effect wins this competition and thereby dominates, must of course be worked out quantitatively. This is done in [27], and the result is that the anti-screening effect is stronger by a factor of twelve. The result of this is remarkable: It enables the coupling constant to be amplified at large distances.

This phenomenon is called *asymptotic freedom*, and it is a property which causes interactions between particles to become weaker at large energy scales, and stronger at small scales. The result is that quarks are confined into either baryons or mesons, which are colourless states consisting of three and two quarks respectively. In fact, coloured states have never been observed in nature, and it is believed that quarks cannot exist freely.

It also turns out that asymptotic freedom is a special property of non-Abelian gauge theories; among renormalizable quantum field theories, only the non-Abelian gauge theories are asymptotically free [28].

One way to study how the coupling α_s depends on the energy scale Λ is via the renormalization group. Here, the behaviour of the *running coupling* $\alpha_s(\Lambda)$ is encoded in the *beta function*. The renormalisation group equation

$$\beta(g_r) \equiv \Lambda \frac{\partial g_r}{\partial \Lambda} = -(11 - \frac{2}{3}N_f)\frac{g_r^3}{16\pi^2} + \mathcal{O}(g^5) \tag{6.15}$$

expresses the evolution of the coupling constant in a differential equation. This equation stems from the relationship between the bare coupling g appearing in the Lagrangian, and the renormalized coupling g_r.

When the beta function is negative, the coupling constant of the theory decreases at high energy. This is obvious from the above equation; as long as the number N_f of quark flavours is less than 17, the coupling g_r decreases with increasing Λ, and the theory is asymptotically free.

The renormalisation group equation can also be expressed in terms of the running coupling strength

$$\alpha_s(\Lambda) \equiv \frac{g_r^2}{4\pi}, \tag{6.16}$$

changing Eq. (6.15) into

$$\Lambda \frac{\partial \alpha_s}{\partial \Lambda} = -\frac{33 - 2N_f}{6\pi}\alpha_s^2. \tag{6.17}$$

Integrating this equation yields

$$\frac{33 - 2N_f}{6\pi}\Big[\ln \Lambda\Big]_{\Lambda_0}^{\Lambda} = \Big[\frac{1}{\alpha_s}\Big]_{\Lambda_0}^{\Lambda}, \tag{6.18}$$

and after tidying up

$$\alpha_s(\Lambda) = \frac{\alpha_s(\Lambda_0)}{1 + \frac{33-2N_f}{12\pi}\alpha_s(\Lambda_0)\ln\frac{\Lambda^2}{\Lambda_0^2}}. \tag{6.19}$$

The integration limit Λ_0 is an arbitrarily chosen reference scale, so the value of $\alpha_s(\Lambda_0)$ must be determined experimentally. To leading order in perturbation theory the above expression is series expanded like $\frac{1}{1+x} \simeq 1 + x + ..$ as follows

$$\begin{aligned}
\frac{\alpha_s(\Lambda_0)}{1 + \frac{33-2N_f}{12\pi}\alpha_s(\Lambda_0)\ln\frac{\Lambda^2}{\Lambda_0^2}} &\equiv \frac{\alpha_{s,0}}{1 + K\alpha_{s,0}} \\
&= \frac{1}{K}\frac{1}{1 + \frac{1}{\alpha_{s,0}K}} \\
&\simeq \frac{1}{K},
\end{aligned} \tag{6.20}$$

yielding the running coupling constant to one-loop order

$$\alpha_s(\Lambda) = \frac{12\pi}{(33 - 2N_f)\ln\frac{\Lambda^2}{\Lambda_0^2}}. \tag{6.21}$$

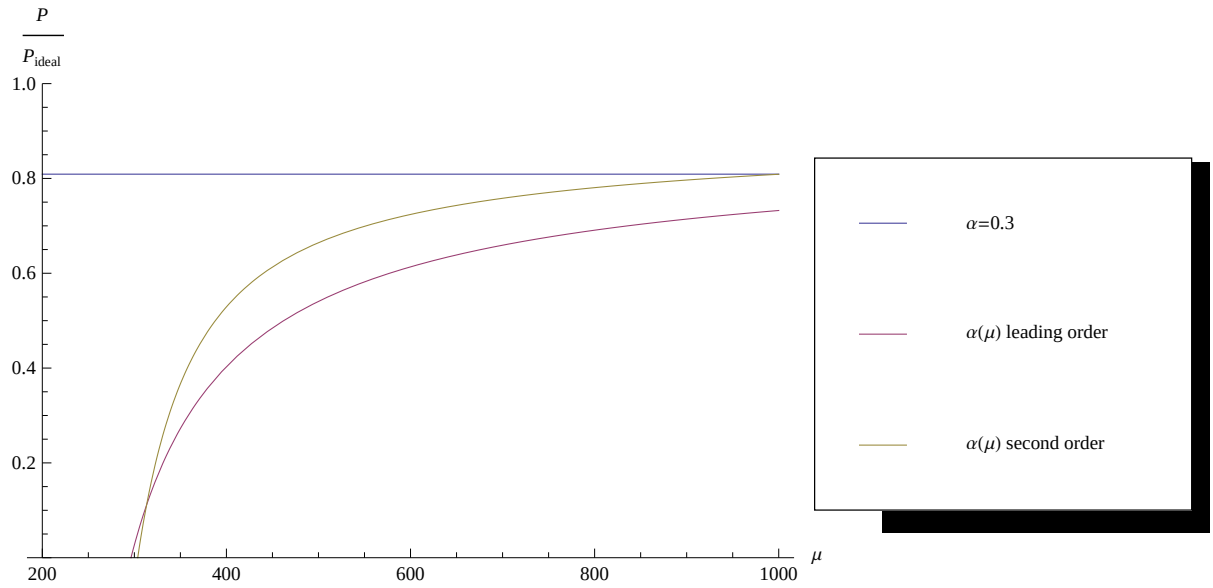

Figure 6.5: The pressure normalized to the ideal pressure, as a function of the chemical potential, for constant α_s, and $\alpha_s(\Lambda)$ to one- and two-loop order. $\Lambda = 2\mu$.

Since the renormalized coupling is a series expansion, the beta function must be a series as well. This can be expressed as

$$\beta(\alpha_s) = -\beta_0\alpha_s^2 - \beta_1\alpha_s^3 - \beta_2\alpha_s^4 - \ldots, \tag{6.22}$$

and it turns out that the two first coefficients, β_0 and β_1, are independent of the renormalisation scheme [22]. Through two loops, the coupling constant is [23]

$$\alpha_s(\Lambda) = \frac{4\pi}{\beta_0 L}\left(1 - 2\frac{\beta_1}{\beta_0^2}\frac{\ln L}{L}\right). \tag{6.23}$$

In this equation,

$$\begin{aligned}\beta_0 &= 11 - \frac{2}{3}N_f \\ \beta_1 &= 51 - \frac{19}{3}N_f \\ L &= \ln\frac{\Lambda^2}{\Lambda^2_{\overline{\text{MS}}}},\end{aligned} \tag{6.24}$$

and the reference scale Λ_0 has been replaced by the renormalisation scale in the $\overline{\text{MS}}$ scheme. The scale $\Lambda_{\overline{\text{MS}}}$ can be determined using experimental data. It is fixed by requiring that $\alpha_s = 0.3089$ at $\Lambda = 2$ GeV [15]; for $N_f = 3$ it is $\Lambda_{\overline{\text{MS}}} = 365$ MeV.

Since the relevant scale in our case is the chemical potential μ, it serves to make the replacement $\Lambda \to \mathcal{K}\mu$, with $\mathcal{K}$ a dimensionless number. Using this replacement, the pressure has been calculated with a constant coupling, and the running coupling to one- and two-loop order. This is displayed in Fig. 6.5, and it is evident that using a constant α_s yields a very different behaviour than with the running $\alpha_s(\Lambda)$.

Chapter 7

General relativity

Einsteins general theory of gravity describes the interaction between matter, including fields, and four-dimensional space-time. In doing so it describes gravity as a geometric property of the curved space-time, and relates the curvature to the mass-energy and momentum of both matter and radiation. These relations are specified by the Einsteins field equations [12], which are discussed in this chapter, Eq. (7.18). In the non-relativistic limit, general relativity reduces to Newtonian dynamics, and for sufficiently small masses it reduces to special relativity. However, its astrophysical applications are more interesting for the present discussion, and these are all in the ultra-relativistic limit. General relativity predicts significant relativistic effects in dense stars [5].

7.1 Formalism

In differential geometry, the metric tensor defined on a manifold, is a function which takes a pair of tangent vectors as input and produces a real number, i.e. a scalar. The metric tensor is a fundamental object in general relativity, since it describes the structure of space-time, and so defines the inner product and physical quantities such as distance, volume, angle and curvature.

With no matter present, special relativity is a good approximation, and space-time is described by the Minkowski metric $\eta_{\mu\nu}$. Euclidean space is the three-dimensional Euclidean plane, as well as its generalizations to higher dimensions, so in Euclidean space the metric tensor is just the Kronecker delta $\delta_{\mu\nu}$.

When treating stars, which have a strong gravitational field and therefore curve space-time, the flat-space metric does not serve to describe the geometry. Under the assumption that the simplest stars are spherical symmetric and that the gravitational field is static and isotropic, the most general metric tensor is [12]

$$g_{\mu\nu} = \begin{pmatrix} -B(r) & 0 & 0 & 0 \\ 0 & A(r) & 0 & 0 \\ 0 & 0 & r^2 & 0 \\ 0 & 0 & 0 & r^2 sin^2\theta \end{pmatrix}. \tag{7.1}$$

Another important tensor is the *Riemann curvature tensor*, and it is defined in terms of *Christoffel symbols*:

$$R^{\lambda}_{\mu\gamma\nu} \equiv \Gamma^{\lambda}_{\mu\nu,\gamma} - \Gamma^{\lambda}_{\mu\gamma,\nu} + \Gamma^{\alpha}_{\mu\nu}\Gamma^{\lambda}_{\alpha\gamma} - \Gamma^{\alpha}_{\mu\gamma}\Gamma^{\lambda}_{\alpha\nu}, \tag{7.2}$$

where the compact notation $\partial_\gamma \Gamma^{\lambda}_{\mu\nu} \equiv \Gamma^{\lambda}_{\mu\nu,\gamma}$ is used. Space-time is considered flat if the Riemann tensor vanishes everywhere. The Christoffel symbol is a purely geometrical object, being a function of only the metric and its derivatives. The curvature at a point in space is fully described by this tensor, defined as

$$\Gamma^{\lambda}_{\mu\nu} \equiv \frac{1}{2} g^{\lambda\rho} \left(g_{\rho\mu,\nu} + g_{\rho\nu,\mu} - g_{\mu\nu,\rho} \right). \tag{7.3}$$

Inserting the expression for the Christoffel symbol into the Riemann tensor, reveals the following symmetries

$$\begin{aligned} R_{\lambda\mu\gamma\nu} &= -R_{\mu\lambda\gamma\nu} = -R_{\lambda\mu\nu\gamma} = R_{\gamma\nu\lambda\mu} \\ R_{\lambda\mu\gamma\nu} &+ R_{\mu\nu\lambda\gamma} + R_{\lambda\nu\mu\gamma} = 0. \end{aligned} \tag{7.4}$$

Because of these symmetries, the Riemann tensor has only twenty independent components in 4-dimensional space-time. The contracted Riemann tensor, often referred to as the *Ricci tensor*, is obtained from the Riemann tensor by contracting over two of the indices

$$R_{\mu\nu} \equiv R^{\gamma}_{\mu\gamma\nu} = \partial_\nu \Gamma^\lambda_{\mu\lambda} - \partial_\lambda \Gamma^\lambda_{\mu\nu} - \Gamma^\rho_{\mu\lambda}\Gamma^\lambda_{\nu\rho} - \Gamma^\rho_{\mu\nu}\Gamma^\lambda_{\lambda\rho}. \tag{7.5}$$

This tensor is symmetric, so it has at most ten independent quantities. It can be contracted further, yielding the curvature scalar, or Ricci scalar

$$\mathcal{R} \equiv g^{\mu\nu} R_{\mu\nu}. \tag{7.6}$$

The Bianchi identities [12] are another important symmetry of the Riemann tensor

$$R_{\lambda\mu\gamma\nu;\alpha} + R_{\mu\lambda\alpha\gamma;\nu} + R_{\lambda\mu\nu\alpha;\gamma} = 0. \tag{7.7}$$

The notation $V_{\mu;\nu}$ with the semicolon denotes covariant differentiation[1], defined as follows

$$V_{\mu;\nu} = V_{\mu,\nu} - \Gamma^\lambda_{\mu\nu} V_\lambda \,. \tag{7.8}$$

This is done because the ordinary derivative of a tensor does not in general yield another tensor, while the covariant derivative always does. A good discussion of the issue as well as a derivation of the above expression can be found in [12]. After contracting, the Bianchi identities yield the following relation

$$R^{\mu\nu}_{;\mu} = \frac{1}{2} g^{\mu\nu} \mathcal{R}_{;\mu}, \tag{7.9}$$

which will be needed shortly. The *Einstein tensor* is defined in terms of the Ricci tensor and Ricci scalar as

$$G_{\mu\nu} \equiv R_{\mu\nu} - \frac{1}{2} g_{\mu\nu} \mathcal{R}. \tag{7.10}$$

From Eq. (7.9), a very important property of the Einstein tensor is

$$G_{\mu\nu;\mu} = 0. \tag{7.11}$$

The *energy momentum tensor* $T^{\mu\nu}$ describes the density and flows of the 4-momentum. The component $T^{\mu\nu}$ is the flow of the μ component in the ν direction, i.e. crossing the surface of constant x^ν. Thus T^{00} represents the energy density, T^{i0} the density of the i-component of momentum, and T^{0i} and T^{ij} flow and stress, respectively.

A *perfect fluid* is a fluid which has no viscosity nor heat conduction. It is thus fully parameterized by its energy density ε and the pressure p. Its energy momentum tensor is

$$T_{\mu\nu} = p\, g_{\mu\nu} + (p + \varepsilon) U_\mu U_\nu, \tag{7.12}$$

where U^μ is the four-velocity. Since p and ε are proper quantities, they must both be scalars, measured by an observer with locally inertial coordinates, moving with the fluid at the instant of the measurement. Conservation equations for the energy and momentum are given by

$$T_{\mu\nu;\nu} = 0. \tag{7.13}$$

The above expression incorporates both energy and momentum conservations in a general metric, and in the limit of flat space-time, it reduces to

$$\frac{\partial T^{\mu\nu}}{\partial x^\nu} = 0, \tag{7.14}$$

from which the traditional expressions for energy-momentum conservation are recovered.

[1] The covariant derivative in general relativity plays the same role as the one defined in the discussion of QED, Eq. (5.27): They both serve to make the theory invariant under transformations, and the gauge covariant derivative is a generalization of the one defined here.

7.2 Einstein's field equations

The gravitational field, its sources and their mutual interactions are described by Einsteins field equations. These equations must describe two parts of a dynamical picture: They must describe how particles behave in response to gravity, and also how particles generate gravitational effects. The first part is answered by the geodesic equation

$$\ddot{x}^\lambda - \Gamma^\lambda_{\mu\nu}\dot{x}^\mu\dot{x}^\nu = 0, \tag{7.15}$$

which is the equation of motion in an arbitrary gravitational field and arbitrary coordinate system [12], i.e. the relativistic analogue of Newton's equation of motion. The second part can be responded to by finding an analogue of the Poisson equation

$$\nabla^2\Phi(\vec{x}) = 4\pi G\rho(\vec{x}), \tag{7.16}$$

which describes how matter curves space-time. Moreover, it is obvious that the field equations must be on tensor form.

When Einstein first derived the field equations, he argued about their form on physical grounds, which is probably the most enlightening way to derive them. From Newtonian gravity it is known that the rest mass generates gravitational effects, and from special relativity that rest mass is just some form of energy. Therefore it is expected that sources of both energy and momentum contribute to the curvature of space-time. Due to this it is natural to assume that the energy momentum tensor is the source of space-time curvature, and one side of the equations should be $\mathcal{C}T^{\mu\nu}$, where $\mathcal{C}$ is some constant. The form of the geodesic equation indicates that the other side of the equations should contain derivatives and second derivatives of the metric. Finally, Eq. (7.13) states that the covariant derivative of this other side must also vanish. According to Eq. (7.11), the Einstein tensor is thus a viable candidate, as it is also a combination of the Ricci tensor, which incorporates the curvature of space-time. Based on this reasoning, it is expected that the field equations are

$$G_{\mu\nu} = R_{\mu\nu} - \frac{1}{2}g_{\mu\nu}\mathcal{R} = \mathcal{C}T_{\mu\nu}. \tag{7.17}$$

By matching this equation in the Newtonian limit to the Poisson equation, the constant is determined, yielding the Einstein's field equations

$$R_{\mu\nu} - \frac{1}{2}g_{\mu\nu}R = -8\pi G T_{\mu\nu}. \tag{7.18}$$

7.3 Relativistic hydrostatic equilibrium

Hydrostatic equilibrium is the condition where a fluid is at rest or moving with a constant velocity. This means that in a comoving reference frame, only the temporal component of the four-velocity U_0 is nonzero. Furthermore, all time-derivatives of $g_{\mu\nu}$, p and ε vanish. In particular,

$$\begin{aligned}
&\partial_\nu\Big((p+\varepsilon)U^\mu U^\nu\Big) = 0,\\
&\Gamma^\mu_{00} = -\tfrac{1}{2}g^{\mu\nu}g_{00,\nu}.
\end{aligned} \tag{7.19}$$

Writing out the equation for energy-momentum conservation (7.13) for a perfect fluid yields

$$\begin{aligned}
T_{\mu\nu;\nu} &= (\partial_\nu p)g_{\mu\nu} + \frac{1}{\sqrt{g}}\partial_\nu\sqrt{g}(p+\varepsilon)U_\mu U_\nu + \Gamma^\mu_{\nu\lambda}(p+\varepsilon)U^\nu U^\lambda\\
&= 0.
\end{aligned} \tag{7.20}$$

Multiplying this last equation by $g_{\mu\lambda}$ and inserting Eqs. (7.19) yields the following relation

$$\partial_\lambda p = -(p+\varepsilon)\partial_\lambda \ln\sqrt{-g_{00}}. \tag{7.21}$$

The above equation thus relates the pressure and energy density of the fluid to a given metric, and will be used shortly.

For the metric described by Eq. (7.1), the four non-vanishing components of the Ricci tensor (7.5) are

$$\begin{aligned}
R_{00} &= \frac{B''}{2B} - \frac{B'}{4B}\left(\frac{A'}{A} + \frac{B'}{B}\right) - \frac{A'}{rA}, \\
R_{11} &= -1 + \frac{r}{2A}\left(-\frac{A'}{A} + \frac{B'}{B}\right) + \frac{1}{A}, \\
R_{22} &= -\frac{B''}{2A} + \frac{B}{4A}\left(\frac{A'}{A} + \frac{B'}{B}\right) - \frac{B'}{rA}, \\
R_{33} &= sin^2\theta\, R_{22},
\end{aligned} \tag{7.22}$$

where the $'$ denotes differentiation with respect to r. All the functions certainly still depend on the coordinate r, though it is not written out explicitly in the compact notation. Inserted into the field equations (7.18) together with Eq. (7.12), the above components yield an equation for $A(r)$;

$$\begin{aligned}
\frac{R_{00}}{2B} + \frac{R_{11}}{2A} + \frac{R_{22}}{r^2} \quad &= \quad -\frac{A'}{rA^2} - \frac{1}{r^2} + \frac{1}{r^2 A} = -8\pi G\varepsilon \\
&\Rightarrow \quad \left(\frac{r}{A}\right)' = 1 - 8\pi G\varepsilon r^2 \\
&\Rightarrow \quad A(r) = \left(1 - \frac{2GM(r)}{r}\right)^{-1}.
\end{aligned} \tag{7.23}$$

In the last line the total mass inside a sphere with radius R has been inserted

$$M(r) = \int_0^R 4\pi r^2 \varepsilon(r) dr, \tag{7.24}$$

and $\varepsilon(r)$ is a function only of r since spherical symmetry is assumed for the metric (7.1) to be valid. Under the assumption that the system is in hydrostatic equilibrium, Eq. (7.21) can be used as an equation for $B(r)$, and inserting $\sqrt{-g_{00}} = \sqrt{B(r)}$ yields

$$\frac{B'}{B} = -\frac{2p'}{p+\varepsilon}. \tag{7.25}$$

This equation and Eq. (7.23) inserted into the component R_{22} in Eq. (7.22) finally yields the following

$$p'(r) = -\frac{G}{r^2}\Big(\varepsilon(r) + p(r)\Big)\Big(M(r) + 4\pi r^3 p(r)\Big)\left(1 - \frac{2GM(r)}{r}\right)^{-1}. \tag{7.26}$$

This is the Tolman-Oppenheimer-Volkoff (TOV) equation, which describes the hydrostatic equilibrium of a general relativistic, static isotropic fluid sphere.

Chapter 8

Stars

The following chapter contains a discussion and numerical calculations for stars. The structure equations are first solved for non-relativistic as well as ultra-relativistic stars consisting of non-interacting matter. After studying the behaviour of these rather simple models, possible solutions for quark stars will be discussed.

Natural units will not be used in this chapter, as we consider it more instructive to derive, calculate and measure stellar properties in kilometers and solar masses $M_\odot$.

8.1 White dwarfs

A white dwarf star is a star composed mostly of electron degenerate matter, meaning that the electron degeneracy pressure is the only thing keeping the star from collapsing. Though dwarf stars are classified as dense stars, they are still not dense enough for relativistic effects to be significant. The largest mass a white dwarf can have is the Chandrasekhar mass [3] of about $1.44M_\odot$, and they typically have radii up to about 10^4 km, i.e. much smaller than our sun. They thus have a gravitational potential of the order $\frac{GM}{c^2R} \sim 10^{-4}$, and can be described using non relativistic structure equations [20].

8.1.1 Mass continuity and hydrostatic equilibrium for Newtonian stars

The mass $M(r)$ enclosed inside a sphere with radius R and mass density $\rho(r)$ is

$$M(r) = 4\pi \int_0^R dr r^2 \rho(r), \tag{8.1}$$

after performing the angular integral, $\int d\Omega = 4\pi$, under the assumption of spherical symmetry. Taking the derivative with respect to r yields

$$\frac{dM}{dr} = 4\pi r^2 \rho(r), \tag{8.2}$$

which is often referred to as the continuity equation. It is a rather trivial equation, as it only states that the mass density is related to the rate of change in the total mass enclosed in a volume.

According to Gauss' law, a spherical symmetric mass distribution $M(r)$ produces the same gravitational force as if it were a point mass, located at the center of mass. Due to this, the gravitational acceleration produced by $M(r)$ can be expressed as

$$g(r) = -\frac{GM(r)}{r^2}, \tag{8.3}$$

where G is the gravitational constant. For a star in hydrostatic equilibrium, the gravitational pressure is balanced by a pressure gradient pointing radially outward from the center of the star. Pressure is defined as force per area, $P = \frac{F}{A}$,

so a change in total pressure along dr corresponds to an increment $dF = A\,dP$ in the force. Since the total force on an object is equal to its mass times acceleration, an increment in the force can be written as

$$dF = \underbrace{\rho(r)A\,dr}_{mass}\ \underbrace{a(r)}_{acceleration}\ . \tag{8.4}$$

Rewriting this and inserting Eq. (8.3) for the acceleration $a(r)$, yields

$$\frac{dp}{dr} = -\frac{GM(r)\rho(r)}{r^2}, \tag{8.5}$$

which is the equation for hydrostatic equilibrium, and the last of two structure equations needed to describe white dwarfs.

The structure equations just derived are differential equations in $p(r)$ and $m(r)$, and since they both involve the density $\rho(r)$, the latter must somehow be related to the pressure $p(r)$. In other words, an equation of state (EoS) is needed.

8.1.2 Equation of state for a polytrope

A polytropic EoS is one which relates the pressure to the mass density as follows

$$p(r) = K\rho(r)^{\gamma}. \tag{8.6}$$

This section contains a brief outline of how to determine K and γ for a white dwarf. A more detailed derivation can be found in [20].

The number of infinitesimal states dn available for free electrons with momentum k is

$$dn = \frac{d^3k}{(2\pi\hbar)^3} = \frac{4\pi k^2 dk}{(2\pi\hbar)^3}, \tag{8.7}$$

so the electron number density n is

$$n = \frac{8\pi}{(2\pi\hbar)^3}\int_0^{k_F} k^2 dk = \frac{k_f^3}{3\pi^2\hbar^3}. \tag{8.8}$$

The Fermi momentum is the highest possible momentum for the electrons, and can also be described as $k_F = \hbar\kappa_F$, where κ_F is the Fermi wave number, i.e. the radius of the Fermi sphere. The additional factor of two has arisen because each electron can be in two spin states. Since stars are overall electrically neutral, every electron must be neutralized by a proton, which is part of an atomic nucleus also containing neutrons. Neglecting the electron mass m_e in comparison with the nucleon mass m_N, the total mass density of the star is essentially given by

$$\rho = nm_N\frac{A}{Z}, \tag{8.9}$$

where $\frac{A}{Z}$ is the inverse ratio of protons per nucleon. Solving Eq. (8.9) for n and equaling it to Eq. (8.8), yields the following relation between the Fermi momentum and the mass density of the star

$$k_F = \hbar\left(\frac{3\pi^2\rho}{m_N}\frac{Z}{A}\right)^{\frac{1}{3}}. \tag{8.10}$$

The total relativistic energy of the electrons is $E_e = \sqrt{k^2c^2 + m_e^2c^4}$, so their energy density is

$$\begin{aligned}\varepsilon_e(k_F) &= 2\int_0^{k_F}\frac{d^3k}{(2\pi\hbar)^3}\left(k^2c^2 + m_e^2c^4\right)^{\frac{1}{2}} \\ &= \frac{m_e^4c^5}{8\pi^2\hbar^3}\left\{\left(3x^3 + x\right)\left(1 + x^2\right)^{\frac{1}{2}} - \sinh^{-1}(x)\right\},\end{aligned} \tag{8.11}$$

where the integral has been solved analytically with $x = \frac{k_F}{m_e c}$. The electrons contribution to the total energy density $\varepsilon = nm_N c^2 \frac{A}{Z} + \varepsilon_e(k_F)$ is comparatively small, though not negligible.

The chemical potential incorporates how many electrons are present in the gas, compared to other particles. I.e. it imparts *how much the energy density fluctuates when changing the number density* of electrons, or put even simpler: How much the energy changes when adding an extra electron to the star. This can be expressed as follows

$$\mu = \frac{d\varepsilon}{dn}. \tag{8.12}$$

The pressure is related to the energy density and chemical potential as $p = n\mu - \varepsilon$, and using Eq. (8.11) yields

$$\begin{aligned} p(k_F) &= \frac{2}{3}\int_0^{k_F} \frac{d^3k}{(2\pi\hbar)^3} k^2 \left(k^2c^2 + m_e^2c^4\right)^{-\frac{1}{2}} \\ &= \frac{m_e^4 c^5}{24\pi^2\hbar^3}\left\{\left(2x^3 - 3x\right)\left(1+x^2\right)^{\frac{1}{2}} + 3\sinh^{-1}(x)\right\}. \end{aligned} \tag{8.13}$$

In the relativistic case when the momenta of the electrons are much larger than their masses, $k_F \gg m_e$ and $x \gg 1$, so Eq. (8.13) can be series expanded, simplifying to

$$\begin{aligned} p(k_F) &\simeq \frac{m_e^4 c^5}{12\pi^2\hbar^3} x^4 \\ &= \frac{\hbar c}{12\pi^2}\left(\frac{3\pi^2 Z\rho}{m_N A}\right)^{\frac{4}{3}} \\ &= K\rho^{\frac{4}{3}}, \end{aligned} \tag{8.14}$$

defining $K \equiv \frac{\hbar c}{12\pi^2}\left(\frac{3\pi^2 Z}{m_N A}\right)^{\frac{4}{3}}$. The above equation constitutes a polytropic EoS for a white dwarf, with $\gamma = \frac{4}{3}$.

Before Eqs. (8.2) and (8.5) can be solved numerically, they must be expressed in terms of dimensionless quantities. This can be achieved by defining

$$\begin{aligned} \bar{M}(r) &= \frac{M(r)}{M_\odot}, \\ \bar{p}(r) &= \frac{p(r)}{\varepsilon_0}, \end{aligned} \tag{8.15}$$

where $M_\odot$ is the solar mass and ε_0 has the dimension of energy density. Being just a scale factor, ε_0 can thus be chosen freely. Using the polytropic EoS yields the following set of equations to be solved

$$\begin{aligned} \frac{d\bar{M}}{dr} &= \beta\,\bar{p}(r)^{\frac{1}{\gamma}} r^2 \\ \frac{d\bar{p}}{dr} &= \alpha\frac{\bar{p}(r)^{\frac{1}{\gamma}}\bar{M}(r)}{r^2}. \end{aligned} \tag{8.16}$$

The constants α and β are defined as follows

$$\begin{aligned} \alpha &= \frac{GM_\odot}{c^2}\left(K\varepsilon_0^{\gamma-1}\right)^{-\frac{1}{\gamma}}, \\ \beta &= \frac{4\pi\varepsilon_0}{M_\odot c^2}\left(K\varepsilon_0^{\gamma-1}\right)^{-\frac{1}{\gamma}}, \end{aligned} \tag{8.17}$$

and the energy density ε_0 is determined by α according to

$$\varepsilon_0 = K^{1-\gamma}\left(\frac{GM}{c^2\alpha}\right)^{\frac{\gamma}{\gamma-1}}. \tag{8.18}$$

Table 8.1: Radius R in km and masses M in terms of solar masses for a white dwarf star with a polytropic EoS.

$\bar{p}_0$	R	M
10^{-13}	2790	1.2469
10^{-14}	4962	1.2469
10^{-15}	8823	1.2469
10^{-16}	15691	1.2469
10^{-17}	27903	1.2469

8.1.3 Numerical calculations and results

Solving Eqs. (8.16) numerically is quite straightforward, and can be done by using a fixed, equal-step Runge Kutta routine. A simple `Python` program has been written for this, but many numerical packages have more sophisticated, built-in solvers which have been optimized and work faster. In accordance with [20], the best numerical results were obtained using the values

$$\alpha = 1.473\,km \tag{8.19}$$

$$\beta = 52.46\,km^{-3}. \tag{8.20}$$

Eq. (8.18) thus fixes the value of the energy density $\varepsilon_0 = 4.17 M_\odot \frac{c^2}{km^3}$, which is quite large, meaning that a very small initial energy density, that is a very small central pressure $\bar{p}_0$, must be used when solving the equations numerically.

The `Python` program used is listed in the Appendix. Briefly explained, it contains a Runge Kutta routine which solves Eqs. (8.16) for $\bar{p}(r)$ and $\bar{M}(r)$ simultaneously. The solver is wrapped in a loop which checks whether the pressure has become negative, since the pressure will decrease and approach zero as we go from the center to the surface of the star. Once this happens, the routine exits. The last value for r is then interpreted as the star's radius R, and the program returns this value, as well as the mass $M(R) = M$. The program also contains an outer loop which runs the routine for different values of the central pressure, and the results obtained are displayed in Table 8.1. The results obtained here are of course not identical with the results in [20]. Though one can in principle never hope to obtain exact results numerically, this problem is unusually sensitive to numerical values of the constants involved. Wrong starting values may give the derivative an entirely wrong initial magnitude and direction, causing the solution to become unstable. Furthermore, as the pressure decreases when approaching R, it does so extremely slowly, almost asymptotically, and an incredibly small precision is needed for determining exactly when the pressure is zero.

However, the most interesting part of the result is that though the central pressure and radius change by orders of magnitude, all the cases have the same mass (the numerical difference in the mass occurs after the eleventh digit in our results). Thus an increasing central pressure will cause the star to contract and vice versa.

As mentioned, the equations can also be solved using built-in solvers, and this has been done for comparison using `Mathematica`'s routine `NDSolve`. The `Mathematica` code is also listed in the Appendix, and it generates the same results as the `Python` program. Plots of the pressure and mass have been generated, and though the `Python` program generates `.dat`-files which can be plotted using `gnuplot`, we choose to include the plots generated by `Mathematica` here, due to better readability. The plots can be seen in Fig. 8.1, and clearly depict a characteristical S-shaped curve for the mass distribution.

8.2 Neutron stars

Neutron stars are much denser than white dwarfs, and they typically have a mass greater than the Chandrasekhar limit. Thus when treating neutron stars a relativistic description is mandatory, and this will be discussed in the following. Nevertheless, at this point the matter which constitutes the stars is still treated as as non interacting. Being created in

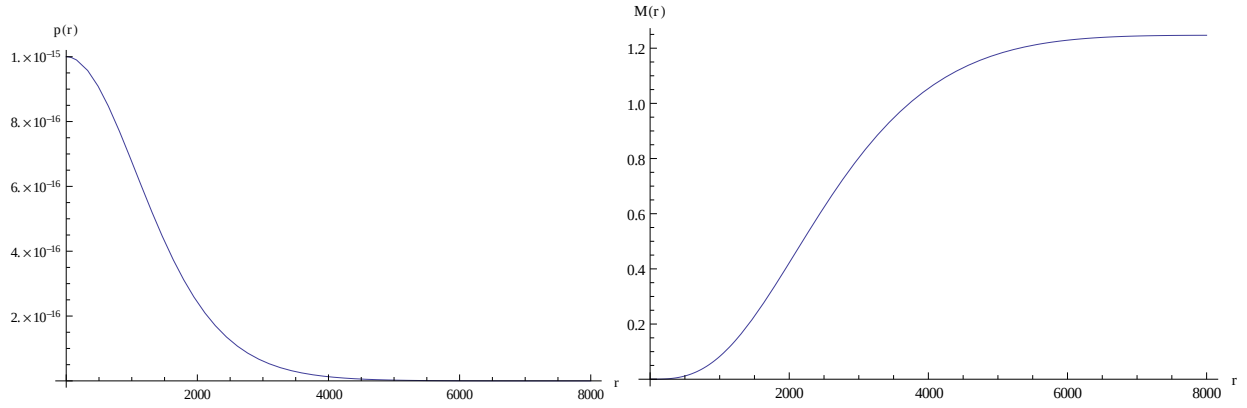

Figure 8.1: Dimensionless pressure and mass distribution in terms of solar masses for a white dwarf with a polytropic EoS. Here with central pressure $\bar{p}_0 = 10^{-15}$.

supernova explosions after a gravitational collapse, neutron stars are so dense that not even the electron degeneracy pressure can withstand the gravitational pressure. In their centers, these stars are five to ten times denser than atomic nuclei ($\rho \sim 2.5 \times 10^{14} \frac{g}{cm^3}$) [5], and most of the electrons and protons have been converted to neutrons through inverse β-decay

$$p + e^- \to n + \nu_e. \tag{8.21}$$

Though neutron stars consist mainly out of neutrons, which have a lifetime of about 15 minutes, they are stable. This is because they are *not* held together by the nuclear force, but gravitational forces. It is due to the fortitude of these gravitational forces that relativistic effects must be taken into account.

8.2.1 General relativistic effects

When treating stars massive enough for relativistic effects to be significant, the TOV-equation derived in Section 7.3, is used. Written out on a slightly different form it reads

$$p'(r) = -\frac{GM(r)\rho(r)}{r^2}\left(1 + \frac{p(r)}{c^2\rho(r)}\right)\left(1 + \frac{4\pi r^3 p(r)}{M(r)c^2}\right)\left(1 - \frac{2GM(r)}{c^2 r}\right)^{-1}. \tag{8.22}$$

Compared to Eq. (8.5), the prefactor is the same, thus the relativistic corrections are all contained in the three brackets of Eq. (8.22).

The first correction factor arises since the mass density ρ must be changed into the inertial mass density, which includes the internal energy; $\rho \to \rho + \frac{P}{c^2}$. The second factor contains an active volume correction from the pressure. Possibly the most interesting and important factor is the third one, which contains the metric of 3-space. It ensures that the surface of the star always be outside the Schwarzschild surface, since solutions with a radius smaller than the Schwarzschild radius are not within the scope of this discussion.

It is worth being aware of what physical implications it has when the correction factors become negligible, and Eq. (8.22) goes over into Eq. (8.5). When $P \ll \rho c^2$, the velocity of sound, which is also the velocity of shock waves, is much smaller than the speed of light. Also, $4\pi r^3 P(r) \ll M(r)c^2$ describes a low pressure-mass and $\frac{2GM(r)}{c^2} \ll r$ low density. Thus taking the non relativistic limit corresponds to treating a lighter, less dense star, which makes sense.

8.2.2 Equation of state for arbitrary relativity

As mentioned earlier, interactions between the particles inside the star are not taken into account here. Furthermore, the simplification of assuming that a neutron star consists entirely out of neutrons is made, although this is somewhat unrealistic. Under these two assumptions, the EoS for a neutron star is that for a non interacting Fermi gas. Since

ultra-relativistic effects are included, the EoS should also hold in both the non-relativistic and the relativistic regime. Considering first the non relativistic case, the same procedure as when finding an EoS for white dwarfs can be used, only making the substitution $m_e \to m_n$, where m_n is the neutron mass. Returning to the integral in Eq. (8.13), and solving it in the non relativistic case, i.e. when $k_F \ll m_n$, again yields a polytropic EoS

$$p(k_F) = K\varepsilon^{\frac{5}{3}}, \tag{8.23}$$

this time with the constant $K \equiv \frac{\hbar^2}{15\pi^2 m_n}\left(\frac{3\pi^2 Z}{m_N c^2 A}\right)^{\frac{5}{3}}$ and $\gamma = \frac{5}{3}$.

In the relativistic case, when $k_f \gg m_n$, the expression for the pressure again reduces to the following

$$p(k_F) \simeq \frac{m_n^4 c^5}{12\pi^2\hbar^3}x^4. \tag{8.24}$$

The expression for the energy density is also the same as the one for electrons, Eq. (8.11), but with m_n instead of m_e, and in the relativistic limit it simplifies to

$$\varepsilon(k_F) \simeq \frac{m_n^4 c^5}{4\pi^2\hbar^3}x^4. \tag{8.25}$$

Comparing this equation to Eq. (8.24) yields the following relation between the energy density and pressure

$$p = \frac{\varepsilon}{3}, \tag{8.26}$$

which is a well-known result for a relativistic gas. Since the EoS should hold for arbitrary relativity, it makes sense to have one term which behaves as Eq. (8.23), and one as Eq. (8.26). As suggested by [20], the general EoS

$$\bar{\varepsilon}(p) = C_N\bar{p}^{\frac{3}{5}} + C_R\bar{p} \tag{8.27}$$

can be used. This equation should hold in general, all simplifications taken into account, since the first term dominates at low pressures, which is in the non relativistic regime, and the second term gradually takes over when the pressure increases, making the star more relativistic.

8.2.3 Numerical calculations and results

The constants C_N and C_R in Eq. (8.27) can be fit using a fitting function, for instance with `Mathematica`. This is done in [20], which obtained the following values

$$C_N = 2.4216, \quad C_R = 2.8663, \tag{8.28}$$

and it should be noted that the constant dominating in the relativistic regime is almost equal to 3, i.e. in accordance with Eq. (8.26).

Before the structure equations (8.22) for a neutron star with arbitrary relativity can be solved numerically, they must be expressed in terms of dimensionless quantities. As before this can be done using the solar mass and defining an energy density ε_0, only in this case the latter is defined as

$$\varepsilon_0 = \frac{m_n^4 c^5}{\left(3\pi^2\hbar\right)^3}. \tag{8.29}$$

The equations have been solved for different central pressures, and compared with the corresponding solutions to the Newtonian structure equations. The results can be seen in Table 8.2, and clearly indicate that including relativistic effects yields a significant difference. Also, the difference in the results increases with the central density, pointing out that higher densities cause more relativistic effects.

Plots of both the pressure and mass have also been generated, and both have the same shape as the corresponding ones for white dwarfs, see Fig. 8.2. A parametric plot for solutions to the equations with different central pressures has been generated in Fig. 8.3, showing how the masses and radii are related. This last plot illustrates the fact that the TOV-equations yield stable solutions for the stars to the right of the maximum, at about $R = 10$ km, while the solutions are unstable for the ones to the left. The interpretation of this is that the stars with the stable solutions are themselves stable, while the ones with the unstable solutions suffer gravitational collapse.

Table 8.2: Solutions to the TOV- and Newtonian equations for neutron stars with a Fermi gas EoS. The radii R are measured in km and the masses M in terms of solar masses.

	TOV		Newtonian	
$\bar{p}_0$	R	M	R	M
0.01	14.810	0.707	16.166	0.911
0.1	9.626	0.773	11.537	1.484
1.0	6.443	0.621	8.094	1.747
10.0	5.513	0.433	5.759	1.510

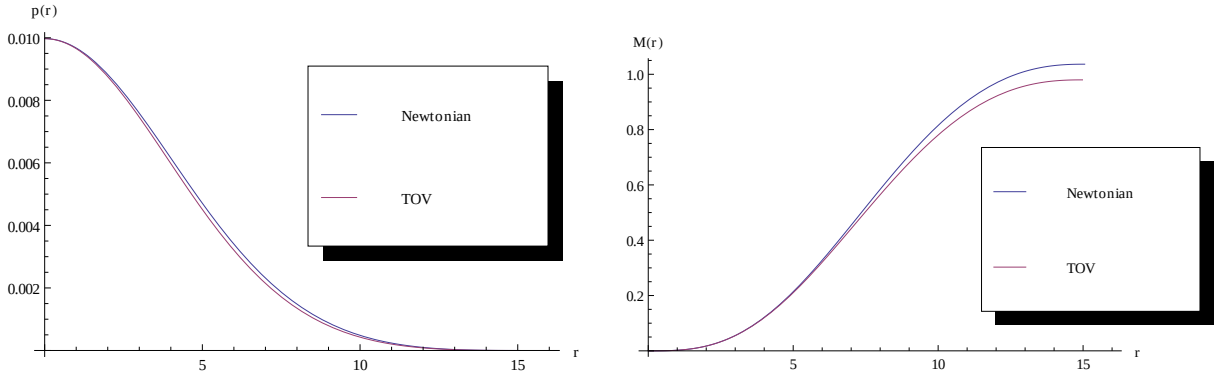

Figure 8.2: Dimensionless pressure and mass distribution in terms of solar masses for a neutron star, displaying the solutions to both the classical Newtonian structure equations and the TOV-equations. The dimensionless central pressure is $\bar{p}_0 = 0.01$.

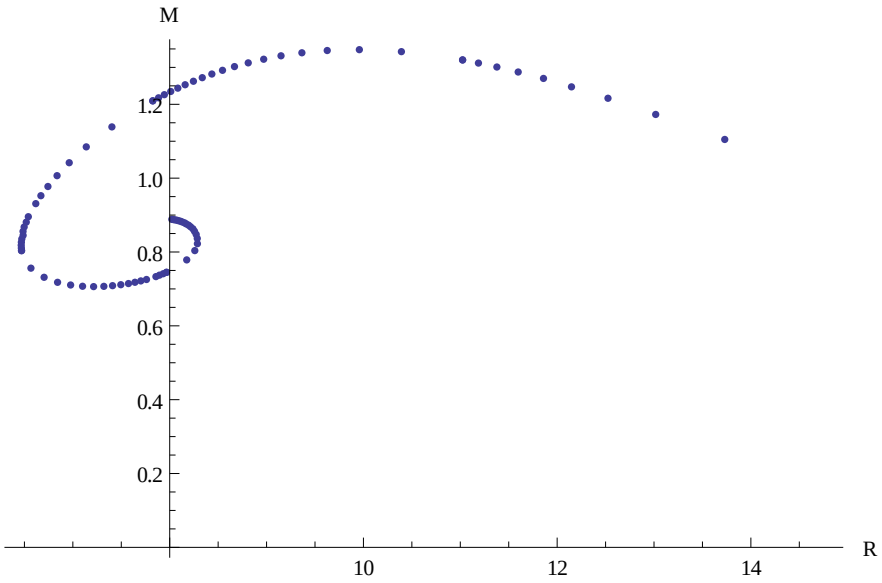

Figure 8.3: Parametric plot of solutions to the TOV-equations with different central pressures. The total radius is measured in km and the mass in terms of solar masses. The stars of low mass and large radius have small values of p_0.

8.3 Quark stars

Finally, the stage is set for the discussion of quark stars. As mentioned briefly in the Introduction, hypothetical quark stars may be formed from very dense and heavy neutron stars. Exactly what happens is still unknown, but the general idea is that the nucleons in the star are squeezed so hard together that the quarks inside the nucleons lose their identity. The neutron consists of one up and two down quarks, with the following electric charges

$$Q_u = \frac{2}{3}e, \quad Q_d = -\frac{1}{3}e. \tag{8.30}$$

Since all stars are originally made out of ordinary matter, i.e. protons and electrons, it can be assumed that all neutrons stem from inverse β-decay. This leads to the assumption that there are just as many protons as electrons left in the star, and that the star should remain electrically neutral, also after the phase transition to quark matter has taken place. However, the conservation law of charge neutrality is a global one; not local. Though it requires overall neutrality, there can and will still be separated charges, if this is energetically favourable. This means that either there are more up than down quarks, giving them different chemical potentials; $\mu_u \neq \mu_d$, or another quark flavour must be included to balance the total charge. Choosing the latter, the strange quark with electric charge $Q_s = -\frac{1}{3}e$ is included. The quarks establish chemical equilibrium via the weak interactions as follows [32]

$$\begin{aligned} d &\longleftrightarrow u + e + \overline{\mu}_e \\ s &\longleftrightarrow u + e + \overline{\mu}_e \\ s + u &\longleftrightarrow d + u, \end{aligned}$$

implying that

$$\begin{aligned} \mu_d + \mu_s &\equiv \mu \\ \mu_u + \mu_e &= \mu. \end{aligned} \tag{8.31}$$

Overall charge neutrality requires that

$$\left(\frac{2}{3}n_u - \frac{1}{3}n_d - \frac{1}{3}n_s - n_e\right)e = 0, \tag{8.32}$$

thus there is only one independent chemical potential left, here denoted by μ. This is referred to as the β-equilibrium condition.

The conversion $d \to s$ is a weak process which takes place when the chemical potential exceeds the rest mass of the strange quark, about 100 MeV. Quark matter consisting of the three lightest quark flavours, i.e. the up, down and strange quarks, is often referred to as *strange matter*. It has been suggested as the absolute ground state of strong interactions [31], although this hypothesis has not been confirmed yet.

Though the strange quark is two orders of magnitude heavier than the other two quarks, all three quarks are approximated to be massless here. Furthermore, since the neutrinos are lost rather quickly, their chemical potential is set to zero [5].

8.3.1 Deviations from ideal gas

As in the previous two cases, an EoS is needed to solve the TOV-equations, and now the EoS for dense quark matter will be used. It was derived in Chapter 6 and is restated here for convenience:

$$p(\mu) = N_f \frac{\mu^4}{4\pi^2} \left\{ 1 - \frac{N_g}{4} \frac{\alpha_s}{\pi} - N_f \left(\frac{\alpha_s}{\pi} \right)^2 \ln \frac{\alpha_s}{\pi} \right\}. \tag{8.33}$$

The thermodynamic relation

$$\varepsilon = -p + \mu n, \tag{8.34}$$

where the number density $n = \frac{dp}{d\mu}$, can be used to express the chemical potential in terms of the energy density. The resulting expression can in turn be inserted into Eq. (8.33), yielding a relation between the energy density and pressure. Treating α_s as a constant, the differentiation of Eq. (8.33) is straightforward, and the energy density goes like $\varepsilon \sim \mu^4$. This results again in a polytropic EoS, with $\gamma = \frac{4}{3}$, and the constant K dependent on α_s, i.e. an ideal gas behaviour with

$$\varepsilon = 3p. \tag{8.35}$$

If one attempts to solve the TOV-equations using this description, one does not obtain physically sensible solutions. This is because the pressure goes asymptotically to zero, effectively resulting in the star having an infinite radius. The solutions are displayed in Fig. 8.4, clearly showing the described behaviour. Furthermore, the total accumulated mass of the star behaves in the same way as for white dwarfs and neutron stars in the inner regions of the star, but without the top of the S-shaped curve in the outer regions.

Since quark matter can only exist under extremely high pressures, it is not surprising that a smooth transition from quark matter to vacuum is hard to accomplish without passing through the hadronic phase at some point.

8.3.2 MIT bag model

A simplified model can be used to describe quark confinement and asymptotic freedom, and one such model will be discussed briefly in the following.

In a 1974 paper, Chodos et al proposed a new model for treating particles as field excitations contained within a bag [24]. This model is called the MIT bag model, and was invented to try to account for hadronic masses in terms of their quark constituents. The basic assumption of the bag model is that quarks are confined into a certain region, where they move freely. Since only colour singlet states are observed nature, and the theory of strong interactions suggests that all regions must be colourless, the QCD vacuum is assumed to have the property that there are no quarks present. Thus within any region containing quarks, the trivial vacuum must be expelled. Expelling the vacuum obviously costs energy, and this energy per volume is called the *bag constant*, denoted by B. The effect of confinement is thus represented phenomenologically by the presence of a bag pressure directed from the outside toward the region inside the bag. One visualization of this is that of an elastic bag which allows quarks to move freely, as long as they are not separated by too large distances. When trying to separate the quarks from each other, the bag would stretch and resist. Furthermore, it would resist with significant amounts of energy, by far exceeding the *pair production energy* of a quark-antiquark pair. This would result in the production of mesons, as illustrated in Fig 8.5.

Although this model can not make precise predictions regarding the critical density at which quarks become disassociated with individual nucleons, it can still be used to some extent when describing confined quarks. Unfortunately,

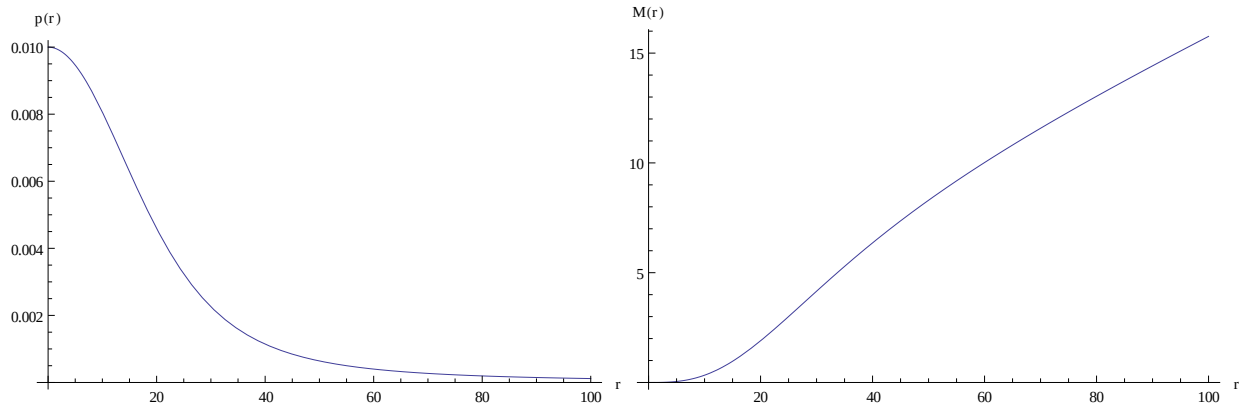

Figure 8.4: Dimensionless pressure and mass distribution in terms of solar masses for a quark star with an ideal gas EoS. The pressure goes asymptotically to zero, without ever crossing the axis, and the total mass is always increasing.

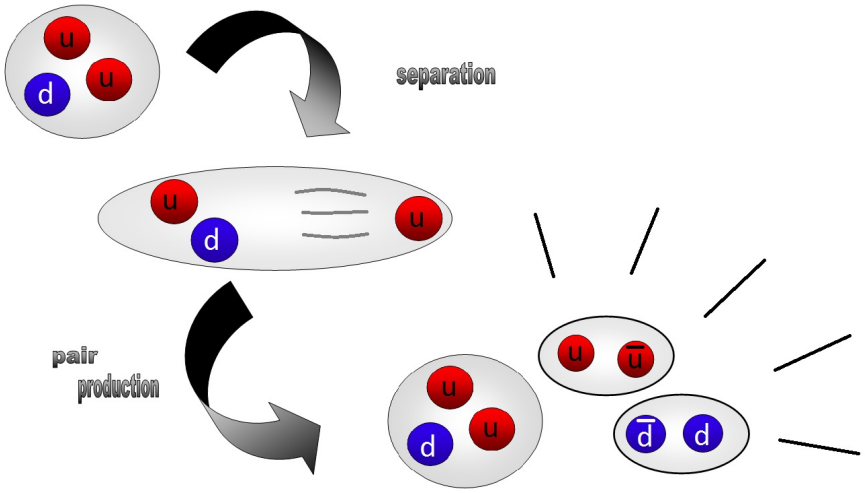

Figure 8.5: Quarks confined into hadrons in the MIT bag model. If one tries to separate the quarks, one has to apply an energy greater than what is required for pair production of quarks and antiquarks.

further details regarding this description of quarks lie outside the scope of this thesis, but it is still interesting to investigate the effects incorporating the bag constant in the equation of state, has on the solutions to the TOV-equations.

When including a bag constant, the equation of state simply changes to

$$\varepsilon = 3p + 4B. \tag{8.36}$$

This results in a nonzero energy density where the pressure vanishes, and the effect is to bind the star closer together. As this lowers the total mass and radius, it may thereby be possible to obtain finite values for both.

The bag constant can be estimated as follows. The vacuum energy is

$$E_{vac}(r) = \frac{4\pi r^3}{3}B, \tag{8.37}$$

and the kinetic energy of the quarks must go as $E_{kin} \sim \frac{C}{r}$, C being some constant, in agreement with Heisenberg's uncertainty relation. The total energy of the bag is thus the sum of these two equations, and a stable bag corresponds to the lowest total energy. Differentiating the total energy thus gives an equation for the value r_b of r which yields a stable bag. This equation is

$$4\pi r_b^2 B - \frac{C}{r_b^2} = 0. \tag{8.38}$$

Solving the above equation for r_b yields the minimum value for the energy,

$$E(r_b) = \frac{16\pi r_b^3}{3}B. \tag{8.39}$$

Assuming that the kinetic energy of the quarks constitute most of the hadrons rest mass, experimental values for the rest mass and radius of hadrons can be used to find B [13]. The radius of the neutron is approximately 10^{-15} m and the neutron mass about 938 MeV. Inserting these values yield a bag constant

$$B^{\frac{1}{4}} \simeq 145\text{MeV}. \tag{8.40}$$

In the following, numerical values close to this one have been used to solve the TOV-equations numerically for a quark star with a bag model EoS. The modifications to the program used for an ideal gas are slight, but the result is significant. By varying the bag constant, while using the same energy scale ε_0 and range of central pressures as for neutron stars, a stable solution was obtained, and the resulting parametric plot of the total masses and radii can be seen in Fig 8.6.

Though the solutions of the TOV-equations are now stable and yield the expected behavior for the mass-radius relation, this model is not ideal. However, it can be used to make qualitative predictions, as the shape of the parametric plot in Fig. 8.6 is the same as those produced my more precise models, to be discussed next.

8.3.3 TOV-equations with running coupling

Including α_s to first order and calculating the energy density $\varepsilon = -p + \mu\frac{dp}{d\mu}$ yields

$$\varepsilon = 3p - \frac{N_f N_g}{16\pi^3}\mu^5\frac{\partial\alpha_s}{\partial\mu}. \tag{8.41}$$

Thus if the coupling constant does not depend explicitly on the chemical potential, $\frac{\partial\alpha_s}{\partial\mu}$=0 and $\varepsilon = 3p$. This indicates that a running coupling constant must be used in order to describe quark stars and obtain a realistic solution in the outer layers of the star. The running coupling constant in QCD is restated here for convenience

$$\alpha_s(\Lambda) = \frac{4\pi}{\beta_0 L}\left(1 - 2\frac{\beta_1}{\beta_0^2}\frac{\ln L}{L}\right), \tag{8.42}$$

with $L = \ln\frac{\Lambda^2}{\Lambda^2_{\overline{\text{MS}}}}$, and $\Lambda = \mathcal{K}\mu$ as before.

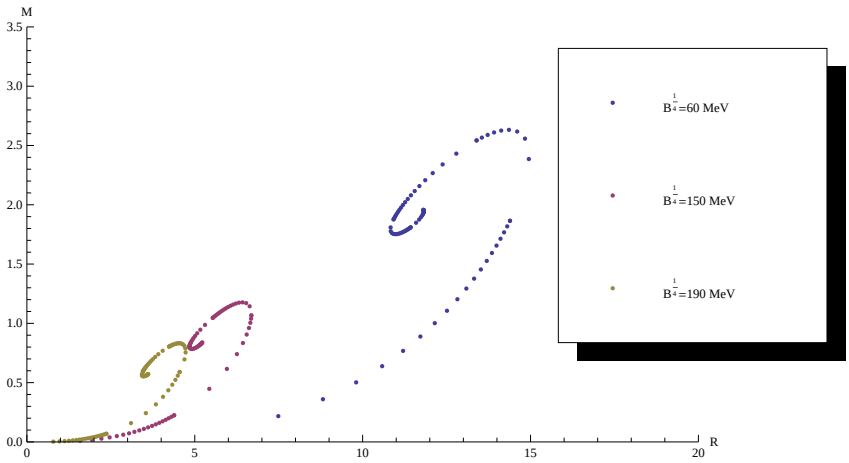

Figure 8.6: Parametric plot of the total mass in terms of solar masses and radius in km, for a quark star described by the bag model EoS, displaying different values of the bag constant B.

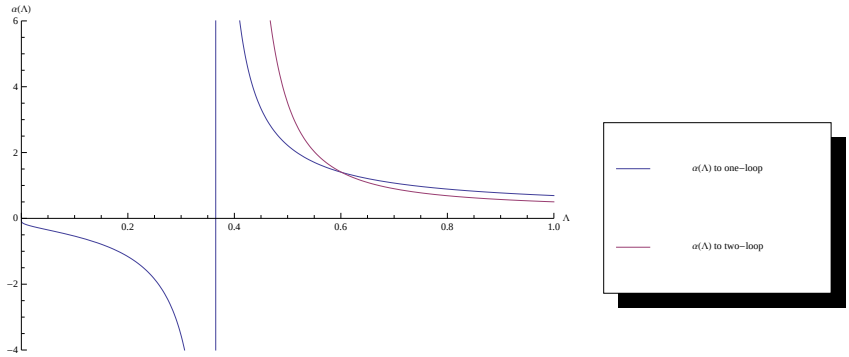

Figure 8.7: The running coupling constant $\alpha_s(\Lambda)$, to one- and two-loop order.

Before the TOV-equations can be solved with the running coupling, there are some potential problems to be discussed. First, there is an obvious problematic value for the chemical potential, since when $\Lambda = \Lambda_{\overline{\text{MS}}}$, the logarithm in Eq. (8.42) is undefined, and the coupling diverges. This is a known infrared problem in QCD, and a possible solution is discussed in [29]. As displayed in the graph in Fig 8.7, this problem seems more severe for the coupling constant to one-loop order; the discontinuous behaviour is not present when including the coupling to two-loop order.

However, the coupling increases rapidly when Λ approaches $\Lambda_{\overline{\text{MS}}}$ from above, so this imposes a lower limit on the chemical potential in the calculations. For any solution to the TOV-equations, the chemical potential has its maximum value at the center of the star [30]. Moving radially outwards from the center of the star, the chemical potential decreases until it equals μ_c, at the point where the pressure vanishes, i.e. $p(\mu_c) = 0$. This μ_c is thus the minimum value of the chemical potential used in the calculations.

A choice for the constant $\mathcal{K}$ must also be made, and Fig 8.8 shows a plot of the pressure normalised to the ideal gas pressure, for different values of $\mathcal{K}$.

The energy density in Eq. (8.41) is now a quite complicated function of μ, so it cannot be inverted and expressed as a function of the pressure as before. A way around this problem is to evaluate ε for different values of μ, starting with μ_c and going up to some large μ. The obtained values for ε can then be interpolated numerically to yield a function representing the energy density, to be used when solving the TOV-equations. The rest of the solving procedure is the

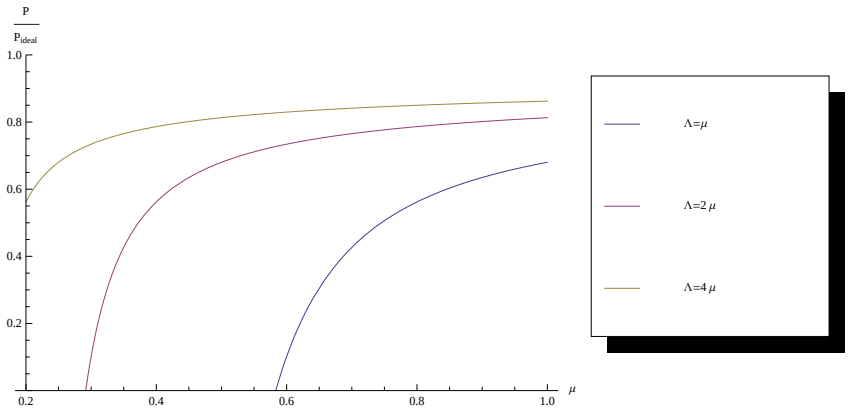

Figure 8.8: The pressure as a function of μ, normalized to the ideal pressure, for different $\Lambda = \mathcal{K}\mu$.

same as before; the mass and radius are evaluated simultaneously for a central pressure p_0, and the radius R is the value where the pressure vanishes. The code is listed in the Appendix, and a parametric plot of the masses and radii of quark stars for different central pressures has been generated, displayed in Fig 8.9.

8.3.4 Generalized stellar structure equations

It is not unusual that the pressure and density of thermodynamic systems are described by complicated functions of μ, which cannot be inverted analytically to yield an EoS relating the pressure and energy density directly. The TOV-equations can be generalized to incorporate the chemical potential to avoid this problem, yielding another set of equations to be solved, yet still describing the same system.

Choosing μ as running variable, the pressure gradient must be changed into a chemical potential gradient through

$$\frac{dp}{dr} = \frac{d\mu}{dr}\frac{dp}{d\mu}. \tag{8.43}$$

Solving $\varepsilon = -p + \mu\frac{dp}{d\mu}$ for $\frac{dp}{d\mu}$ yields

$$\frac{dp}{d\mu} = \frac{p+\varepsilon}{\mu}. \tag{8.44}$$

The differential equation for μ is thus

$$\frac{d\mu}{dr} = \frac{dp}{dr}\frac{\mu}{p+\varepsilon}, \tag{8.45}$$

and the generalized stellar structure equations in the presence of μ are

$$\begin{aligned}\frac{dM}{dr} &= \frac{4\pi r^2 \varepsilon(r)}{c^2}\\ \frac{d\mu}{dr} &= -\frac{\mu(r)G}{c^2 r^2}\left(M(r) + \frac{4\pi r^3 p(r)}{c^2}\right)\left(1 - \frac{2GM(r)}{c^2 r}\right)^{-1}.\end{aligned} \tag{8.46}$$

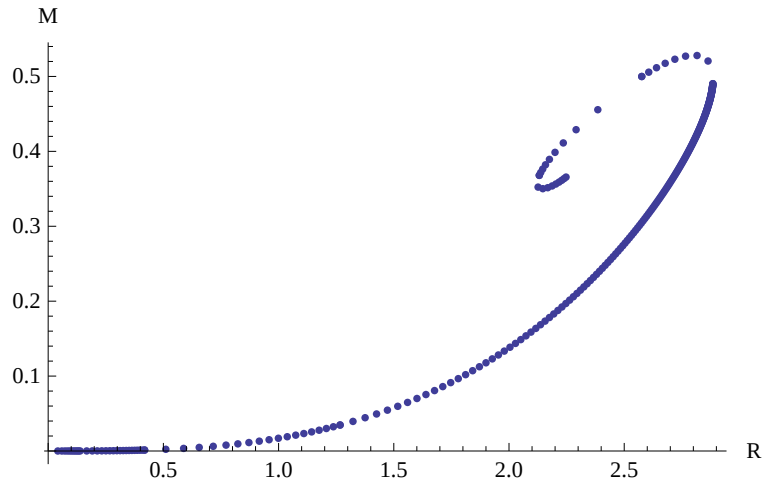

Figure 8.9: Parametric plot of the total mass in terms of solar masses and radius in km, for a quark star described by the EoS from QCD with a running coupling constant, $\Lambda = \mu$.

Chapter 9

Conclusions and outlook

The first chapters of this thesis were dedicated to the basics of thermal field theory, and much time was also spent studying the perturbative expansions and equation of state in simpler theories before QCD was considered. In the present work, the pressure in thermal field theory for a single scalar field was calculated up to order g^5, but it has been calculated to higher orders by others [33]. It turned out that conventional perturbation theory is valid only when the coupling constant is much smaller than unity, which is certainly not always the case.

Extending the discussion to include several kinds of fields, it turned out that QED with its small coupling constant, the fine structure constant, can be suitably described using perturbation theory. In the discussion of QED, vacuum effects were also taken into account, and it turned out that the quantum mechanical vacuum is in fact a very busy place.

Using QED as a stepping stone to understand QCD, new fermions and charges were introduced when going from the Abelian $U(1)$ local gauge symmetry group to the non-Abelian $SU(3)$, and the strong interactions mediated by gluons acting on quarks were described.

Finally, the thermodynamics of QCD at zero temperature and finite quark chemical potential were studied. The equation of state for cold quark matter was derived with the result

$$p = N_f \frac{\mu^4}{4\pi^2}\left\{1 - \frac{N_g}{4}\frac{\alpha_s}{\pi} - N_f\left(\frac{\alpha_s}{\pi}\right)^2 \ln\frac{\alpha_s}{\pi}\right\},$$

and the behavior of the QCD coupling α_s was thoroughly discussed. The conclusion is that the EoS for cold and dense quark matter, arising from a perturbative expansion in the coupling, yields a fairly realistic description.

Before this EoS was used to model stars, one chapter was dedicated to the discussion of general relativity, as general relativistic effects in dense stars are expected to be very significant. The discussion of general relativity led to a derivation of Einstein's field equations as well as the Tolman-Oppenheimer-Volkoff-equations. These last equations were then used as structure equations for dense stars, and starting with white dwarfs and neutron stars, the results in [20] were reproduced.

Next, quark stars were modelled using different equations of state for quark matter. It turned out that the EoS from QCD with a constant coupling yields an unphysical behavior, so these solutions were not considered further. A similar EoS, predicted by the MIT bag model, is the following

$$\varepsilon = 3p + 4B,$$

i.e. nonzero energy density even when the pressure vanishes. The structure equations were solved for this model also, using different values for the bag constant B. Upon comparing the parametric plot obtained this way, with the parametric plot obtained using the QCD EoS with a running coupling constant and $\Lambda = \mu$, we see that the largest bag constant is the one with the most fitting result. Furthermore, the bag model plot indicates that this model is more accurate in the low density region. Both these conclusions are in agreement with [34].

The parametric plot obtained for quark stars with a running coupling constant are also as expected from the literature [35]. The numerical results obtained in this thesis indicate that a star with mass $0.5M_\odot$ has a radius of roughly

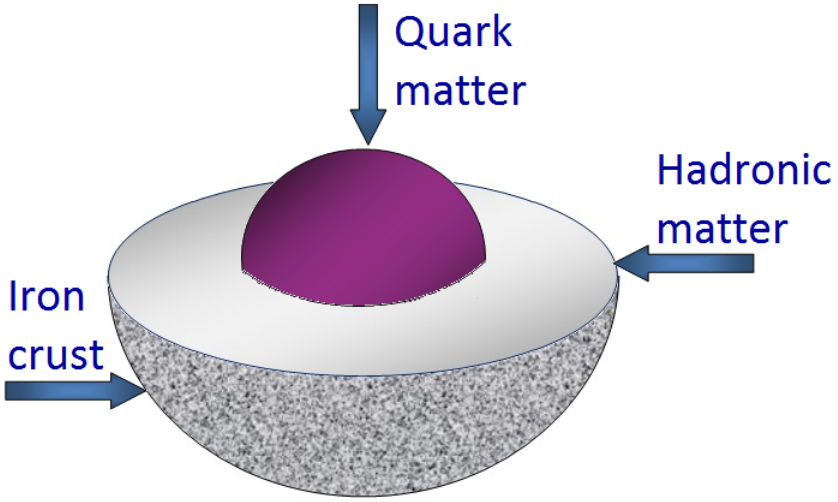

Figure 9.1: Cross section illustrating the internal structure of a star with a quark core, a mantle consisting of hadronic matter, and a thin iron crust.

2.58 km. Calculating several masses and their corresponding radii yields a ratio $\frac{M}{R}$ in the range $0.15 - 0.2$ for the most common quark stars, i.e. the central stars in the parametric plot.

If quark stars do in fact exist, they would serve as good laboratories where cold quark matter could be observed. The existence of quark stars in hydrostatic equilibrium was first suggested almost forty years ago [36], and an observational confirmation of the existence of quark stars would be conclusive evidence of quark confinement at large baryon densities.

However, at present the existence of quarks stars still remains to be confirmed by observations. Such a positive identification of a quark star would require a complement of consistent observations, being physical properties such as mass and radius, both dependent on the equation of state for dense quark matter. Thus, given more time, it would have been very interesting to modify the EoS used in this thesis, to something more realistic. For instance, it would be natural to continue this discussion of thermal field theory and quark stars by trying to find an EoS which takes into account that a dense star is most likely to have a quark core surrounded by a mantle consisting of hadronic matter, and a thin iron crust at the surface, as illustrated in Fig 9.1.

Such a model could be implemented for instance by approximating a value μ_T of the chemical potential for which matter is assumed to undergo a transition from hadronic matter to quark matter. The integration of the structure equations could then have been performed starting at $\mu > \mu_T$ with the EoS from QCD, and switching to the EoS describing hadronic matter when crossing the point $\mu = \mu_T$, as is done in [37].

Other improvements on the EoS could consist in incorporating the mass of the strange quark, since treating it as massless for low chemical potentials is a somewhat crude approximation. The quark mass could also be treated as density dependent, requiring a dynamical EoS for strange quark matter, as discussed in [38].

From astrophysical observations it is known that neutron stars have a circumferential radius of roughly 6 km or larger, as the numerical calculations in this thesis also indicate. Furthermore, detailed simulations of supernovae do not predict remnant masses of less than $1.2M_\odot$[39]. As mentioned, the pressure in the interior regions of neutron stars could be high enough to cause a transition to deconfined quark matter. If this were to happen throughout the entire star, i.e. not only in the innermost regions, a pure quark star would be the result. This is the kind of quark star which has been discussed in this thesis. If the density is high enough, quark matter is stable with respect to nuclear matter. This means that a bare quark star would be self-bound, as opposed to a neutron star, which requires gravitational forces for its binding. This again indicates that bare quark stars could be both smaller and lighter than a neutron star, and it is

possible that a few of the approximately 1500 neutron stars detected thus far are really quark stars [40].

Another avenue of interest would have been to study the effects present in rotating stars. It is improbable for a dense star not to be rotating at all; in fact conservation of angular momentum predicts that the denser a star becomes when collapsing, the faster it should rotate. A rotating compact star curves space-time, causing very interesting general relativistic effects, for instance singularities in the Kerr metric and the resulting ergosphere [41]. Furthermore, it is known that rotating neutron stars have strong magnetic fields, assigning them the name *magnetars*, or *pulsars*, as we observe them by their strong magnetic pulses. Currently, the exact mechanisms which generate these strong magnetic fields are unknown, so there is no exact way of predicting what would happen to them if the matter constituting a neutron star went through a phase transition to quark matter. There are several good articles discussing the matter[41][42], but the subject is certainly still open for further research.

Across the sea of space the stars are other suns. We have traveled this way before and there is much to be learned. – Carl Sagan

Appendix A

Identities

This Appendix contains some identities and relations used in the thesis. Any ket describing a state $|\phi\rangle$ can be written as

$$|\phi\rangle = \sum_a \langle\psi_a|\phi\rangle|\psi_a\rangle. \tag{A.1}$$

The commutativity of kets with complex scalars thus yields the identity

$$\sum_a |\psi_a\rangle\langle\psi_a| = 1. \tag{A.2}$$

For a three dimensional vector $\vec{p} = (p_1, p_2, p_3)$ and the Pauli matrices $\vec{\sigma} = (\sigma^1, \sigma^2, \sigma^3)$, the following relation is valid

$$\begin{aligned}
(\vec{\sigma}\cdot\vec{p})^2 &= \left(\sigma^1 p_1 + \sigma^2 p_2 + \sigma^3 p_3\right)^2 \\
&= \tfrac{1}{2}\begin{pmatrix} p_3 & p_1 + i\,p_2 \\ p_1 - i\,p_2 & -p_3 \end{pmatrix}\begin{pmatrix} p_3 & p_1 + i\,p_2 \\ p_1 - i\,p_2 & -p_3 \end{pmatrix} \\
&= \tfrac{1}{2}\left(2\,p_1^2 + 2\,p_2^2 + 2\,p_3^2\right) \\
&= \vec{p}^{\,2}.
\end{aligned} \tag{A.3}$$

The determinant of a slashed operator in d dimensions is

$$\begin{aligned}
\det(\not{P}) &= \sqrt{\det(\not{P})^2} \\
&= \sqrt{\det(P^2)} \\
&= \sqrt{(P^2)^d}.
\end{aligned} \tag{A.4}$$

A relation between the trace and the determinant of a complex matrix D can be found by using that the trace operation sums all the matrix' diagonal elements, which is equal to the sum of its eigenvalues. This yields

$$\det \exp D = \exp \operatorname{Tr} D. \tag{A.5}$$

Furthermore, every eigenvalue λ of the matrix D corresponds to the exponential eigenvalue $\exp\lambda$ of $\exp D$. Thus for a matrix E satisfying $\exp E = D$, the above equation yields

$$\det D = \exp \operatorname{Tr} E. \tag{A.6}$$

Taking the logarithm on both sides and substituting $E = \ln D$, yields

$$\ln\det D = \operatorname{Tr}\ln D. \tag{A.7}$$

Appendix B

Calculations of integrals

This appendix contains a brief outline of dimensional regularization and calculations of integrals needed throughout the thesis. The imaginary-time formalism is used, so the four-momentum is $P = (p_0, \vec{0})$, and $P^2 = p_0^2 + \vec{p}^2$. The Matsubara frequencies are $p_0 = 2n\pi T$ for bosons and $p_0 = (2n+1)\pi T$ for fermions, as derived in Chapter 3.

B.1 Dimensional regularization

In dimensional regularization, a Feynman diagram is formally computed as a function of the dimensionality of space-time d, considering one time dimension and $d-1$ space dimensions. By formally evaluating integrals in d dimensions, where d need not be an integer, one effectively performs an analytic continuation in the dimensions, which is where the name of the technique stems from. When taking the limit $d \to 4$, the resulting final expression for observable quantities should have a well-defined limit. Integrals which diverge for integer d give finite results for non-integer d. Two integrals often needed are

$$\int \frac{d^d p}{(2\pi)^d} \frac{1}{(p^2+m^2)^n} \tag{B.1}$$

and

$$\int \frac{d^d p}{(2\pi)^d} \frac{p^2}{(p^2+m^2)^n}. \tag{B.2}$$

In order to evaluate the first one, the rotational invariance of the integrand is used to switch to polar coordinates and factor out the spherical part,

$$\int \frac{d^d p}{(2\pi)^d} \frac{1}{(p^2+m^2)^n} = \int \frac{d\Omega_d}{(2\pi)^d} \int dp \frac{p^{d-1}}{(p^2+m^2)^n}. \tag{B.3}$$

Thus an expression for the area of the unit sphere in d dimensions is needed. This can be obtained by studying the Gaussian integral

$$\int dx e^{-x^2} = \sqrt{\pi} \tag{B.4}$$

in d dimensions

$$\begin{aligned}(\sqrt{\pi})^d &= \left(\int dx e^{-x^2}\right)^d \\ &= \int d^d x \exp\left\{-\sum_{i=0}^{d} x_i^2\right\} \\ &= \int d\Omega_d \int_0^\infty dx x^{d-1} e^{-x^2} \\ &= \frac{1}{2}\int d\Omega_d \int_0^\infty d(x^2)\,(x^2)^{\frac{d}{2}-1} e^{-x^2} \\ &= \frac{1}{2}\int d\Omega_d \Gamma\left(\tfrac{d}{2}\right), \end{aligned} \tag{B.5}$$

where the Γ-function has been inserted in the last line;

$$\Gamma(z) = \int_0^\infty e^{-t} t^{z-1} dt. \tag{B.6}$$

So the area of a d-dimensional unit sphere is

$$S_d = \int d\Omega_d = \frac{2\pi^{\frac{d}{2}}}{\Gamma(\frac{d}{2})} \tag{B.7}$$

which is an expression that makes sense for both integer and non-integer d, so that analytical continuation to non-integer dimensions is possible.

Returning to the integral over p, the substitution $x = \frac{p^2}{m^2}$ with $dx = \frac{2p}{m^2} dp$ yields the following

$$\begin{aligned}\int \frac{d\Omega_d}{(2\pi)^d} \int dp \frac{p^{d-1}}{(p^2+m^2)^n} &= \frac{S_d}{(2\pi)^d} \int dx \frac{m^{d-2n}}{2} \frac{x^{\frac{d}{2}-1}}{x+1} \\ &= \frac{S_d m^{d-2n}}{2(2\pi)^d} \int \frac{dx}{x} \frac{x^{\frac{d}{2}}}{(x+1)^n}. \\ &= \frac{S_d m^{d-2n}}{2(2\pi)^d} \frac{\Gamma(\frac{d}{2})\Gamma(n-\frac{d}{2})}{\Gamma(n)} \end{aligned} \tag{B.8}$$

having identified

$$\int \frac{dt}{t} \frac{t^z}{(t+1)^{z+\omega}} = \frac{\Gamma(z)\Gamma(\omega)}{\Gamma(z+\omega)} \tag{B.9}$$

in the last line. After inserting the area of the unit sphere in Eq. (B.7), a general expression for the integral in Eq. (B.1) is

$$\int \frac{d^d p}{(2\pi)^d} \frac{1}{(p^2+m^2)^n} = \frac{1}{(4\pi)^{\frac{d}{2}}} m^{d-2n} \frac{\Gamma(n-\frac{d}{2})}{\Gamma(n)}. \tag{B.10}$$

The integral in Eq. (B.2) can be calculated using exactly the same procedure, and the result is

$$\int \frac{d^d p}{(2\pi)^d} \frac{p^2}{(p^2+m^2)^n} = \frac{1}{(4\pi)^{\frac{d}{2}}} \frac{d}{2} m^{d-2n+2} \frac{\Gamma(n-\frac{d}{2})}{\Gamma(n)}. \tag{B.11}$$

B.2 Spatial integrals

The integral in Eq. (B.10) often appears with $n = 1, 2$ in the calculations of this thesis, and the evaluations in $d = 3 - 2\varepsilon$ dimensions will be performed here. The first one reads

$$\begin{aligned}\int \frac{d^{3-2\varepsilon}p}{(2\pi)^{3-2\varepsilon}} \frac{1}{p^2+m^2} &= (4\pi)^{\varepsilon-\frac{3}{2}} m^{1-2\varepsilon} \frac{\Gamma\left(-\frac{1}{2}+\varepsilon\right)}{\Gamma(1)} \\ &= -\frac{m}{4\pi},\end{aligned} \tag{B.12}$$

after Taylor expanding about $\varepsilon = 0$ and dropping linear terms. Using exactly the same procedure for $n = 2$ yields

$$\begin{aligned}\int \frac{d^{3-2\varepsilon}p}{(2\pi)^{3-2\varepsilon}} \frac{1}{(p^2+m^2)^2} &= (4\pi)^{\varepsilon-\frac{3}{2}} \frac{1}{m^{1+2\varepsilon}} \left(\frac{3}{2}-\varepsilon\right) \frac{\Gamma\left(\frac{1}{2}+\varepsilon\right)}{\Gamma(2)} \\ &= \frac{1}{8\pi m}.\end{aligned} \tag{B.13}$$

Next follows the evaluation of the integral

$$\int_p \ln\left(\vec{p}^2+m^2\right), \tag{B.14}$$

again in $d = 3 - 2\varepsilon$ dimensions. An easy way to proceed is by first differentiating with respect to m^2, using dimensional regularization to evaluate the integral, and then integrate over dm^2 to get back the original integral:

$$\begin{aligned}\frac{d}{dm^2} \int_p \ln\left(\vec{p}^2+m^2\right) &= \int_p \frac{1}{\vec{p}^2+m^2} \\ &= \frac{1}{(4\pi)^{\frac{3}{2}}} (4\pi)^{\varepsilon} \Gamma(\varepsilon-\tfrac{1}{2}) m^{1-2\varepsilon} \\ &= \frac{1}{(4\pi)^{\frac{3}{2}}} (4\pi)^{\varepsilon} \Gamma(\varepsilon-\tfrac{1}{2}) \int_p m^{1-2\varepsilon} dm^2 \\ &= \frac{1}{(4\pi)^{\frac{3}{2}}} (4\pi)^{\varepsilon} \Gamma(\varepsilon-\tfrac{1}{2}) \frac{2}{d} m^{3-2\varepsilon}.\end{aligned} \tag{B.15}$$

In the limit $\varepsilon = 0$ this is

$$\int_p \ln\left(\vec{p}^2+m^2\right) = -\frac{m^3}{6\pi}. \tag{B.16}$$

B.3 Bosonic sum-integrals

This section contains calculations of sum-integrals over bosonic matsubara frequencies, $p_0 = i\omega_n$, with $\omega_n = 2ni\pi T$. First follow some explicit calculations, before a general expression is derived. The simplest sum-integral encountered in this thesis is

$$\sum\!\!\!\!\!\!\int_P \frac{1}{P^2}, \tag{B.17}$$

which is evaluated using the method of residues, described in detail in section 3.4.1.

$$\begin{aligned}
\sum\!\!\!\!\!\!\int_P \frac{1}{P^2} &= \int \frac{d^3p}{(2\pi)^3} T \sum_n \mathrm{Res}\left\{ \frac{1}{\omega^2 - p^2} \coth\left(\frac{\beta\omega}{2}\right)\right\} \frac{\beta}{2} \\
&= \int \frac{d^3p}{(2\pi)^3} \frac{1}{2p} \coth\left(\frac{\beta p}{2}\right) \\
&= \frac{1}{2\pi^2}\frac{1}{2}\int_0^\infty dp\, p + \frac{1}{2\pi^2}\int_0^\infty dp \left(\frac{p}{e^{\beta p}-1}\right) \\
&= \frac{T^2}{12},
\end{aligned} \tag{B.18}$$

where in the last line a shift in the vacuum energy has been omitted. Next follows the evaluation of the sum-integral

$$\sum\!\!\!\!\!\!\int_P \ln P^2, \tag{B.19}$$

which can be done by writing out P and next differentiating with respect to p_0^2, solving the resulting integral with Equation (B.10), and then integrating over p_0^2. This yields the following

$$\begin{aligned}
\sum\!\!\!\!\!\!\int_P \ln P^2 &= \sum\!\!\!\!\!\!\int_P \ln(\vec{p}^2 + p_0^2) \\
&= \sum\!\!\!\!\!\!\int_P \frac{1}{\vec{p}^2 + \vec{p_0}^2} dp_0^2 \\
&= \left(\frac{e^{\gamma_E}\Lambda^2}{4\pi}\right)^\varepsilon T \sum_{p_0 = 2\pi n T} \int_p \frac{1}{\vec{p}^2 + \vec{p_0}^2} dp_0^2 \\
&= -\frac{2\pi^2 T^4}{\sqrt{\pi}} \left(\frac{e^{\gamma_E}\Lambda^2}{4\pi^2 T^2}\right)^\varepsilon \Gamma(\varepsilon - \tfrac{1}{2}) \frac{1}{\frac{3}{2} - \varepsilon} \zeta(2\varepsilon - 3) \\
&= -\frac{\pi^2 T^4}{45},
\end{aligned} \tag{B.20}$$

having identified the Riemann Zeta function

$$\zeta(z) = \sum_{n=1}^\infty \frac{1}{n^z}, \tag{B.21}$$

and Taylor expanded about $\varepsilon = 0$. When replacing the sum over $p_0 = 2\pi n T$, i.e. the Matsubara frequencies, with the Zeta function a factor 2 arises, since the sum includes both negative and positive frequencies. By using the Zeta function, it is also possible to derive a general expression for the following sum-integral

$$\sum\!\!\!\!\!\!\int_P \frac{1}{(P^2)^n} \equiv \left(\frac{e^{\gamma_E}\Lambda^2}{4\pi}\right)^\varepsilon T \sum_{p_0 = 2\pi k T} \int \frac{d^d p}{(2\pi)^d} \frac{1}{(p_0^2 + \vec{p}^2)^n}. \tag{B.22}$$

Inserting Eq. (B.10) with $d = 3 - 2\varepsilon$ yields

$$\begin{aligned}
\sum\!\!\!\!\!\!\int_P \frac{1}{(P^2)^n} &= \left(e^{\gamma_E}\Lambda^2\right)^\varepsilon T \sum_{p_0 = 2\pi k T} \frac{1}{(4\pi)^{\frac{3}{2}}} p_0^{3-2n-2\varepsilon} \frac{\Gamma(n - \frac{3}{2} + \varepsilon)}{\Gamma(n)} \\
&= \left(e^{\gamma_E}\Lambda^2\right)^\varepsilon \frac{T}{2^3 \pi^{\frac{3}{2}}} \frac{\Gamma(n - \frac{3}{2} + \varepsilon)}{\Gamma(n)} \sum_{p_0 = 2\pi k T} \frac{1}{p_0^{2n+2\varepsilon-3}} \\
&= \left(e^{\gamma_E}\Lambda^2\right)^\varepsilon \frac{T}{2^2 \pi^{\frac{3}{2}}} \frac{\Gamma(n - \frac{3}{2} + \varepsilon)}{\Gamma(n)} \frac{\xi(2n + 2\varepsilon - 3)}{(2\pi T)^{2n-3}(4\pi^2 T)^\varepsilon}.
\end{aligned} \tag{B.23}$$

As announced, the sum over p_0 has been replaced with the Zeta function, Eq. (B.21) with $z = 2n + 2\varepsilon - 3$. The $n = 0$ term contributes only to a shift in the vacuum energy, and can be renormalized away. Tidying up a bit yields the general result

$$\sum\!\!\!\!\!\!\int_P \frac{1}{(P^2)^n} = \left(\frac{e^{\gamma_E}\Lambda^2}{4\pi^2 T^2}\right)^{\varepsilon} \frac{T^{4-2n}}{2^{2n-1}} \pi^{\frac{3}{2}-2n} \frac{\Gamma(n-\frac{3}{2}+\varepsilon)}{\Gamma(n)} \xi(2n+2\varepsilon-3). \tag{B.24}$$

B.4 Fermionic sum-integrals

This section contains first evaluations of some fermionic sum-integrals, and next a relation which can be used to go from bosonic to fermionic integrals. First the method of residues, described in detail in section 3.4.1, is used to evaluate the sum-integral

$$\sum\!\!\!\!\!\!\int_{\{P\}} \frac{1}{P^2}, \tag{B.25}$$

recalling that the poles of the hyperbolic tangent are the fermionic Matsubara frequencies $\omega_n = (2n+1)i\pi T$. Furthermore, a chemical potential can be included by adding $\pm\mu$ to the frequencies, which does not alter the procedure.

$$\begin{aligned}
\sum\!\!\!\!\!\!\int_{\{P\}} \frac{1}{P^2} &= \int \frac{d^3p}{(2\pi)^3} T \sum_n \mathrm{Res}\left\{\frac{1}{\omega^2 - p^2} \tanh\left(\frac{\beta(\omega \pm \mu}{2}\right)\right\} \frac{\beta}{2} \\
&= \int \frac{d^3p}{(2\pi)^3} \left[\frac{1}{p}\tanh\left(\frac{\beta(p+\mu)}{2}\right) + \frac{1}{p}\tanh\left(\frac{\beta(p-\mu)}{2}\right)\right]\frac{1}{4} \\
&= \frac{1}{2\pi^2}\int_{-\infty}^{\infty} p\,dp\left(1 - \frac{2}{e^{\beta(p+\mu)}+1} + 1 - \frac{2}{e^{\beta(p-\mu)}+1}\right)\frac{1}{4} \\
&= \frac{1}{2\pi^2}\frac{1}{4}\int p\,dp - \frac{1}{2\pi^2}\int p\,dp\left(\frac{1}{e^{\beta(p+\mu)}+1} + \frac{1}{e^{\beta(p-\mu)}+1}\right)\frac{1}{2} \\
&= -\frac{1}{2\pi^2}\left(\frac{\mu^2}{4} + \frac{\pi^2 T^2}{12}\right),
\end{aligned} \tag{B.26}$$

where the shift in the vacuum energy has been omitted.
Now, the sum-integral

$$\sum\!\!\!\!\!\!\int_{\{P\}} \ln P^2 \tag{B.27}$$

can be calculated by using almost exactly the same procedure as in the bosonic case, the only difference arising due to the fermionic Matsubara frequencies. It is evaluated as follows

$$\begin{aligned}
\sum\!\!\!\!\!\!\int_{\{P\}} \ln P^2 &= \sum\!\!\!\!\!\!\int_{\{P\}} \ln(\vec{p}^2 + p_0^2) \\
&= \sum\!\!\!\!\!\!\int_{\{P\}} \frac{1}{\vec{p}^2 + p_0^2} dp_0^2 \\
&= \left(\frac{e^{\gamma_E}\Lambda^2}{4\pi}\right)^{\varepsilon} T \sum_{p_0=(2n+1)\pi T} \int_p \frac{1}{\vec{p}^2 + p_0^2} dp_0^2 \\
&= \frac{T}{(4\pi)^{3/2}} \left(e^{\gamma_E}\Lambda^2\right)^{\varepsilon} \sum_{p_0=(2n+1)\pi T} p_0^{1-2\varepsilon} \Gamma(\varepsilon - \tfrac{1}{2}) dp_0^2 \\
&= \frac{T}{(4\pi)^{3/2}} \frac{\left(e^{\gamma_E}\Lambda^2\right)^{\varepsilon} \Gamma(\varepsilon - \frac{1}{2})}{\frac{3}{2} - \varepsilon} \sum_{p_0=(2n+1)\pi T} p_0^{3-2\varepsilon} \\
&= -\frac{T}{3\pi} \sum_n \left((2n+1)\pi T\right)^3 + \mathcal{O}(\varepsilon) \\
&= -\frac{8\pi^2 T^4}{3} \zeta(-3, \tfrac{1}{2}) \\
&= \frac{7\pi^2 T^4}{360},
\end{aligned} \tag{B.28}$$

so the only difference in the calculation is that the Generalized Zeta function must be used.
Next, it is shown that

$$\sum\!\!\!\!\!\!\int_{\{P\}} \frac{\vec{p}^2}{P^4} = \frac{d}{2} \sum\!\!\!\!\!\!\int \frac{1}{P^2}. \tag{B.29}$$

Inserting the definition of the sum-integral with $d = 3 - 2\varepsilon$ and going to polar coordinated yields

$$\begin{aligned}
\sum\!\!\!\!\!\!\int \frac{\vec{p}^2}{(\vec{p}^2 + p_0^2)^2} &= \left(\frac{e^{\gamma_E}\Lambda^2}{4\pi}\right) T \sum_{p_0=(2n+1)\pi T} \int \frac{d^d p}{(2\pi)^d} \frac{\vec{p}^2}{(\vec{p}^2 + p_0^2)^2} \\
&= \left(\frac{e^{\gamma_E}\Lambda^2}{4\pi}\right) T \sum_{p_0=(2n+1)\pi T} \int \frac{d\Omega_d}{(2\pi)^2} \int dp \frac{p^{d+1}}{(p^2 + p_0^2)^2},
\end{aligned} \tag{B.30}$$

and after partial integration the integral is

$$\int dp \frac{p^{d+1}}{(p^2 + p_0^2)^2} = \left[-\frac{1}{2} \frac{p^d}{p^2 + p_0^2}\right] + \frac{d}{2} \int dp \frac{p^{d-1}}{p^2 + p_0^2}, \tag{B.31}$$

where the first term on the right-hand side vanishes when taking the limits from 0 to ∞. Inserting this and going back from polar coordinates yields

$$\begin{aligned}
&\left(\frac{e^{\gamma_E}\Lambda^2}{4\pi}\right)^{\varepsilon} T \frac{d}{2} \sum_{p_0=(2n+1)\pi T} \int \frac{d\Omega_d}{(2\pi)^2} \int dp \frac{p^{d-1}}{p^2 + p_0^2} \\
&= \left(\frac{e^{\gamma_E}\Lambda^2}{4\pi}\right)^{\varepsilon} T \frac{d}{2} \sum_{p_0=(2n+1)\pi T} \int \frac{d^d p}{(2\pi)^d} \frac{1}{p^2 + p_0^2} \\
&= \frac{d}{2} \sum\!\!\!\!\!\!\int \frac{1}{P^2}.
\end{aligned} \tag{B.32}$$

The fermionic sum-integrals on the form

$$\sum\!\!\!\!\!\!\int_{\{P\}} \frac{1}{(P^2)^m} \tag{B.33}$$

can be obtained from the bosonic ones by scaling arguments which are

$$\sum\!\!\!\!\!\!\int_{\{P\}} \frac{1}{(P^2)^m} = \left(2^{2m+1-d}-1\right) \sum\!\!\!\!\!\!\int_{P} \frac{1}{(P^2)^m}. \tag{B.34}$$

Appendix C

Python numerics

This Appendix contains the `Python` [43] code I wrote for solving the TOV-equations numerically. As mentioned in the thesis, the results obtained with these programs are good for the simplest stars, i.e. white dwarfs and neutron stars, but time did not allow for writing a program which yielded acceptable results for quark stars. The numerical equations describing quark stars were thus solved only in `Mathematica`, for which the code is contained in App. D.

C.1 White dwarf calculations in Python

Listing C.1: dwarfstar.py

```
a=1.473
b=52.46
c=3./4.
h=1./6. #for RK
dr=10e-3 #step size

#Defining functions
def f(r,p,m):
  if r != 0:
    return -a*(p**c)*m/(r**2)
  else:
    return 0

def g(r,p):
    return b*(r**2)*(p**c)

#for writing numerical results (p0, R, M) to file
res=open('resdwarf.dat','w')

p0=1e-18
while p0.real<1e-13:
  print "p0=",p0
  p0*=10
  r=complex(10e-10) #radius, start just above zero to avoid infinity
  p=complex(p0) #pressure at center
  m=complex(0) #mass at center
  ps=[p]
  ms=[m]
  rs=[r]
  svar=[0]*2

#for creating .dat-files with the data produced. to be used for plotting.
  #wp=open('pressure.dat','a')
  #wm=open('mass.dat','a')
  #wr=open('radius.dat','a')

  while p.real > 0:
    k1 = f(r,p,m)*dr
    l1 = g(r,p)*dr
    k2 = f(r+0.5*dr,p+0.5*k1,m+0.5*l1)*dr
    l2 = g(r+0.5*dr,p+0.5*k1)*dr
    k3 = f(r+0.5*dr,p+0.5*k2,m+0.5*l2)*dr
    l3 = g(r+0.5*dr,p+0.5*k2)*dr
    k4 = f(r+dr,p+k3,m+l3)*dr
    l4 = g(r+dr,p+k3)*dr
    p+=h*(k1+2*k2+2*k3+k4)
    m+=h*(l1+2*l2+2*l3+l4)
    r+=dr
```

```
49        ps.append(p.real)
50        ms.append(m.real)
51        rs.append(r.real)
52        # w=str(p.real)
53        # wp.write(w)
54        # wp.write("\n")
55        # w=str(m.real)
56        # wm.write(w)
57        # wm.write("\n")
58        # w=str(r.real)
59        # wr.write(w)
60        # wr.write("\n")
61        #wp=open('pressure.dat','r')
62        #wm=open('mass.dat','r')
63        #wr=open('radius.dat','r')
64      n=len(ps)
65      pos1=0.
66      pos2=0.
67      neg1=0.
68      neg2=0.
69      i=0
70      while n>i and ps[i].real>0:
71        pos1=rs[i]
72        pos2=ms[i]
73        if i<(n-1):
74          neg1=rs[i+1]
75          neg2=ms[i+1]
76          #print 'counting'
77        else:
78          print "Functions has no zeroes"
79        i+=1
80      svar[0]=(pos1+neg1)*0.5
81      svar[1]=(pos2+neg2)*0.5
82      for i in range(1,n):
83        if ps[i]==0:
84          svar[0]=rs[i]
85          svar[1]=ms[i]
86      print 'r=', svar[0]
87      print 'm=', svar[1]
88      wr=str(svar[0])
89      wm=str(svar[1])
90      wp=str(p0.real)
91      res.write('p0=')
92      res.write(wp)
93      res.write('\n')
94      res.write('R=')
95      res.write(wr)
96      res.write(', M=')
97      res.write(wm)
98      res.write('\n')
99      res.write('\n')
100     print 'loop done, and p0=', p0, '\n' 'real p0=',p0.real
```

```
101 res=open('resdwarf.dat','r')
102 print 'DONE'
```

C.2 Neutron star calculations in Python

Listing C.2: neutronstar.py

```
from math import pi
c=3*10e5
G=6.673*10e-20
M=1.98892*10e30
e0=0.003006*M*c**2
a=G*M/c**2
b=4*pi*e0/(M*c**2)
An=2.4216
Ar=2.8663
g1=3.0/5.0
g2=-2.0/5.0
h=1./6. #for RK
dr=10e-7 #step size

#Defining functions
def f(r,p,m):
 #TOV-equation for pressure:
   return -a*m/(r**2)*(An*p**g1+Ar*p)*(1+1/(An*p**g2+Ar))*(1+b*p*r**3/m)*1/(1-2*a*m/r)
 #Newtonian equation for pressure:
 #return -a*m/(r**2)*(An*p**(3.0/5.0)+Ar*p)

def g(r,p):
   return b*r**2*(An*p**(3.0/5.0)+Ar*p)

#for writing numerical results (p0, R, M) to file
res=open('results.txt','w')

p0=1e-3
while p0.real < 1e1: #Increase central pressure by factor 10 in each loop.
   p0*=10
   print p0
   r=complex(10e-10) #radius, start just above zero to avoid infinity
   p=complex(p0) #pressure at center
   m=complex(10e-14) #mass at center
   ps=[p]
   ms=[m]
   rs=[r]
   svar=[0]*2
#Runge Kutta
   while p.real > 0: #Run loop until real part of pressure >0.
     k1 = f(r,p,m)*dr
     l1 = g(r,p)*dr
     k2 = f(r+0.5*dr,p+0.5*k1,m+0.5*l1)*dr
     l2 = g(r+0.5*dr,p+0.5*k1)*dr
     k3 = f(r+0.5*dr,p+0.5*k2,m+0.5*l2)*dr
     l3 = g(r+0.5*dr,p+0.5*k2)*dr
     k4 = f(r+dr,p+k3,m+l3)*dr
     l4 = g(r+dr,p+k3)*dr
```

```
49        p+=h*(k1+2*k2+2*k3+k4)
50        m+=h*(l1+2*l2+2*l3+l4)
51        r+=dr
52        ps.append(p.real)
53        ms.append(m.real)
54        rs.append(r.real)
55    #Find zero of p(r)
56      n=len(ps)
57      pos1=0.
58      pos2=0.
59      neg1=0.
60      neg2=0.
61      i=0
62      while n>i and ps[i].real>0:
63        pos1=rs[i]
64        pos2=ms[i]
65        if i<(n-1):
66          neg1=rs[i+1]
67          neg2=ms[i+1]
68          #print 'counting'
69        else:
70          print "Functions has no zeroes"
71        i+=1
72      svar[0]=(pos1+neg1)*0.5
73      svar[1]=(pos2+neg2)*0.5
74
75      for i in range (1,n):
76        if ps[i]==0:
77          svar[0]=rs[i]
78          svar[1]=ms[i]
79          print 'p0=', p0
80          print 'r=' , svar[0]
81          print 'm=' , svar[1]
82      wr=str(svar[0])
83      wm=str(svar[1])
84      wp=str(p0.real)
85      res.write('p0=')
86      res.write(wp)
87      res.write('\n')
88      res.write('R=')
89      res.write(wr)
90      res.write(', M=')
91      res.write(wm)
92      res.write('\n')
93      res.write('\n')
94    res=open('results.txt','r')
95    print 'DONE'
96
97    #Write to file. Should be placed inside the loop, to write one file for each p0.
98    #If commented in here, it will only write the result for the last p0.
99    #wp=open('pressuretov.dat','a')
100   #wm=open('masstov.dat','a')
```

```
101 #wr=open('radiustov.dat','a')
102 #for i in range (1,n):
103 # w=str(ps[i])
104 # wp.write(w)
105 # wp.write("\n")
106 # w=str(rs[i])
107 # wr.write(w)
108 # wr.write("\n")
109 # w=str(ms[i])
110 # wm.write(w)
111 # wm.write("\n")
112 #wp=open('pressure.dat','r')
113 #wr=open('radius.dat','r')
114 #wm=open('mass.dat','r')
```

Appendix D

Mathematica numerics

The following pages contain the `Mathematica` [44] code used to produce the results and graphs in this thesis.

```
Clear["Global`*"]

Needs["PlotLegends`"]
```

White Dwarf

```
α := 1.473
β := 52.46
γ := 4 / 3
s[p0_] := NDSolve[{p'[r] == -α / (r^2) * p[r]^(1 / γ) * m[r], m'[r] == β * r^2 * p[r]^(1 / γ),
    p[10^-10] == p0, m[10^-10] == 0}, {p, m}, {r, 10^-10, 100 000}]
P[r_, p0_] := First[Re[p[r] /. s[p0]]]
Mass[r_, p0_] := First[Re[m[r] /. s[p0]]]
R[p0_] := Last[Last[FindRoot[P[r, p0] == 0, {r, 1}]]]

(*Plotting solution for central pressure 10^-15*)
sol = s[10^-15];
Plot[p[r] /. sol[[1]], {r, 10^-14, 8000}, AxesLabel → {"r", "p(r)"}]
Plot[m[r] /. sol[[1]], {r, 10^-14, 8000}, AxesLabel → {"r", "M(r)"}]
```

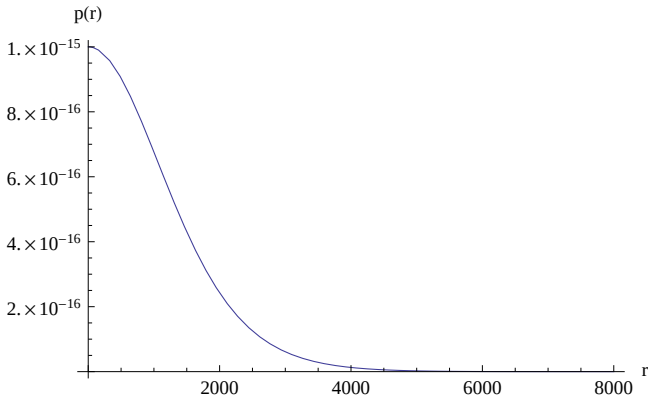

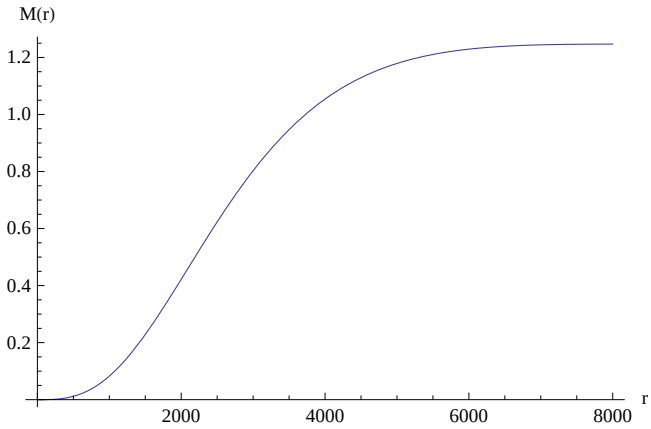


```
Clear[α, β, γ, s, p, m, Mass, R, P, sol]
```

Neutron Star

```
c := 3 * 10^5 (*km/s*)
G := 6.673 * 10^-20 (*km^3/(kg*s*)
M := 1.98892 * 10^30 (*kg*)
α := G * M / (c^2)
β := 4 * Pi * ϵ 0/ (M * c^2)
An := 2.4216
Ar := 2.8663
ϵ 0:= 0.003006 * M * c^2
```

■ TOV equations

```
s[pc_] := NDSolve[{p'[r] == -α / (r^2) * (An * p[r]^(3.0 / 5.0) + Ar * p[r]) * m[r] *
      (1 + 1 / (An * p[r]^(-2.0 / 5.0) + Ar) * (1 + β * r^3 * p[r] / m[r]) * 1 / (1 - 2 α * m[r] / r)),
   m'[r] == β * r^2 * (An * p[r]^(3.0 / 5.0) + Ar * p[r]), p[10^-10] == pc,
   m[10^-10] == 10^-14}, {p, m}, {r, 10^-10, 30}, MaxSteps → 100 000]
P[r_, pc_] := First[Re[p[r] /. s[pc]]]
Mass[r_, pc_] := First[Re[m[r] /. s[pc]]]
R[pc_] := Last[Last[FindRoot[P[r, pc] == 0, {r, 1}]]]

(*Generating parametric plot for different central pressures*)
T1 := Table[{R[i * 10^-2], Mass[R[i * 10^-2], i * 10^-2]}, {i, 1, 10}];
T2 := Table[{R[i * 10^-1 * 0.5], Mass[R[i * 10^-1 * 0.5], i * 10^-1 * 0.5]}, {i, 2, 20}];
T3 := Table[{R[i * 0.5], Mass[R[i * 0.5], i * 0.5]}, {i, 2, 20}];
T4 := Table[{R[i * 5.0], Mass[R[i * 5.0], i * 5.0]}, {i, 2, 20}]
T5 := Table[{R[i * 50], Mass[R[i * 50], i * 50]}, {i, 2, 20}]
parameters := Join[T1, T2, T3, T4, T5]
Quiet[ListPlot[parameters, PlotRange → Automatic, AxesLabel → {"R", "M"}]]
```

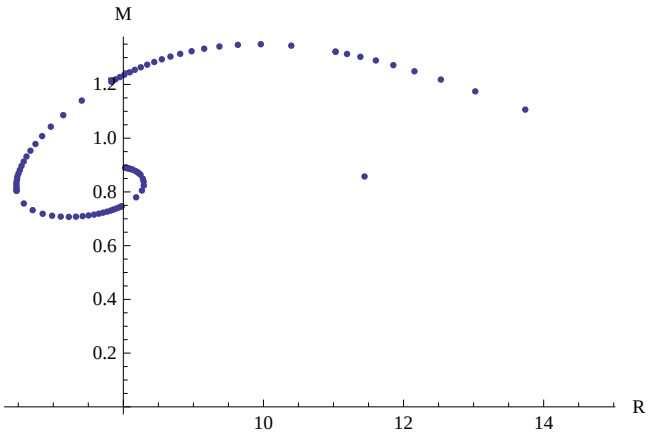

■ Newtonian equations

```
t[pc_] := NDSolve[{pn'[r] == -α / (r^2) * (An * pn[r]^(3.0 / 5.0) + Ar * pn[r]) * nm[r],
   nm'[r] == β * r^2 * (An * pn[r]^(3.0 / 5.0) + Ar * pn[r]), pn[10^-10] == pc,
   nm[10^-10] == 10^-14}, {pn, nm}, {r, 10^-10, 100}, MaxSteps → 100 000]
NP[r_, pc_] := First[Re[pn[r] /. t[pc]]]
NMass[r_, pc_] := First[Re[nm[r] /. t[pc]]]
NR[pc_] := Last[Last[FindRoot[NP[r, pc] == 0, {r, 1}]]]
```

```
(*Plotting solutions to TOV and Newtonian equations, for central pressure 0.01*)
sol = s[0.01];
tol = t[0.01];
Plot[{pn[r] /. tol[[1]], p[r] /. sol[[1]]}, {r, 10^-14, 16}, AxesLabel → {"r", "p(r)"},
 PlotLegend → {"Newtonian", "TOV"}, LegendPosition → {0.001, -0.2}]
Plot[{nm[r] /. tol[[1]], m[r] /. sol[[1]]}, {r, 10^-14, 16}, AxesLabel → {"r", "M(r)"},
 PlotLegend → {"Newtonian", "TOV"}, LegendPosition → {0.3, -0.4}]
```

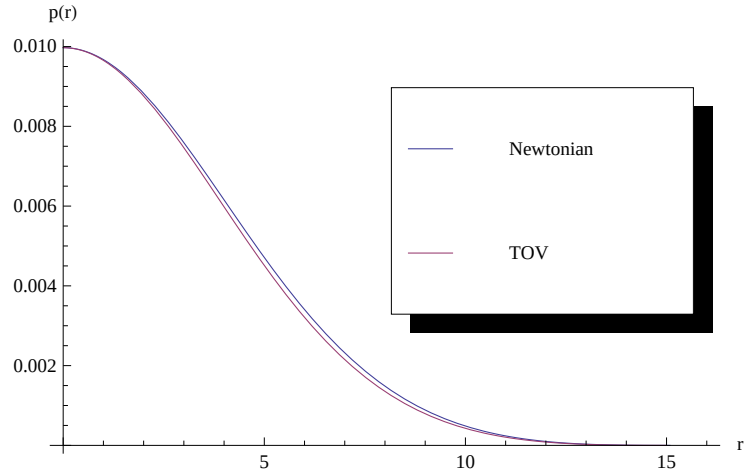

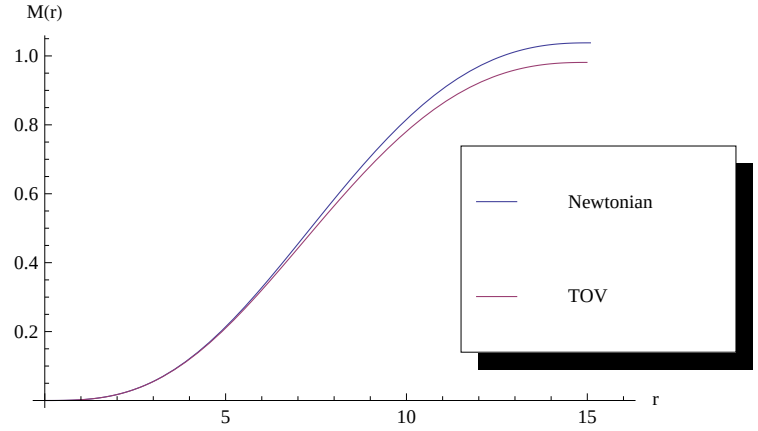


```
Clear[c, G, M, α, β, An, Ar, ϵ0, p, m, s, P, Mass, R, parameters, t, pn, nm, NP, NMass, NR]
```

Quark star

```
c := 3 * 10^5 (*km/s*)
G := 6.673 * 10^-20 (*km^3/(kg*s*)
M := 1.98892 * 10^30 (*kg*)
α := G M / c^2
β := 4 * Pi * ϵ0 / (M * c^2)
ϵ0 := 0.003006 * M * c^2
```

■ Ideal gas

```
s[pc_] := NDSolve[
  {p'[r] == -α / (r^2) * 4 p[r] * (m[r] + β * r^3 * p[r]) / (1 - 2 α m[r] / r), m'[r] == β * r^2 * 4 p[r],
   p[10^-10] == pc, m[10^-10] == 10^-14}, {p, m}, {r, 10^-10, 60}, MaxSteps → 100 000]
```

```
(*Plotting solution for central pressure 0.01*)
sol = s[0.01]
Plot[p[r] /. sol[[1]], {r, 10^-14, 60}, AxesLabel → {"r", "p(r)"}]
Plot[m[r] /. sol[[1]], {r, 10^-14, 60}, AxesLabel → {"r", "M(r)"}]
```

```
{{p → InterpolatingFunction[{{1. × 10^-10, 60.}}, <>],
  m → InterpolatingFunction[{{1. × 10^-10, 60.}}, <>]}}
```

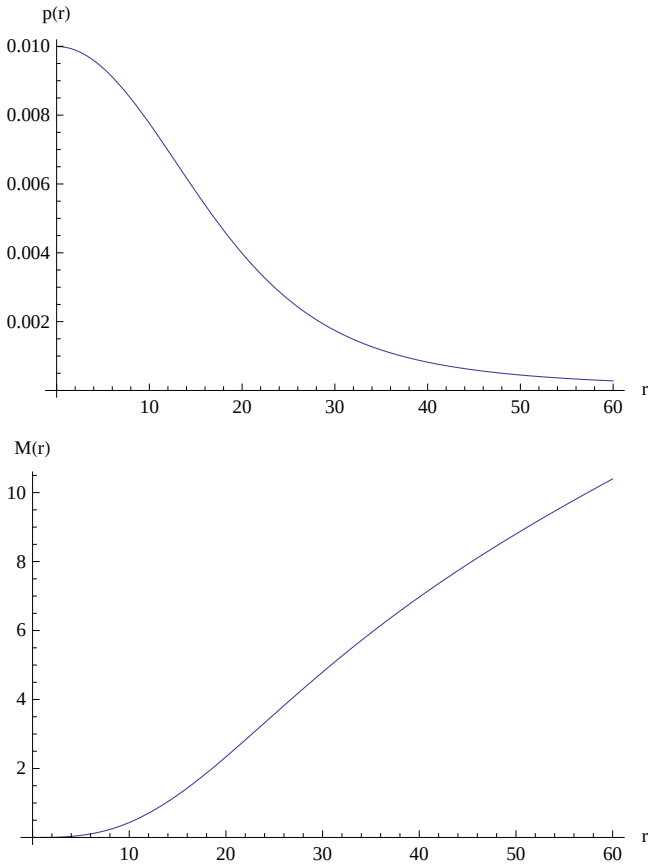

■ Bag model

```
s[pc_, B_] := NDSolve[{p'[r] == -α / (r^2) * 4 (p[r] + B) * (m[r] + β * r^3 * p[r]) / (1 - 2 α * m[r] / r),
    m'[r] == β * r^2 * (3 p[r] + 4 B), p[10^-10] == pc, m[10^-10] == 10^-14},
  {p, m}, {r, 10^-10, 50}, MaxSteps → 100 000]
P[r_, pc_, B_] := First[Re[p[r] /. s[pc, B]]]
Mass[r_, pc_, B_] := First[Re[m[r] /. s[pc, B]]]
R[pc_, B_] := Last[Last[FindRoot[P[r, pc, B] == 0, {r, 1}]]]
```

```
(*Generating parametric plot for different central pressures,
and different bag constants*)
parameters[B_] :=
 Join[Table[{R[i * 10^-3 * 0.5, B], Mass[R[i * 10^-3 * 0.5, B], i * 10^-3 * 0.5, B]}, {i, 2, 20}],
  Table[{R[i * 10^-2, B], Mass[R[i * 10^-2, B], i * 10^-2, B]}, {i, 1, 10}],
  Table[{R[i * 10^-1 * 0.5, B], Mass[R[i * 10^-1 * 0.5, B], i * 10^-1 * 0.5, B]}, {i, 2, 20}],
  Table[{R[i * 0.5, B], Mass[R[i * 0.5, B], i * 0.5, B]}, {i, 2, 20}],
  Table[{R[i * 5.0, B], Mass[R[i * 5.0, B], i * 5.0, B]}, {i, 2, 20}],
  Table[{R[i * 50], Mass[R[i * 50], i * 50]}, {i, 2, 20}]]
Quiet[ListPlot[{parameters[0.01], parameters[0.05], parameters[0.1]},
  PlotRange → {{0, 20}, {0, 3.5}}, AxesLabel → {"R", "M"},
  PlotLegend → {"B=60 MeV", "B=150 MeV", "B=230 MeV"}, LegendPosition → {0.5, -0.3}]]
```

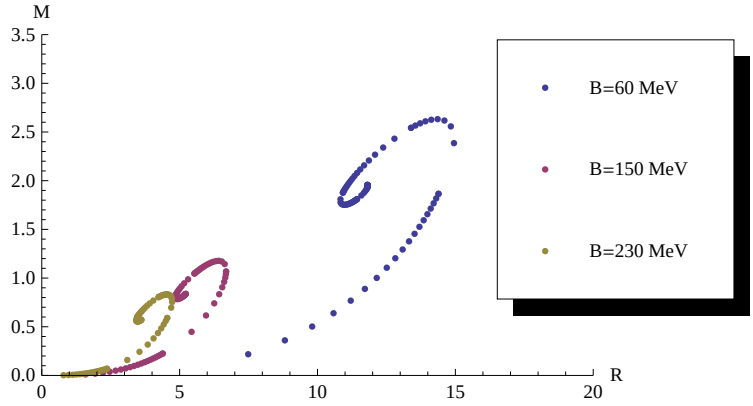


```
Clear[c, G, M, α, β, ϵ 0 p, m, s, sol, P, Mass, R, parameters]
```

■ Running coupling

```
ħ c:= 0.197
Nc := 3 (*Number of colours*)
Nf := 3 (*Number of flavours*)
P0 := μ^4 Nc Nf / (12 Pi^2) (*Ideal pressure*)
E0 := 3 * P0
β 0:= 11 - 2 Nf / 3
β 1:= 51 - 19 Nf / 3
Λ msbar:= 0.365 (*GeV*)
conv := 1.783 * 10^18(*(GeV/fm^3)/(kg/(m s^2)) converts between Gev/fm^3 and Joule/m^3*)
G := 6.67 * 10^(-11)(*m^3/(kg s^2)*)
c := 299 792 458(*m/s*)
r0 := 10^(-15)(*initial radius in meters*)
rmax := 13 000(*max radius in meters*)
M := 1.989 * 10^(30)(*kg*)
step := 10^(-4)(*step size used to sample central pressures*)
k := 10^-3

(*Defining coupling and pressure correction*)
Clear[α]
L[Λ_] = Log[Λ^2 / Λ msbar^2];
α[Λ_] = 4 π / (β 0 L[Λ]) (1 - 2 β 1 / β 0^2 Log[L[Λ]] / L[Λ]);
F[Λ_, mu_] = 1 - 2 α[Λ] / π(*-Nf(α[Λ]/π)^2 Log[α[Λ]/π]*) (*With comment: to one-loop*);
```

```
(*Calculating energy*)
ϵ[K_, μ_] = 1 / 3 (3 F[K μ, μ] + μ D[F[K μ, μ], μ]);
K = 1;
μ Min= μ /. FindRoot[F[K μ, μ] == 0, {μ, 0.65, 0.3, 0.8}, AccuracyGoal → 14, MaxIterations → 20]
(*P(μ)=0*)
μ Max= 10;
EPTable := Table[{P0 / ħ c^3 F[K μ, μ], E0 / ħ c^3 ϵ[K, μ]}, {μ, μ Min, μ Max, 0.01}]
(*could have smaller step size*)
Energy = Interpolation[EPTable]
```

```
0.583227
```

```
InterpolatingFunction[{{1.2768 × 10^-16, 88817.7}}, <>]
```

```
s[pc_] := NDSolve[{m'[r] == 4 Pi r^2 (conv Energy[p[r] / conv]),
   p'[r] == -(G / (r^2 c^2)) (conv Energy[p[r] / conv] + p[r]) (m[r] + 4 Pi r^3 p[r]) /
       (1 - 2 G m[r] / (c^2 r)), p[r0] == pc, m[r0] == 0}, {m, p}, {r, r0, rmax}]
P[r_, pc_] := First[Re[p[r] /. s[pc]]]
Mass[r_, pc_] := First[Re[m[r] /. s[pc]]] / M
R[pc_] := Last[Last[FindRoot[P[r, pc] == 0, {r, 100}]]]
```

```
(*Generating parametric plot*)
p0 := i * step * conv
T1 := Table[{k R[p0], Mass[R[p0], p0]}, {i, 1, 10}];
T2 := Table[{k R[p0], Mass[R[p0], p0]}, {i, 11, 101, 5}];
T3 := Table[{k R[p0], Mass[R[p0], p0]}, {i, 101, 1001, 50}];
T4 := Table[{k R[p0], Mass[R[p0], p0]}, {i, 1001, 20001, 100}];
T5 := Table[{k R[p0], Mass[R[p0], p0]}, {i, 20001, 100001, 10000}];
T6 := Table[{k R[p0], Mass[R[p0], p0]}, {i, 100001, 1000001, 100000}];
T7 := Table[{k R[p0], Mass[R[p0], p0]}, {i, 1000001, 10000001, 1000000}];
parameters := Join[T1, T2, T3, T4, T5, T6, T7]
Quiet[ListPlot[parameters, PlotRange → All, AxesLabel → {"R", "M"}]]
```

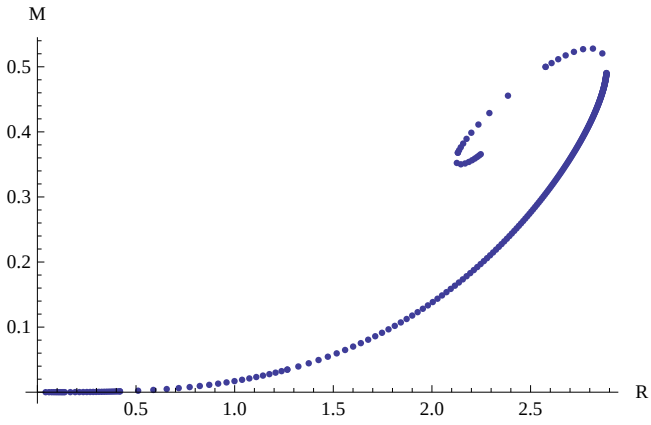


```
Clear[ħ, ç, Nc, Nf, P0, E0, β0, β1, Λmsbar, conv, G, c, M, k, L, α,
 F, ϵ, K, μ Min, μ Max, EPTable, Energy, s, p, m, P, Mass, R, parameters]
```

Bibliography

[1] Kenneth G. Wilson, *Confinement of quarks*, Physical Review Letters D10, 2445-2459, 1974.

[2] K. Fukushima and T. Hatsuda, *The phase diagram of dense QCD*, hep-ph/1005.4814, 2010.

[3] Subrahmanyan Chandrasekhar, *The Maximum Mass of Ideal White Dwarfs*, The Astrophysical Journal 74, 81-82, 1931.

[4] E. Noether, *Invariante Variationsprobleme*, Nachr. D. Knig. Gesellsch. D. Wiss. Zu Gttingen, Math-phys. Klasse 235 – 257, 1918.

[5] Norman K. Glendenning, *Compact Stars*, 1997.

[6] Michel Le Bellac, *Thermal Field Theory*, 1996.

[7] Peskin and Schröder, *An Introduction to Quantum Field Theory*, 1995.

[8] J. I. Kapusta and C. Gale, *Finite-Temperature Field Theory Principles and Applications*, 1989.

[9] Lewis Ryder, *Quantum Field Theory*, 1996.

[10] Mandl and Shaw, *Quantum Field Theory*, 1988.

[11] A. Zee, *Quantum Field Theory in a Nutshell*, 2010.

[12] Steven Weinberg, *Gravitation and Cosmology*, 1972.

[13] Jens O. Andersen, *Introduction to Statistical Mechanics*, 2011.

[14] R. D. Pisarski, *Scattering Amplitudes in Hot Gauge Theories*, Physical Review Letters 63 1129, 1989.

[15] Particle Data Group, 2004.

[16] D. J. Gross et al, *QCD and Instantons at Finite Temperature*, Modern Physics 53 43-80, 1981.

[17] R. P. Feynman, *Space-Time Approach to Non-Relativistic Quantum Mechanics*, Reviews of Modern Physics 20 367, 1948.

[18] P. Arnold and C. Zhai, *Three-loop Free Energy for pure Gauge QCD*, Physical Review Letters D50 7603, 1994.

[19] R.Parwani and H. Singh, *The Pressure of hot $g^2\phi^4$ Theory at order g^5*, Physical Review Letters D51 4518-4524, 1994.

[20] Richard R. Silbar and Sanjay Reddy, *Neutron Stars for Undergraduates*, American Journal of Physics 72 892-905, 2004.

[21] I. Levine et al, *Measurement of the Electromagnetic Coupling at Large Momentum Transfer*, Physical Review Letters 78 424-427, 1997.

[22] S. J. Brodsky et al, *On the Elimination of Scale Ambiguities in Perturbative Quantum Chromodynamics*, Physical Review Letters D1 28, 1983.

[23] E. S. Fraga and P. Romatschke, *Role of Quark Mass in cold and dense Perturbative QCD*, Physical Review Letters D71 105014, 2005.

[24] A. Chodos, R.L. Jaffe et al, *New extended Model of Hadrons*, Physical Review Letters D9 3471, 1974.

[25] V. Gogohia, *Failure of the Ladder Approximations to QCD*, Physics Letters B611 129-136, 2005.

[26] E. S. Fraga et al, *Small, Dense Quark Stars from Perturbative QCD*, Physical Review D63 121702, 2001.

[27] T. Appelquist, M. Dine and I. Muzinich, Physical Letters B 70 231, 1977.

[28] S. Coleman and D. J. Gross, *Price of Asymptotic Freedom*, Physical Review Letters 31 851, 1973.

[29] D.V. Shirkov and I.L. Solovstov, *Analytic Model for the QCD Running Coupling with Universal* $\bar{\alpha}_s(0)$ *Value*, Physical Review Letters 79 1209, 1997.

[30] E. S. Fraga et al, *Small, dense Quark Stars from Perturbative QCD*, Physical Review D63 121702, 2001.

[31] A. R. Bodmer, *Collapsed Nuclei*, Physical Review Letters D4 1601-1606, 1971.

[32] Frédérique Grassi, *Zero temperature quark matter equation of state*, Fermilab-Conf-87/167-A, 1987.

[33] J. O. Andersen et al, *Pressure to order* $g^4 log\, g$ *in* ϕ^4*-theory at weak coupling*, hep-ph/0903.4596v2, 2009.

[34] Hua Li et al, *Bag Model and Quark Star*, arXiv:1008.5019v1, 2010.

[35] J. O. Andersen and M. Strickland, *The Equation of State for Dense QCD and Quark Stars*, Physical Review Letters D66 105001, 2002.

[36] N. Itoh, *Hydrostatic equilibrium of hypothetical quark stars*, Progress of Theoretical Physics 44 291, 1970.

[37] A. Kurkela et al, *Cold Quark Matter*, Physical Review Letters D81 105021, 2009.

[38] G. H. Bordbar and B. Ziaei, *The effect of dynamical quark mass in the calculation of strange quark star structure*, astro-ph/1201.3228v1, 2012.

[39] F. X. Timmes et al, *The Neutron Star and Black Hole initial Mass Function*, Astrophysical Journal 457 834, 1996.

[40] Ren-Xin Xu, *The birth of quark stars*, Chinese Journal of Astronomy and Astrophysics 2 279-286, 2006.

[41] http://astro.cornell.edu/

[41] M. Orsaria et al, *Magnetars as highly magnetized quark stars: An analytical treatment*, The Astrophysical Journal 734 1, 2011.

[42] P. Jaikumar, *Surface structure of quark stars with magnetic fields*, hep-ph/0604179v1, 2006.

[43] G. van Rossum and J. de Boer, *Interactively Testing Remote Servers Using the Python Programming Language*, CWI Quarterly, Volume 4, Issue 4, Amsterdam, pp 283-303, 1991.

[44] W. R. Inc., Mathematica 8.0.

All figures in this thesis, except from Fig 1.1, have been produced by myself. The front page figure is based on a photograph of our sun, taken from nasa.gov, and modified for artistic purposes.